The average wave overtopping discharge for a composite slope

A case study to the Afsluitdijk rehabilitation project

L.M.A. Jordans December 2019

TU Delft

Van Oord
Marine ingenuity

LEVVEL
LELY'S ERFGOED VEILIGGESTELD

Predicting the average wave overtopping discharge for a composite slope

A case study to the Afsluitdijk rehabilitation project

by

L.M.A. Jordans

In partial fulfilment of the requirements for the degree of

Master of Science
in Hydraulic Engineering

at the Delft University of Technology (TU Delft)

to be defended publicly in december 2019

TU Delft   Van Oord — Marine ingenuity   LEVVEL — LELY'S ERFGOED VEILIGGESTELD

Acknowledgements

Abstract

The Afsluitdijk failed on the current safety standards regarding flood protection. Contractors were free to send in new designs. To prove that the new design can resist the design wave conditions, tests are performed in a wave flume on a large and on a small scale. Between the two scales, clear differences in the average wave overtopping discharge were observed. The large scale tests showed higher average wave overtopping discharges than would be expected based on the small scale tests. The new design of the Afsluitdijk has a complex geometry, including a berm, armour units on the lower slope and on the upper slope ribs are constructed using roughness elements. The armour units and the roughness elements are of a new type and not much information about the roughness of these elements is available. Also, the combined influence of the berm and roughness elements has not been fully investigated yet. Since the Wadden Sea has a protected status the area to widen the Afsluitdijk is limited, which makes it harder to satisfy the overtopping requirements. The research objective of this study, is to develop a method to accurately predict the average wave overtopping discharge for a composite slope on a large scale.

The research started with modelling the wave conditions at the toe of the structure using the computational wave model SWASH. The effect of the foreshore on the wave conditions was considered. Then the influence of structural parameters such as the berm width, protrusion of ribs and the density of the ribs on the average wave overtopping discharge was investigated by comparing different test results. The method from EurOtop Manual (2018) and Capel (2015) are both treated to check their performance in predicting the average wave overtopping discharge. Since the method of Capel (2015) predicted the wave overtopping better than the method from the EurOtop Manual (2018), this equation was further adapted to predict the wave overtopping discharge more accurately for the case of the Afsluitdijk. The first adaptation was the area over which the roughness influence factor was considered. Based on observations during the flume tests was decided that only the roughness influence factor of the ribs on the upper slope should be taken into account in the equation of Capel (2015) when the water level is around the berm height. The second adaptation in the method of Capel (2015), was the influence of the shallow foreshore on the wave height distribution, which affects the run-up. This effect is taken into account by an influence factor in the equation of the average wave overtopping discharge. The third adaptation was the use of the deep water wave steepness instead of the local wave steepness. The wave steepness can not adapt quickly to the foreshore. Thus the wave steepness based on the equation of the deep water wavelength, is a better parameter. For each of these adjustments, the root means square error was calculated. These three adjustments resulted in lower values of the root mean square error. Afterwards, the cause of the difference in average wave overtopping discharge between the large and small scale flume tests was investigated. To do so the model effects and scale effects are elaborated. The differences in the modelled wave conditions and the structures were analyzed and the critical limits for scale effects were checked. The main difference between the two structures is the shape of the ribs. The squared ribs on a small scale might result in flow detachment and thus in a smaller average wave overtopping discharge. Scale effects might occur due to air entrainment, affecting the flow depth over the ribs. A larger flow depth will result in less effective ribs and a higher average wave overtopping discharge. Also, the accuracy of several parameters and the sensitivity of these parameters on the wave overtopping discharge was investigated.

From this research it was concluded that wave measurements at deep water cannot be used to accurately predict the wave overtopping discharge for the case of the Afsluitdijk. The ribs formed by the roughness elements on the upper slope resulted in a large reduction of the wave overtopping discharge. The influence of the ribs on the wave overtopping discharge becomes negligible for an average wave overtopping discharge larger than 20 l/m/s. The exact relation between the characteristics of the rib profile and the reduction on the wave overtopping discharge could not be derived from the available data set. Also, the combined influence of the berm and the roughness elements on the wave overtopping discharge could not be derived from the data set. The performed tests lack a systematic approach, as a consequence of the different objective from the contractors' side. The wave overtopping discharge on large scale for the composite slope as designed for the Afsluitdijk can best be predicted if the wave conditions at the toe of the structure are used. Still, the equation of Capel (2015) with some adjustments, which takes only the influence of the roughness elements on the upper slope, an extra influence factor for the shallow water effects and the deep water wave steepness into account, resulted in a good prediction of the wave overtopping discharge on both large and small scale. The average wave overtopping discharge on a large scale can be predicted with an average deviation of 30%, on a small scale the average deviation is 170%. The largest uncertainty in the prediction of the average wave overtopping discharge is the roughness influence factor of the structure.

Finally, recommendations regarding the wave model in SWASH are propesed. Also, a systematic approach to assess the combined influence of the berm and roughness elements is suggested. Furthermore, advice for extra measurements is provided.

Contents

Nomenclature

Fr	Froude number	[-]
u	Velocity	[m/s]
g	Gravity constant	[m/s^2]
L	Length scale	[m]
v_l	Viscosity	[m^2/s]
Re	Reynolds number	[-]
We	Weber number	[-]
Ca	Cauchy number	[-]
ρ_w	Water density	[kg/m^3]
σ	Surface tension	[N/m]
E	Bulk modulus of elasticity	[Pa]
T	Wave period	[s]
h	Water depth	[m]
H_{m0}	Spectral significant wave height	[m]
α	Slope angle	[°]
s	Wave steepness	[m]
$s'_{m-1,0}$	Local wave steepness	[-]
q	Mean overtopping discharge	[l/m/s]
R_c	Crest freeboard	[m]
γ_f	Friction reduction factor	[-]
γ_b	Berm reduction factor	[-]
γ_β	Oblique incident wave reduction factor	[-]
γ_v	Reduction factor crest wall	[]
r_b	Influence of berm width	[-]
r_{db}	Vertical difference between still water line and middle of the berm	[-]
ξ	Breaker parameter	[-]
α	Representative slope of the structure	[-]
K_r	Reflection coefficient	[-]
H_r	Reflected wave height	[m]
H_i	Incoming wave height	[m]
d	Water depth below plane of reference	[m]
ζ	Surface elevation	[m]
γ_h	Reduction factor foreshore	[-]
$H_{2\%}$	Exceedance wave height by the two percent highest waves	[m]
H_s	Significant wave height	[m]
H_{m0}	Significant wave height	[m]
$T_{m-1,0}$	Spectral mean energy wave period	[s]
T_p	Peak period	[s]
L_{berm}	Berm length	[m]
B	Berm width	[m]
SWL	Still water level	[m]
L_0	Deep water wave length	[m]
h_b	Water depth at berm	[m]
h_t	Water depth at toe	[m]
γ_f	Roughness reduction factor	[-]
f_h	Rib height	[m]
f_L	Center to center distance between elements	[m]
f_b	Width of elements	[m]
L	Length over which roughness is applied	[m]
ρ_{yf}	Roughness density parameter	[-]
γ_{fw}	Roughness width	[-]
$h_{protrusion}$	Height of the ribs	[m]
z	Location on the upper slope	[m]

$Ru_{2\%}$	Two percent run up height	[m]
h_a	Water layer thickness	[m]
k	Wave number	[radians/m]
	Permeability porous flow	[m/s]
n	Scaling factor	[-]
v_k	Kinematic viscosity	[m^2/s]
N	Stability number	[-]
D_n	Nominal diameter	[m]
Δ	Relative density	[-]
Λ	Leakage length	[m]
D	Thickness soil layer	[m]

1
Introduction

1.1. Background

After 70 years of making plans about the closure of the Zuiderzee and land reclamation in the Zuiderzee, in 1918 the Zuiderzeewet was signed. The storm surge which occurred in 1916 played an important role in the decision to sign the Zuiderzeewet. This storm surge flooded the land around the former Zuiderzee and caused a sudden change in the public opinion about the closure of the Zuiderzee by means of a dam, according to Vrouwenvelderk and Struik (1990). In 1927 the construction of the Afsluitdijk started and in 1932 the closure of the Zuiderzee was completed. A 32 kilometre long dike separates the Zuiderzee from the Waddensea. In the last 87 years, the Afsluitdijk has continued to prove its worth, for example during the storm surge of 1953.

During the last safety assessment of Rijkswaterstaat in 2006, the dike failed on the current safety standards for flood protection. The results of the safety assessment showed that the height of the dike was not sufficient and the revetment at the seaward side and the lake side need major reinforcements. Also the height and stability of the sluice complexes could not be guaranteed during extreme storm events. A new design was needed, which ensured continued protection against flooding in the future for The Netherlands.

In 2016 the tendering procedure opened for the DBFM contract of the Nieuwe Afsluitdijk. Rijkswaterstaat awarded the project of the Nieuwe Afsluitdijk to the Levvel consortium, consisting of Van Oord (with Aberdeen/APG), BAM (with PGGM) and Rebel. According the planning process the Afsluitdijk should meet the requirements of flood safety again by the end of 2023.

1.2. Problem statement

The contractors were free to send in their designs, but Rijkswaterstaat required large scale tests in the Delta flume to prove that the design can resist the design wave conditions, this ensures the requirements for water safety and wave overtopping are met. Prior to the execution of the tests on a large scale, small scale tests were performed to optimise the design of the different dike sections. During the tests, differences in the wave overtopping discharge are observed for the different model scales under the same wave conditions. The large scale tests showed higher overtopping discharges than would be expected based on the small scale tests.

From the flume tests, no information is available about the wave conditions at the toe of the structure. During the large scale tests wave conditions are mainly measured at deep water. Later extra wave gauges are installed at the foreshore.

The new design of the Afsluitdijk has a complex geometry composed of armour units on the lower slope, a berm and a block revetment with ribs constructed on the upper slope. The armour units and the block revetment with ribs constructed on it are both of a new type. The ribs are constructed to enhance roughness and reduce the amount of overtopping. Thus far not much information about the roughness of the new type of armour elements and the block revetment with ribs is available.

The complex geometry with the combination of a berm and roughness elements further complicates the task of accurately predicting the overtopping. This is mainly because the combined influence of the berm and roughness elements has not been fully investigated yet.

The area to widen the Afsluitdijk for the reinforcement is limited, since the Wadden Sea has a protected status as a nature reserve and it is a World Heritage site, according to Ministerie van Infrastructuur en Milieu (2016a) and UNESCO Centre (2019). This makes it harder to satisfy the requirements regarding wave overtopping.

In brief, differences in overtopping discharge between large and small scale, lack of measurements from wave conditions at the toe, the uncertainties in roughness of the new type of elements, the complex geometry and the restricted space for reinforcing the Afsluitdijk ask for a more accurate way to predict the wave overtopping discharge on large scale.

1.3. Research objective and research question

The objective of this research is to develop a method to accurately predict the average wave overtopping discharge for a composite slope on a large scale.

Research question:

How can the average wave overtopping discharge for a composite slope as designed for the Afsluitdijk rehabilitation project accurately be predicted?

Subquestions:

- Can deep water wave conditions be used to accurate predict the average wave overtopping discharge?
- Which mechanisms influence the average wave overtopping discharge?
- How can the roughness of the rib profile accurately be determined?
- How can existing methods be adapted to better predict the average wave overtopping discharge?
- What causes the difference in wave overtopping discharge between large scale and small scale?

1.4. Scope

Regarding safety in the rehabilitation project of the Afsluitdijk only the average wave overtopping discharge is in the scope of this project. Individual wave overtopping and stability of the structure are out of the scope. Measurements of the wave conditions, still water level and the wave overtopping discharge from the tests in the Delta flume and Scheldt flume are provided. Furthermore, the data set contains information of the structural parameters.

1.5. Outline of the report

An overview of the different chapters and their content is presented below.

- Chapter 2: **Approach**
  The approach explains the different steps and the sequence of the steps that will be taken during the research.

- Chapter 3: **Theoretical background**
  The theoretical background summarizes the current state of knowledge, regarding the design of the Afsluitdijk, overtopping discharge, friction due to ribs, wave models and scale effects.

- Chapter 4: **Model setup**
  This chapter contains information about the setup of the experiments that are analyzed in this study. It can be separated in two parts. The first part explains the setup of the physical experiments in the different wave flumes. The second part discusses the setup of the computational wave model SWASH. Which is used to model the wave conditions at the toe of the structure.

- Chapter 5 and chapter 6: **Results and analysis**
  Chapter 5 describes the wave conditions at different locations in the flume. These wave conditions will be used as a starting point in the roughness determination of the upper slope in the next chapter, chapter 6. These chapters are separated, because they consider two different aspects. Chapter 5 and chapter 6 consider respectively the hydraulic loading and the structural response.

- Chapter 7: **Discussion**
  In this chapter results of the computational wave model, the model setup of the wave flume experiments and the empirical equations are discussed.

- Chapter 8: **Conclusion**
  First the subquestions will be answered and finally the main research question is answered.

- Chapter 9: **Recommendations**
  Here the recommendations for improvements in the model setup and for future research are given.

2
Approach

The approach intends to answer the research questions in a structured way and also acquire enough insight into the subject to fulfill the research objective. The approach follows the sub questions from top to bottom.

To visualize the approach a test setup will be used consisting of several steps, these are explained in figure 2.1 and figure 2.2. The method consists of two main parts: the hydraulic loading and the structural response. The hydraulic loading comprises the wave conditions while the structural response considers the capability of the structure to reduce the wave overtopping discharge.

2.1. Hydraulic loading

The tests in the wave flumes are executed with different bottom profiles. The bottom profiles can be divided into three parts. From left to right, see figure 2.1, deep water, foreshore and the structure. Exactly between the foreshore and the structure, the toe is located. The length of the foreshore, the height of the foreshore, the slope between the foreshore and the toe and the start of the toe are varied between the bottom profiles.

Tests are executed on different scales in the wave flumes. Tests in the Delta flume are on scale 1:2.95, which will be referred to as large scale. Tests in the Scheldt flume are on scale 1:19.8, this is called small scale. In the wave flume, wave gauges were installed. The majority of the tests in the Delta flume are performed with only three wave gauges located in deep water. Later an extra set of three wave gauges is installed at the flat part of the foreshore. In the Scheldt flume, two sets of four wave gauges were installed from the beginning of the tests. One set was installed at deep water, the other set was installed at the flat part of the foreshore.

Since the number of wave gauges is limited in the wave flume, a computational wave model is used to assess the effect of the foreshore on the wave conditions at the toe of the structure. Section 3.2 describes which physical processes are important when waves approach the structure and go from deep to shallow water. Also, the effect on the wave parameters is described here. Then a trade-off is made between the models SWAN, SWASH and OpenFOAM to decide which wave model is best to predict the wave conditions at the toe of the structure.

The setup of the wave model is described in chapter 4. The cases that will be tested in the wave model are based on the target wave conditions, still water level and the bottom profile. The wave model will be calibrated based on the wave conditions at deep water. Once the model is calibrated, it will be validated. For the validation, the measurements from the wave gauges in the wave flume on the foreshore are compared to the measurements from the wave model at the same locations to see if they give accurate results. Afterward, it is verified if the reflection in the wave model is negligible such that the measured wave height is indeed the incoming wave height. The amount of reflection will be checked in deep water.

The wave model will be used to gather more information about the physical processes that affect the wave conditions across the length of the wave flume due to changes in the bathymetry of the bottom profiles. In the wave model, extra output locations are placed at the toe of the structure to determine the wave conditions there. With spectral analysis, the significant wave height, peak period and spectral mean wave energy period are calculated. The highest two percent waves are calculated with a time domain analysis. The results of the wave parameters are presented in chapter 5 and will be used as a starting point for the structural response. The results of the wave conditions will also be used to check if differences are occurring between the Delta flume and the Scheldt flume.
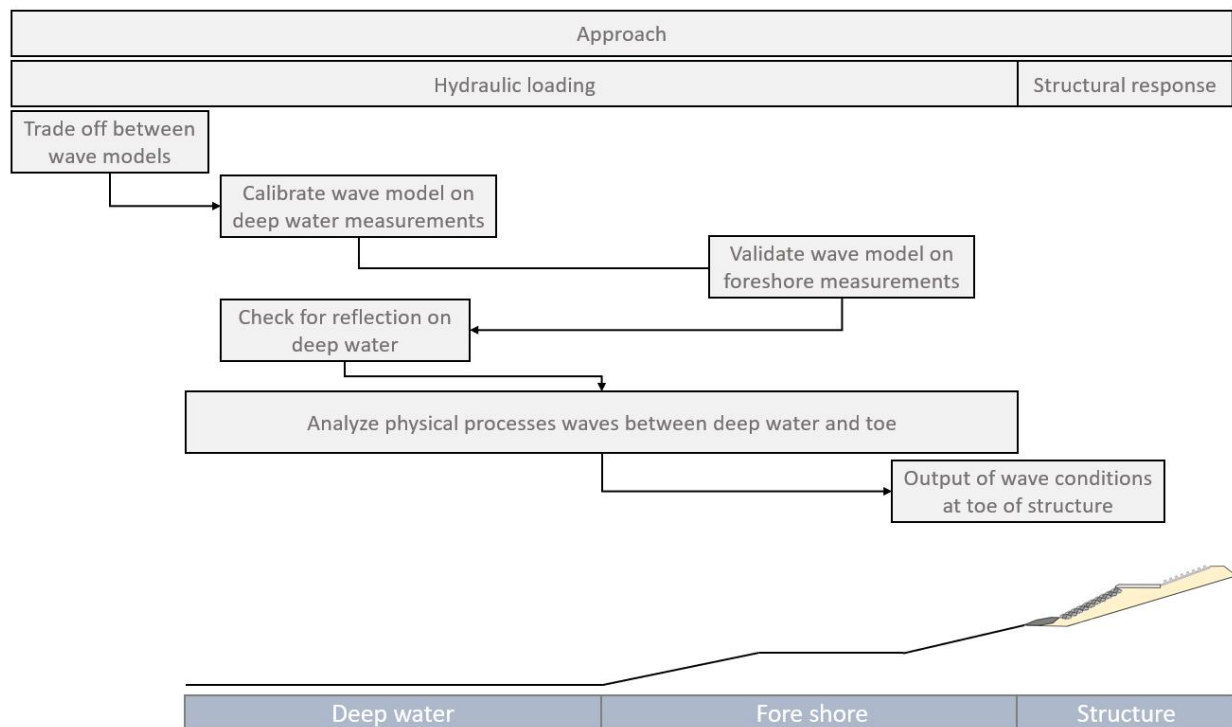
Figure 2.1: Approach hydraulic loading

2.2. Structural response

Based on the results of the wave conditions from the wave model, the wave overtopping measurements and the structural parameters the mechanisms which are important for the wave overtopping discharge are investigated. The wave conditions showed that they are affected by the foreshore. The relation $H_{2\%}/H_{m0}$ at the toe of the structure is not 1.4 anymore and the local wave steepness increases. The structural parameters that are considered are the lower slope, berm and upper slope. Considered characteristics of the ribs on the upper slope are the exposed area, protrusion, density of the ribs and the number of ribs.

Then the performance of the current theories in predicting the average wave overtopping discharge is looked at. The theory of EurOtop Manual (2018) and Capel (2015) are considered. The root mean square error will be used as a measure for the performance in predicting the average wave overtopping discharge and the roughness of the upper slope. Subsequently, the theory of Capel (2015) will be adjusted to estimate the average wave overtopping discharge more precise. The area over which the roughness elements are influencing the wave overtopping discharge, the influence of the shallow foreshore on the wave overtopping discharge, the wave steepness, the location of the used wave conditions and the water layer thickness of the run-up are treated.

Since there is a clear difference in average wave overtopping discharge between small and large scale, possible model and scale effects are considered. First is dealt with the hydraulic conditions and afterward with the structural response. For the scale effects, some theoretical critical limits are defined which should be exceeded to avoid scale effects. These limits will be checked. The model effects that are evaluated are the bottom friction, the wave gauges and the shape of the ribs on the upper slope.

The uncertainty in several parameters is determined. The sensitivity of the adjusted equation of Capel to these uncertainties is calculated. This gives an indication of the performance of the adjusted equation.
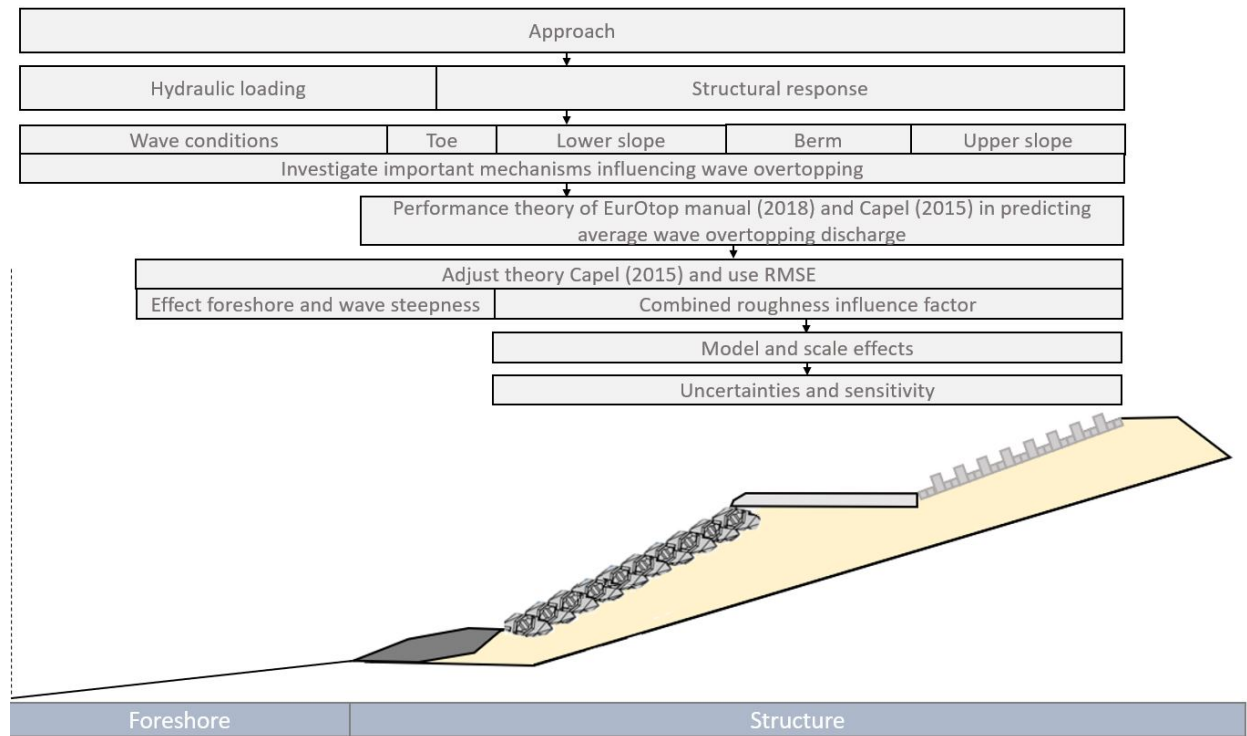
Figure 2.2: Approach structural response

3
Theoretical background

The purpose of this chapter is to inform about the design of the Afsluitdijk. Then the current knowledge about the hydraulic loading of the waves is summarized and a trade off between different wave models is made. After that a deeper insight in the structural parameters of the design of the Afsluitdijk is presented. Finally the current methods to predict wave overtopping are described.

3.1. Design Afsluitdijk
3.1.1. Afsluitdijk
The Afsluitdijk was built between 1927 and 1932. The main function of the Afsluitdijk is to provide protection against flooding of the inland. It separates the Zuiderzee from the North sea. Figure 3.1 shows a typical cross section of the Afsluitdijk nowadays, which is uniform over the whole length of the Afsluitdijk.
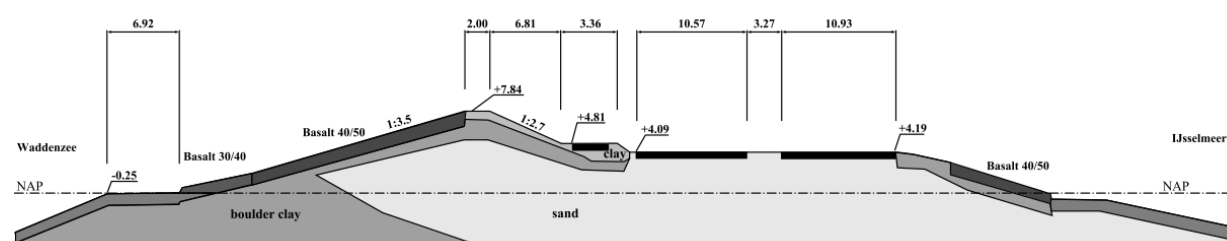
Figure 3.1: Typical cross section existing Afsluitdijk, Landa (2014)

The toe of the structure has been built of quarry run and the protection of the seaward slope consists mainly of basalt columns. The lake side slope has a grass cover and the lower part is made of natural basalt columns. This is a characteristic Dutch seadike profile, with a gentle slope at the seaside and a steeper lake side slope.

3.1.2. Requirements nieuwe Afsluitdijk
The Afsluitdijk should be able to withstand a storm that occurs 1/10 000 years. The normative situation for the Afsluitdijk is an extreme heavy north-western storm during spring tide. Regarding the safety of the design of the Nieuwe Afsluitdijk there are two requirements that should be fulfilled till 2050 according the Ministerie van Infrastructuur en Milieu (2016b).

- Stability of the armour and the toe construction should be guaranteed.
- Average wave overtopping discharge should be lower than 10 l/m/s.

To preserve the historic profile of the Afsluitdijk there is another set of requirements. A small selection of the relevant requirements is shown below.

- The crest height is limited to NAP +10 meter and the crest width is limited to 3.5 meter.
- The vegetation on the inner slope should be preserved.
- The slope at the seaward side should be gentler than at the lake side.
- The structure on the upper outer slope should be fine and regular.
- The boulder core should be retained.
- There should be a bicycle path, although the location of it is not fixed.

To fulfill all the criteria set by Rijkswaterstaat the dike is separated in different dike sections, each with their own specific details for their case.

3.1.3. Dike sections and design of the nieuwe Afsluitdijk

The Afsluitdijk is separated in several dike sections. The dike sections have different cross sections. The dike sections are numbered and showed in table 3.1. The Afsluitdijk is evaluated from West to East, starting at 0.00 km in Den Oever onwards. In figure 3.2 an overview of the considered dike sections is shown.

Table 3.1: Dike sections Afsluitdijk, from East to West

Section	From (km)	To (km)	Description
6b	4.40	6.90	Afsluitdijk
8a	7.60	11.00	Afsluitdijk
8b	11.00	15.05	Afsluitdijk
17	27.90	31.92	Kornwerderzand

Figure 3.2: Dike sections overview

Figure 3.3 shows a schematization including the most important aspects of two typical cross sections of the Nieuwe Afsluitdijk that are considered in the report. The top figure shows the typical cross section of dike sections 6b, 8a and 8b. The cross section shows the toe, lower slope with armour units, asphalt berm and on the upper slope the block revetment with ribs. The structural parameters are varied during the different tests. The second cross section shows the cross section of dike section 17. Here, both the lower and upper slope are covered by a block revetment. On the upper slope ribs are constructed in the block revetment. Based on these cross sections the different elements and their function will be explained.
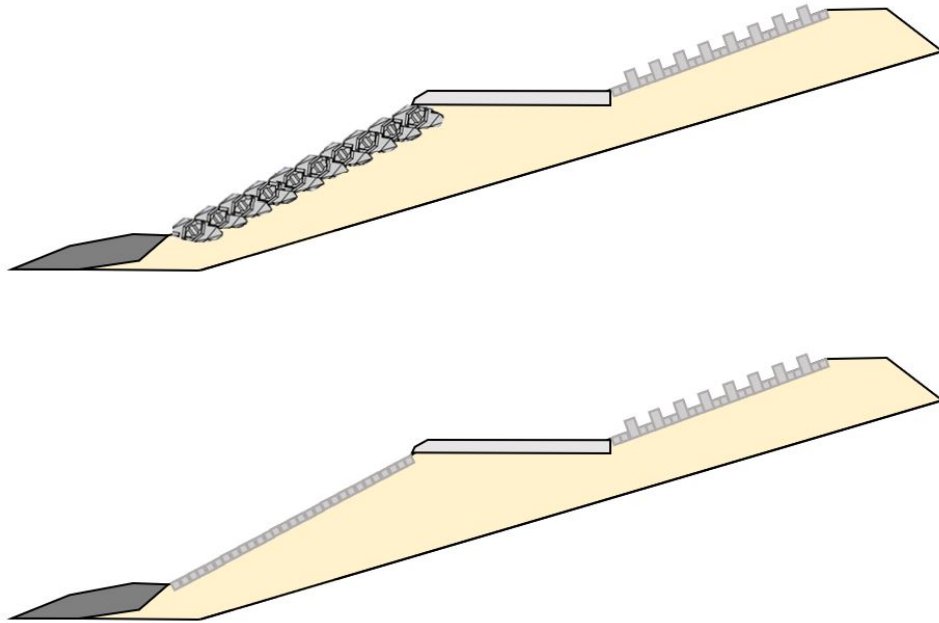
Figure 3.3: Schematization of typical cross section Afsluitdijk, upper figure shows dike section 6b, 8a and 8b. Lower figure shows dike section 17. Figures are not to scale

Foreshore

The foreshore is the part in front of the structure. The foreshore is not shown in figure 3.3. If the foreshore is in shallow water waves start to break, the incoming wave height reduces and the wave spectrum changes. In very shallow water more waves will break, more different wave periods will exist and the spectrum changes even more. Also, the wave steepness reduces and thus the breaker parameter changes, resulting in other types of wave breaking, according to Van der Meer (2002). During the flume tests different foreshores are tested. The foreshore is modelled as a 1:10 slope, than a flat part which is a transition zone and towards the structure there is again a slope. The different foreshores are shown in chapter 4.
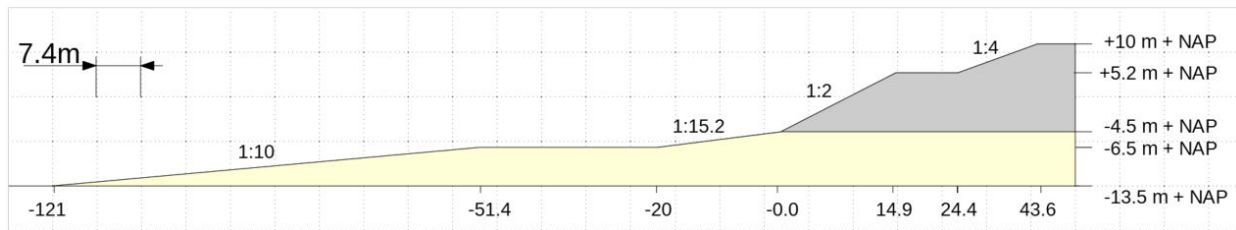
Figure 3.4: Schematization of slopes of foreshore and structure on scale. Bottom profile 8b-208 and structural parameters of testcase O1-8b-DG-2

Toe of the structure

The toe of the structure is located where the lower outer slope of the structure meets the foreshore, in figure 3.3 the toe is coloured dark grey. The stability of the toe is an important element for the stability of the armour units on the lower slope. During low water waves might break on the toe. The toe of the Afsluitdijk consists of quarried rock. The gradings of the quarried rock vary for the different dike sections.

Lower slope

The lower part of the seaward slope of dike section 6b, 8a and 8b consist of the armour units Xbloc^{plus}, which are called Levvel-blocs in this project. The Xbloc^{plus} is a new designed armour unit. This interlocking armour unit is placed on a staggered grid. The Xbloc^{plus} units are resting on the slope of the structure and on two units of the lower row, see figure 3.5. All the units are placed with a uniform orientation, which is different from other single layer armour units. In the design of these units extra attention is paid to achieve optimal interlocking between blocks, prevention of pressure build up during run up and run down by the central opening and fast and easy placement of the blocks, according to Reedijk et al. (2018).
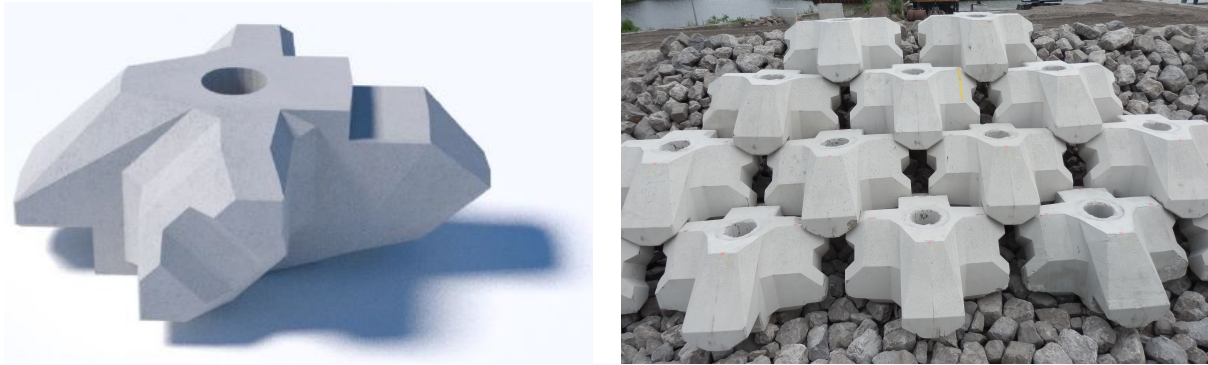
Figure 3.5: Side view of the Xbloc^{plus} and the regular pattern after placement, Reedijk et al. (2018)

The lower schematization of figure 3.3 shows dike section 17, without the Xbloc^{plus} on the lower slope. Here a smooth block revetment is placed on the lower slope.

Berm

The berm is the horizontal part of the structure, between the lower slope and the upper slope. In the case of the Afsluitdijk the berm also functions as bicycle path during calm weather conditions. The berm is located around design water level, because there it is most effective in reducing wave overtopping. In this way the berm ensures that the crest height of the structure can be reduced. The berm is made of asphalt resulting in a smooth surface with a low friction factor. To fixate the Xbloc^{plus} on the lower part of the outer slope berm blocks are put on top of the Xbloc^{plus}. These blocks form the transition between the lower slope and the berm.

Upper slope

On the upper part of the outer slope of all dike sections a revetment of Quattroblocks is constructed. The Quattroblock is the successor of the Basalton column. Quattroblocks are four columns which are connected as one element. Four of those elements together form a set, as can be seen in figure 3.6. Between the columns there is open space where gravel will be washed in.

Figure 3.6: Set of Quattroblocks (left) and the placement on the upper slope of dike section 17 (right), Holcim Coastal B.V.

The right figure shows the Quattroblocks as constructed on the upper slope of dike section 17. In this figure also the rib pattern is visible. This pattern is constructed to enhance roughness and reduce the wave overtopping discharge. The ribs are formed by elements of Quattroblocks with larger heights. The amount of ribs, the rib height and the configurations for various dike sections differ. The characteristics of the ribs depend on the hydraulic loading of the dike section.

3.2. Hydraulic loading

3.2.1. Physical processes

Waves go through several processes such as shoaling, breaking and reflection when they travel from deep water over the foreshore towards the structure. In this section is explained how wave parameters evolve when they approach the structure. At the end is explained how these processes affect the wave spectrum.

Classification shallowness

First a classification of the shallowness on the foreshore is defined in table 3.2. The paper of Hofland et al. (2017) describes four classes that can be present along the foreshore. This classification is based on the deep water wave height and the local water depth.

Table 3.2: Classifications shallowness foreshore

Classification	Limits
Deep water	$\frac{h}{H_{m0,deep}} > 4$
Shallow water	$1 < \frac{h}{H_{m0,deep}} < 4$
Very shallow water	$0.3 < \frac{h}{H_{m0,deep}} < 1$
Extremely shallow water	$\frac{h}{H_{m0,deep}} < 0.3$

In deep water waves are not breaking or shoaling due to depth, yet bottom friction and refraction may change the waves. In shallow water waves are influenced by depth induced processes. First waves may start to shoal and later start breaking. The wave spectrum looks similar as the deep water wave spectrum, but now higher and lower frequencies appear because of second order effects. In very shallow water breaking of the waves continues and the wave spectrum is different from the deep water spectrum. Low-frequency energy becomes dominant and

the spectrum is flattened. In extremely shallow water the spectrum mainly consists of infragravity waves. The provided test cases of this research only considered foreshore with deep and shallow conditions.

Shoaling
When waves enter shallow water, the wave frequency will be retained. The wave length and the wave velocity decrease with a decreasing water depth, since the dispersion relation remains valid. The decrease of the group velocity increases the amplitude of the waves. The effect of shoaling on the wave height becomes visible on the slope of the foreshore. Since the wave length decreases and the wave height increases, waves become steeper. Shoaling enhances triad wave-wave interactions. This distorts the profile of the wave, resulting in shallower troughs and higher peaks compared to the waves in deep water. The waves are no longer linear.

Breaking
White capping is the type of wave breaking that occurs in deep water. The individual water particles at the crest of the wave have a larger velocity than the phase speed of the wave, causing the front face of the wave to become too steep and it will break. Hasselmann (1974). In shallow water, the wave height is limited by depth induced breaking or surf-breaking. A typical ratio between the maximum significant wave height and the water depth for a horizontal bottom is 0.45.

The breaking parameter or surf similarity parameter describes the different types of breaking that occur. The main types of breaking are surging, collapsing, plunging and spilling. The transition between the different types of breaking is gradually changing. Battjes (1974)

$$\xi = \frac{\tan(\alpha)}{\sqrt{\frac{H_0}{L_0}}} = \frac{1}{2\pi} \frac{\tan(\alpha)}{\sqrt{H_0/gT^2}} \tag{3.1}$$

Equation 3.1 is used for deep water. To describe the interaction between the waves and the structure the deep water wave height is replaced by the significant wave height on the toe and the deep water wave length is replaced by the spectral mean wave energy period at the toe.

Reflection
When waves interact with the structure wave energy can be reflected from the slope back to deep water. The relative amount of wave energy that is reflected depends on the breaking process. The reflection coefficient is defined as the ratio between the amplitude of the reflected wave and the amplitude of the incident wave, as described in equation 3.2.

$$K_r = \frac{H_r}{H_i} \tag{3.2}$$

To determine the amplitude of the reflected wave there are two common methods, the method of Mansard and Funke (1980) and the method of Zelt and Skjelbreia (1992). In the study of Mansard and Funke three wave gauges are installed. Based on the on the linear superposition of wave components it is possible to seperate the incoming and the reflected wave from the total wave. Here the least square method with uniform weighting is applied. The method of Zelt and Skjelbreia is able to estimate the incoming and reflected wave height using an arbitrary number of wave gauges. The least square method is used with a weighting function. The weighting for each of the wave gauges is associated with the reliability of the information these wave gauges provide. The reliability depends for example on the distance between the wave gauges. The research of Zelt and Skjelbreia (1992) shows that choosing appropriate weighting coefficients increases the accuracy.

Wave spectrum
To express the irregular wave spectrum of a young sea state the JONSWAP spectrum with a peak enhancement factor of 3.3 is used.

3.2.2. Wave parameters

Wave height

There are a lot of ways to define the wave height. In this research two wave heights are considered. The significant wave height, based on the spectral analysis and the wave height which is exceeded by the highest two percent waves. This wave height is based on the time domain analysis. On deep water the waves are Rayleigh distributed, when the waves enter shallow water the distribution can better be described by a combination of the Rayleigh distribution and a Weibull distribution. Battjes and Groenendijk (2000)

To figure out how the wave conditions change over the spatial domain the wave height is determined at several locations in the spatial domain. The wave conditions at deep water, the flat part of the foreshore and at the toe of the structure will be calculated. Here only the incident wave height will be examined, because the reflection of the structure will be taken into account.

Wave period

Two wave periods from the wave spectrum are analyzed. These are the peak period, which corresponds to the frequency with the highest energy density and the spectral mean wave energy period which can be described with equation 3.3.

$$T_{m-1,0} = \frac{m_{-1}}{m_0} \tag{3.3}$$

On deep water the relation between the peak period and the spectral mean wave energy period is assumed to be 1.1. Yet the waves enter shallow water when approaching the structure. Energy is redistributed to the lower frequencies. This changes the constant relation between the peak period and the spectral mean wave energy period. The peak period and the spectral mean wave energy period will be determined at deep water, the flat part of the foreshore and at the toe of the structure.

Wavelength

The wavelength of free waves at arbitrary water depth can be described with the dispersion relation, equation 3.4. It is an iterative procedure to calculate this wavelength.

$$L = \frac{gT^2}{2\pi} \tanh \frac{2\pi h}{L} \tag{3.4}$$

In deep water $\tanh(2\pi h / L)$ approaches 1 and the deep water wavelength can be described with equation 3.5.

$$L_0 = \frac{gT^2}{2\pi} \tag{3.5}$$

3.2.3. Wave models

To decide which model to use to predict the wave parameters, a small comparison based on several characteristics of the computational models is made. Based on the characteristics of the models a trade off is made.

	SWAN	SWASH	OpenFOAM
Type	Phase averaged	Phase resolving	Phase and depth resolving
Area of application	Near shore	Till shore	Fluid-structure interaction
Equation to solve	Wave action balance	Non-linear Shallow water	Reynolds averaged Navier Stokes
Rotational flow	Irrotational flow	Rotational flow	Rotational flow
Shoaling	✓	✓	✓
Breaking	Depth-induced	Steepness-induced	Depth- & steepness-induced
Wave interaction	Triad and quadruplets	Triad and quadruplets	Triad and quadruplets
Reflection and transmission	✓	✓	✓
Bottom friction	Madsen and Rosengaus (1988)	Manning	Manning
Computation time	●●●●●	●●●○○	●○○○○

Table 3.3: Comparison wave models

Since SWAN is not designed for simulating the wave processes till the shore and the computational time of OpenFOAM is too long for the amount of tests that need to be simulated, is decided to use SWASH as wave model.

In SWASH the Reynolds-averaged Navier-Stokes equations are solved, so all hydrodynamic processes are included. A small description but more extensive elaboration about SWASH is provided below.

Numerical wave-flow model SWASH

SWASH is a wave-flow model which is essentially applicable in the coastal regions up to the shore. This resulted in the acronym SWASH, Simulating WAves till SHore. It can be used to predict the transformation of dispersive surface waves from offshore to the beach for studying the surf zone and swash zone dynamics. It is a general-purpose numerical tool for simulation non-hydrostatic, free-surface, rotational flows and transport phenomena in one, two or three dimensions, The SWASH team (2014). Below some important terms are explained.

- Non-hydrostatic: The effect of vertical accelerations is included.
- Free surface: SWASH simulates the changes of the wave-form, thus the free surface of the water.
- Rotational flow: Fluid particles move along the flow, but at the same time they rotate about their own axis with some angular velocity.

The governing equations in the model are the nonlinear shallow water equations, including non-hydrostatic pressure and some transport equations. This gives the following Navier-Stokes equations, Zijlema et al. (2011).

$$\frac{\delta \zeta}{\delta t} + \frac{\delta hu}{\delta x} + \frac{\delta hv}{\delta y} = 0 \tag{3.6}$$

$$\frac{\delta u}{\delta t} + u\frac{\delta u}{\delta x} + v\frac{\delta u}{\delta y} + g\frac{\zeta}{x} + \int_{-d}^{\zeta} \frac{\delta q}{\delta x} dz + c_f \frac{u\sqrt{u^2 + v^2}}{h} = \frac{1}{h}\left(\frac{\delta h\tau_{xx}}{\delta x} + \frac{\delta h\tau_{xy}}{\delta y}\right) \tag{3.7}$$

$$\frac{\delta v}{\delta t} + u\frac{\delta v}{\delta x} + v\frac{\delta v}{\delta y} + g\frac{\delta \zeta}{\delta y} + \frac{1}{h}\int_{-d}^{\zeta} \frac{\delta q}{\delta y} dz + c_f \frac{u\sqrt{u^2 + v^2}}{h} = \frac{1}{h}\left(\frac{\delta h\tau_{yx}}{\delta x} + \frac{\delta h\tau_{yy}}{\delta y}\right) \tag{3.8}$$

The integral of the non-hydrostatic pressure gradient over the water depth can be expressed as follows:

$$\int_{-}^{\zeta} d\frac{\delta q}{\delta x} dz = \frac{1}{2} h\frac{\delta q_b}{\delta x} + \frac{1}{2} q_b \frac{\delta(\zeta - d)}{\delta x} \tag{3.9}$$

The equations are phase-resolved meaning that the water surface is resolved. On every grid point the vertical displacement of the water surface is calculated.

These equations make use of four types of boundaries conditions, all considered at the boundary of the physical domain. These boundaries can be the bottom, free surface, open boundary and closed boundary. At these boundaries at least one normal and one tangential component of the velocity and/or shear stress need to be described. The boundary conditions for each type of boundary are considered below.Zijlema and Stelling (2005)
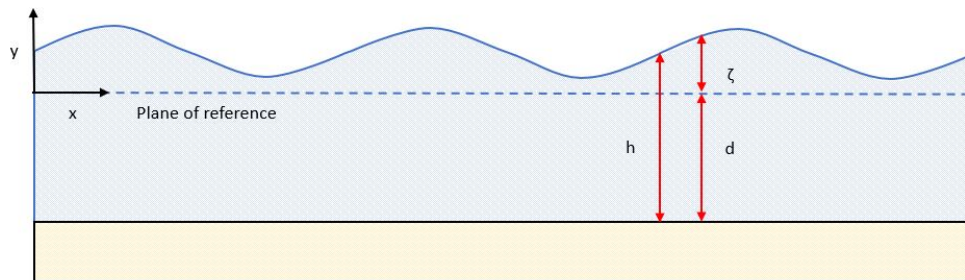

Figure 3.7: Indication of variables in SWASH

- Bottom: The normal velocity is imposed through the dynamic condition, which gives $w = -u\frac{\delta d}{\delta x}$. The tangential stress is the bottom stress in the model. In this model the velocity perpendicular to the bottom is zero and there is bottom friction.

- Free surface: The normal velocity at the surface is obtained by solving the momentum equation. The tangential stress concerns only the wind stress. Concerning infragravity waves the surface tension can be neglected and thus the pressure at the free surface is zero. The assumption is made there is no windstress in this model.
- Open boundary: Two types of open boundaries can be distinguished.
  - Inflow: The surface elevation is prescribed at the inflow. In this model the offshore boundary is an open boundary with inflow. Here is assumed that q = 0 and the tangential stress is also zero.
  - Outflow: The normal stress and tangential velocity are imposed. At the outflow the flow is assumed to be hydrostatic, which results in the water level. The shoreline is modelled with a sponge layer. This layer absorbs the incoming wave, so no reflection occurs.
- Closed boundary: At this type of boundary both the normal velocity and the tangential stress are set to zero. This type of condition is also known as the free-slip condition. This type of boundary is not used in this model.

The model can be employed to resolve the dynamics of wave transformation. So it can be applied for waves that approach the coast.

SWASH differs from other wave-models as it is not a Boussinesq-type wave model. In SWASH multiple vertical layers can be added, so the wave celerity is calculated for every layer. In this way the wave celerity due to frequency dispersion can be better modelled, because the wave celerity varies over depth. In this way the SWASH model improves the frequency dispersion by increasing the amount of vertical layers, where Boussinesq-type of wave models increase the order of derivatives of the dependent variables. This makes SWASH faster and more robust. The SWASH team (2014)

3.3. Structural parameters overtopping

Many theories use influence factors to express the effect of structural parameters on the wave overtopping. In the wave overtopping these influence factors are multiplied with each other under the assumption that the effect of each of the parameters is independent of the others. No information about the independence of these influence factors can be found . Below the effect of structural parameters are described on the basis of those influence factors.

3.3.1. Toe

If the water depth at the toe of a structure is larger than 4 times the significant wave height, the wave height distribution follows the Rayleigh distribution. For a shallow foreshore, where the water depth is smaller than 4 times the significant wave height waves will break and the distribution starts to deviate from the Rayleigh distribution. In a Rayleigh distribution, the relation between $H_{2\%}/H_{m0} = 1.4$. This relation becomes smaller when the largest waves start breaking and varies between approximately 1.1 up to 1.4.

To represent the influence of the water depth at the toe on the run-up an empirical relation between the wave height that is exceeded by the highest two percent of the waves and the significant wave height is given by Van der Meer and Janssen (1994) as described in equation 3.10.

$$\gamma_h = \frac{H_{2\%}}{1.4 \cdot H_s} \tag{3.10}$$

For this equation holds that the significant wave height at the toe of the construction should be used, instead of the deep water significant wave height. This influence factor, to take the depth induced breaking on the foreshore into account, might possibly be used to predict the wave overtopping discharge more accurate.

3.3.2. Berm

The berm reduces the amount of wave overtopping due to dissipation of wave energy. Therefore the wave reaches the upper slope with a lower energy, which result in a smaller run up height and thus lower wave overtopping volumes. The effect of the berm on the wave overtopping discharge is expressed in equation 3.11, which follows from the study of Van der Meer and Janssen (1994).

$$\gamma_b = 1 - r_b(1 - r_{db}) \tag{3.11}$$

Where $0.6 \leq \gamma_b \leq 1.0$

The influence of the berm width (r_b) can be calculated with the equation below.

$$r_b = 1 - \frac{2 \cdot H_{m0}/L_{berm}}{2 \cdot H_{m0}/(L_{berm} - B)} \tag{3.12}$$

The influence of the location of the berm with respect to the still water level is expressed in equation 3.13. The berm is most effective when it is located around the still water level according this equation.

$$r_{db} = 0.5 - 0.5 \cdot (\pi \frac{d_h}{x}) \tag{3.13}$$

Where x depends on the location of the berm. If the berm is located above the still water level x = $R_{u2\%}$ if the berm is located below the still water level x = 2 H_{m0}.

Ahrens and Ward (1991) also conducted a study to determine the effectiveness of a berm in reducing wave run-up and overtopping at a rip rap revetment. The research involves three terms to estimate the run-up on a riprap revetment. Two terms describe the relative run-up on a riprap revetment with a 1:2 slope without berm. The third term can be regarded as the berm reduction factor. Given by equation 3.15, which consists of a dimensionless value of the berm width, as described in equation 3.14 and a dimensionless regression coefficient. During the tests in this research the water level was equal or larger than the berm level, so the berm was submerged during the tests. However the tested geometry differs (rip-rap revetment and submerged berm) from the geometry used in this study, still it is worth to have a look at the performance of this equation. Mainly, because this equation also considers so many structural parameters in the dimensionless berm width.

$$B' = \frac{B}{\sqrt{(H_{m0} \cdot L_0)}} \cdot \frac{(h_b - h_t)}{SWL - h_t} \tag{3.14}$$

$$\gamma_b = \exp(c2 \cdot B') \tag{3.15}$$

c2 is a dimensionless regression coefficient with a value of -0.158 according the study of Ahrens and Ward (1991).

The study of Huppes (2019) validated the berm reduction factor calculated with equation 3.11. It considered a berm width of 5 meter, with the Xbloc^{plus} on the lower slope and a smooth upper slope. Three tests, scale 1:36.2, using the same hydraulic loading resulted in a small adaptation of equation 3.11. Huppes (2019) suggests to increase the γ_b with a constant value of 0.027.

3.3.3. Roughness of the structure
Combined roughness
In this report two studies that express the roughness influence factor of the structure are considered. Both methods try to capture the roughness of a composite slope of the entire structure in a combined roughness influence factor. For this a weighted influence factor is used, see equation 3.16. The weighted influence factor considers the roughness applied for a distance below the still water line and above still the waterline. The distance both methods take into account differs, as indicated in table 3.4. Figure 3.8 shows the distance over which the roughness is considered.
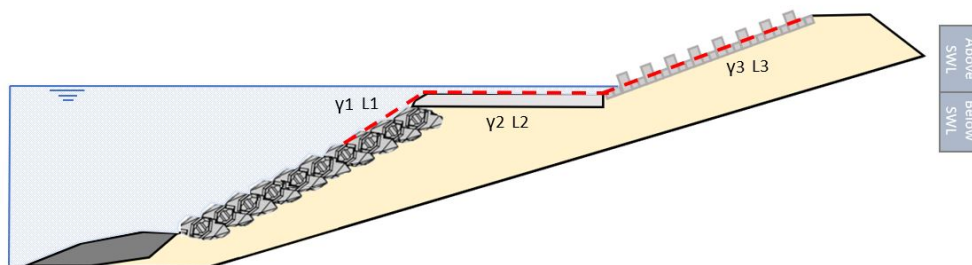

Figure 3.8: Combined roughness influence distance indicated by red dashed line

The method in EurOtop Manual (2018) takes the roughness between 0.25 $R_{u2\%,smooth}$ below the still water line and 0.50 $R_{u2\%,smooth}$ above the still waterline into account.

This means that the average roughness influence factor over the elements of part of the lower slope, the length of the berm and part of the upper slope is used as combined roughness influence factor of this structure.

The method of Capel (2015) uses a slightly different area over which the roughness influence factor is calculated. The distance below the still water level is described by equation 3.17, above still water level the area which is taken into account is the minimum of $Ru_{2\%}$ or the crest height.

Table 3.4: Area of influence for roughness elements

Method	Below SWL	Above SWL
EurOtop (2018)	0.25 $R_{u2\%,smooth}$	0.50 $R_{u2\%,smooth}$
Capel (2015)	equation 3.17	min($R_{u2\%}$, Crest height)

$$\gamma_{f,weighted} = \frac{\sum_{i=1}^{n} \gamma_{f,i} \cdot L_i}{\sum_{i=1}^{n} L_i} \tag{3.16}$$

$$\frac{d_{rough}}{H_{m0}} = min(0.35; 0.24 \cdot \xi_{m-1,0}^{1/3}) \tag{3.17}$$

To calculate the combined roughness influence factor the roughness influence factors of the lower slope, berm and upper slope should be evaluated.

The structure of the Afsluitdijk is a composite slope including a berm. The method of the combined roughness influence factor is never validated for this purpose. The equation in EurOtop Manual (2018) is based on the CLASH database. After filtering and selecting the sources less than 2% of the CLASH database remains with a structure including a berm and roughness on the upper slope. Even from this 2% it is questionable if it corresponds to a sea dike, with a composite slope and ribs on the upper slope. Since there is no source of the study enclosed of these remaining data points. The filtering of the database can be found in Appendix E. During the tests of Capel (2015) also no berm was included in the tested cross sections.

In the study of Kriebel (2019) a method is applied to calculate the combined roughness for a composite slope based on Chen et al.. It includes an extra parameter, the location-weighting factor, for the location where the roughness is applied. It assumes that the lower located roughness elements are less effective in reducing wave overtopping. The used location-weighting factors are 0.65 for the upper slope, 0.22 for the berm and 0.13 for the lower slope. Implementing the location weighting factor results in equation 3.18, where α is the location-weighting factor.

$$\gamma_{f,weighted} = \frac{\sum_{i=1}^{n} \alpha_i \cdot \gamma_{f,i} \cdot L_i}{\sum_{i=1}^{n} L_i} \tag{3.18}$$

Lower slope

The lower slope of the structure consists of the armour element Xbloc[plus] or a placed block revetment of Quattroblocks, as showed in figure 3.3. Since this block revetment is smooth the roughness influence factor is set to 1.0. The roughness of the armour units on the lower slope might decrease the wave overtopping, even when they are located below the still water line. The roughness influence factor of the Xbloc[plus] is investigated in several studies, but these studies did not result in one unique value.

The study of Huppes (2019) focused on the parameters that reduce the wave overtopping discharge at the Afsluitdijk. Tests are executed to determine the roughness coefficient of the lower slope. The dike section consisted of a composite slope, with Xbloc[plus] on the lower slope, a berm around the still water level and a smooth upper slope. Tests are executed on a 1:36.2 scale. The tests resulted in the following roughness influence factors for the Xbloc[plus] on the lower slope:

- 1:2 slope, $\gamma_f = 0.96$
- 1:1.5 slope, $\gamma_f = 0.51$

Reedijk et al. (2019) conducted a research to the roughness coefficient of the Xbloc[plus] as breakwater and shore protection armour unit. These tests did not include a berm.

Tests are performed on a 2:3 slope with a wave steepness varying between 0.01 and 0.04. From the tests followed that the roughness influence factor for the Xbloc^{plus} was 0.45.

The study of Moreno (2017) focused on the wave overtopping over a rubble mound structure using the Xbloc^{plus} as armour unit. So, the entire slope consists of Xbloc^{plus}. All the tests are executed on a 1:50 scale. The measurements showed that the roughness influence factor for the Xbloc^{plus} was:

- 3:4 slope, $\gamma_f = 0.55$
- 1:2 slope, $\gamma_f = 0.55$

Berm

Besides the berm width and the berm height which influence the wave overtopping, the berm has also a roughness. The roughness influence of the berm depends on the material of the berm. For the tested cases where the berm was made of concrete, wood or PVC, the surface is assumed to be smooth and impermeable. The roughness influence factor is assumed to be equal to 1.

Upper slope

Revetments form in general a smooth slope where the top of the revetment is levelled. To reduce the wave overtopping a rib pattern or chess board pattern can be constructed in the revetment. The pattern increases the roughness of the revetment which leads to a reduction of the wave run up and thus wave overtopping. The most common theories to determine the reduction factor of the block revetment are the method of Van der Meer (2002) and the method of Capel and Klein Breteler (2016). An elaboration of both methods is showed in the next sections.
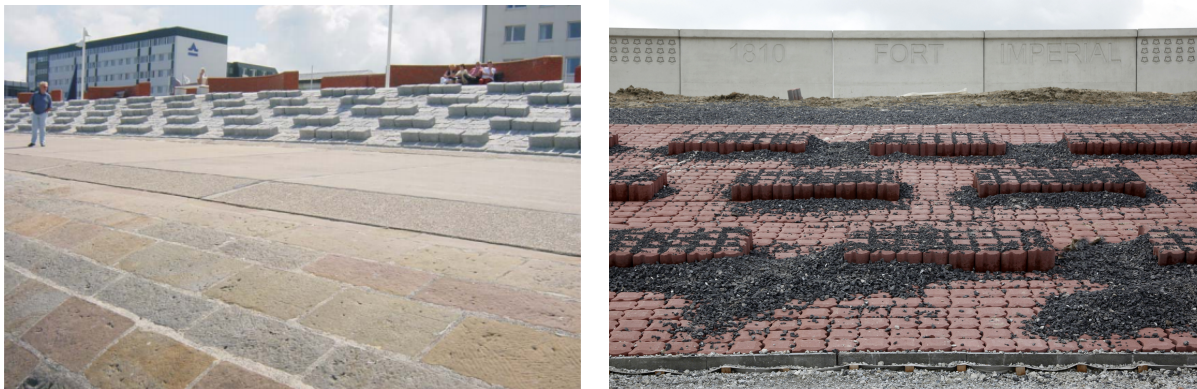

Figure 3.9: Block revetments with rib pattern, (left) Van der Meer et al. (2018) and (right) Haringman Beton

EurOtop Manual (2018)

The method in the EurOtop Manual (2018) to describe the roughness influence of the upper slope is based on the study of Van der Meer (2002), where the results of several wave run-up tests are presented. To present the roughness of the different configurations the following parameters are used.

- f_h: height of element.
- f_L: center to center distance of elements at right angles to the waterline.
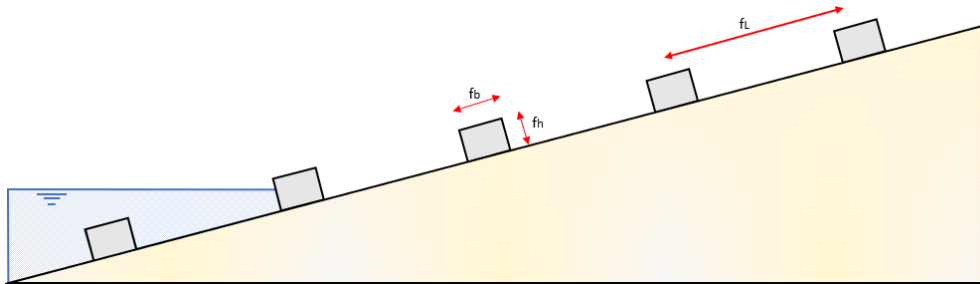- f_b: width of element at right angles to the waterline.

Figure 3.10: Dimensions roughness elements

The optimum distance between the ribs, according this method is f_L/f_b=7. In the case of $5 < f_h/f_b < 8$ and if the total surface is covered by blocks or ribs and the height has a minimum of $f_h/H_{m0} = 0.15$ than the following minimum reduction factors might be assumed;

- Blocks, covers 1/25 of total surface, optimum height: $\gamma_{f,min}$=0.85
- Blocks, covers 1/9 of total surface, optimum height: $\gamma_{f,min}$=0.80
- Blocks, 1/4 of revetments blocks is higher $\gamma_{f,min} = 0.90$
- Ribs, with rib distance of f_L/f_b=7: $\gamma_{f,min}$=0.75

A larger height than $f_h/H_{m0} = 0.15$ has no effect on the roughness influence factor. If the height of the blocks or ribs is smaller, than a linear interpolation to $\gamma_f = 1$ for $f_h/H_{m0} = 0$ should be performed as showed in equation 3.19.

$$\gamma_f = 1 - (1 - \gamma_{f,min} \cdot (\frac{f_h}{0.15 \cdot H_{m0}})) \tag{3.19}$$

Roughness elements only cover parts of the slope, hence a roughness influence factor is applied which only takes into account the parts that actually effect the roughness. Roughness elements have little or no effect to 0.25 $R_{u2\%,smooth}$ below the still water line or 0.50 $R_{u2\%,smooth}$ above the still waterline. A combined influence factor for the structure is calculated by the weighted average of the different influence factors, including the lower slope and the berm. Equation 3.16 is used for this, based on Van der Meer et al. (2018). This equation is used if the EurOtop Manual (2018) method is mentioned in the report.

Capel method 2015

Based on the research of Capel (2015) the effect of different parameters on the roughness will be explained. Here is explained how the equation to determine the roughness reduction factor for a rib profile is developed.

Mean overtopping discharge
The roughness influence due to the pattern decreases if the average wave overtopping discharge increases. A larger wave overtopping discharge is caused by a larger flow depth over the roughness elements. If the flow depth is larger the water experiences less roughness of the pattern.

The flow depth depends on the relative wave run-up compared to the relative crest height. The flow depth and the average overtopping discharge show a very strong relation. Therefore is decided to express a relation between the roughness influence factor in a dimensionless value of the average wave overtopping discharge.

$$1 - \gamma_f = -0.033 \cdot \ln\left(\frac{q}{\sqrt{g \cdot H_s^3}}\right) \tag{3.20}$$

Wave steepness
An increase in wave steepness leads to a reduction of the roughness of the patterns. There are two possible reasons for this. The first reason is that the ratio between $H_{2\%}/H_s = 1.4$ for waves with a steepness of 4-5%, for long waves with a wave steepness of 2% this ratio is 1.3. This means that the highest waves in the spectrum of steep waves are higher than the highest waves in the spectrum of the long waves. This results in a higher average wave overtopping discharge for steep waves and thus these will experience less roughness.

Another possible reason for the decrease in roughness that is experienced by steeper waves is the run down level that is lower for a smaller wave steepness. So the run up distance for the incoming wave with a steepness of 2% will be larger than for a wave with a steepness of 5%. Thus the roughness experienced will be lower for steeper waves.

To express the relation between wave steepness and the roughness reduction factor. First the effect of the wave overtopping discharge is excluded by dividing $1 - \gamma_f$ by $-\ln(q^*)$. The values are compared to the wave steepness. The wave steepness is calculated based on the water depth at the toe of the construction and the $T_{m-1.0}$. The wave steepness is expressed as $0.075 - s_{m-1.0}$, because 0.075 can be seen as the maximum wave steepness.

Slope gradient
In the research of Capel (2015) a rib pattern of 6 rows of protruding sets above the waterline on a slope of 1:3 and 1:4 is applied. The distance along the slope between the waterline and the crest was equal, which resulted in a lower crest height for the 1:4 case. The results show the same behaviour. Which means that the slope gradient does not influence the roughness coefficient. The roughness coefficient is influenced by the distance over which the rib pattern is applied.

Protrusion of the ribs
An increase in protrusion of the ribs results in an increase of the roughness. Test are executed with three different protrusion heights. From the results the following relation is found:

$$\frac{1 - \gamma_f}{-\ln(q*)} = c \cdot \sqrt{0.075 - s'_{m-1.0}} \tag{3.21}$$

In this equation c is the factor that differs for the heights of the elements. For c the following dimensionless relation is found, $c = 0.13(h_{protrusion}/h_{reference})^{0.25}$. The reference height is assumed to be 0.20 meter, because this height starts to make a relevant difference in the reduction of the wave overtopping.

Another result is the reduced effect of the protrusion height below the water level for high wave steepness conditions. In particular the upper part is determining the roughness of the slope.

Roughness width and roughness density
Not only the location of the roughness pattern is of importance, also the size of the front face area that is exposed to wave run-up is important. The exposed area is expressed in the roughness density parameter. The definition of the roughness density parameter is: "the total exposed area of all protruding elements from the waterline to the crest level, divided by the width and length of the slope". The roughness width ($\gamma_{f,w}$) is the length of roughness elements per meter dike length.

$$\rho_{\gamma f} = \frac{\gamma_{f,w} \cdot sin(\alpha) \cdot h_{prot}}{R_c} \tag{3.22}$$

Equation 3.22 is a dimensionless parameter, including the effect of the protrusion. So, the need of the reference protrusion is gone in the final equation as showed in equation 3.21.

Run-up
For smaller amounts of overtopping the layer thickness of the overflowing water might be smaller than the protrusion of the ribs. In the roughness density equation, equation 3.22, only the effective height of the ribs should be taken into account. The effective height of the wave run-up at different locations on the slope can be determined based on Schüttrumpf and Oumeraci (2005). The effective height is indicated in figure 3.11 with the yellow arrows.
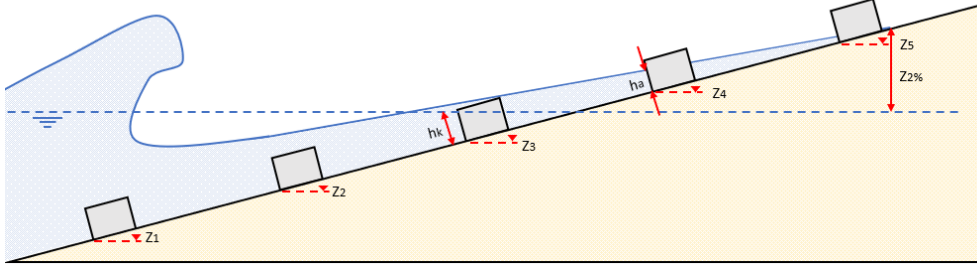
Figure 3.11: Effective protrusion of ribs by run-up

$$h_a(z) = 0.216 \cdot (Ru_2\% - z) \tag{3.23}$$

$$R_{u2\%} = 3.45 \cdot \tanh(0.65 \cdot \xi_{m-1,0}) \cdot \gamma_b \cdot \gamma_f \cdot H_s \tag{3.24}$$

So if the height of the ribs is larger than the thickness of the layer of water that runs up, the effective height consists only of the area that is in touch with the water. Also the ribs that are located further than the 2% wave run-up are not taken into account.

Roughness coefficient and overtopping equations
The research of Capel (2015) resulted in a new equation to assess the roughness coefficient for special rib patterns on the revetment of the upper slope and in an equation for the wave overtopping.

$$\gamma_f = 1 - (0.585 \cdot \sqrt{0.075 - s'_{m-1,0}} \cdot \rho_{\gamma f}^{0.5} \cdot (6.9 \cdot \frac{Rc}{R_{u2\%}} - \ln(q_0)) \tag{3.25}$$

$$\frac{q}{\sqrt{g \cdot H_s^3}} = \frac{0.027}{\sqrt{\tan(\alpha)}} \cdot \xi_{m-1,0} \cdot \exp(-6.5 \cdot \frac{R_c}{3.45 \cdot \tanh(0.65 \cdot \xi_{m-1,0}) \gamma_f \cdot H_s}) \tag{3.26}$$

The validity of these equations can not be guaranteed outside the tested range as given in table 3.5.

Table 3.5: Tested range Capel (2015)

Parameter	Small scale (1:22)	Large scale (1:11)
H_{m0}/h [-]	0.04-0.25	0.08-0.25
$s_{m-1,0} = H_{m0}/L_{m0}$ [-]	1.8%-5.0%	0.7%-5.9%
$s'_{m-1,0}$ [-]	1.8%-5.2%	1.3%-6.0%
kh [-]	1.0-5.3	0.5-4.0
$\xi_{m-1,0}$ [-]	1.1-2.5	0.9-2.2
R_c/H_{m0} [-]	1.2-2.7	0.07-0.2
q [l/m/s]	0.5-10/40	0.1-0.5
$\tan\alpha$ [-]	1:3-1:4	1:4-1:6
$\rho_{\gamma f}$ [-]	0.012-0.094	0.015-0.051

3.4. Predicting wave overtopping

3.4.1. Definition wave overtopping

Wave overtopping occurs if incoming waves break on the slope of the dike and the wave front runs up. If the run-up level is higher than the crest level, overtopping takes place. Two types of overtoppping can be distinguished, green water and white water. Green water is the type of overtopping that large sheets of water run over the crest of the dike. White water is also called spray overtopping, this tends to occur when waves break seaward of the structure. This results in non-continuous amounts of overtopping.

Because wave overtopping is random in time, space and volume the magnitude of overtopping is averaged over 1000 waves and expressed in l/m/s. This averaging is based on the paper of Verhaeghe et al. (2008), it states that this parameter will be stable over a period of 1000 waves.

3.4.2. Prediction methods wave overtopping

Different methods are available to predict wave overtopping at structures. Every methods has its own strengths and weaknesses. The most common method is the empirical method. It relates the structural parameters and the wave conditions to the wave overtopping. Two other methods are based on wave overtopping measurements of field work and model tests gathered during the CLASH project. The first method uses the CLASH database, which describes all the model tests and field work cases by 31 parameters. The other method uses a Neural Network tool, which is trained on the CLASH database, to predict the wave overtopping discharge.

Another way to determine the wave overtopping for a structure is the use of a numerical model. Numerical models always imply simplifications of the overtopping process and are therefore limited to specific types of structures or wave conditions. However, the advantage is that these models run wave sequences and are able to give individual wave overtopping volumes. The last method is physical modelling. The prototype and the wave conditions are correctly scaled down. The physical model is often tested in a 2-dimensional wave flume. For more complex structures a 3-dimensional wave basin is used. Physical modelling is prone to scale effects and model effects.

In this research attention is paid to empirical methods and physical modelling. So these methods will be elaborated further below.

3.4.3. Empirical methods

Several studies have been executed in the past to find a method to estimate the overtopping discharge empirically. The first empirical equation that took irregular waves formulated in the paper of Owen (1980). Later Van der Meer (1998) describes the wave overtopping discharge based on breaking and non-breaking waves. These equations are later improved resulting in the overtopping discharge equations that can be found in EurOtop Manual (2018). Also, Capel (2015) based the form of his overtopping equation on the equation of Van der Meer (1998).

EurOtop Manual

The dutch guideline TAW by Van der Meer (2002) suggested to replace T_p by $T_{m-1,0}$ in the equation of Van der Meer (1998). The values of a_v and b_v are now replaced by respectively 0.067 and 4.75. This results in the wave overtopping equation as presented in EurOtop Manual (2007).

$$\frac{q}{\sqrt{gH_{mo}^3}} = \frac{0.067}{\sqrt{\tan(\alpha)}}\gamma_b\xi_{m-1,0}\exp(-4.75\frac{R_c}{H_{m0}}\frac{1}{\xi_{m-1,0}\gamma_b\gamma_f\gamma_\beta\gamma_v})$$ (3.27)

With a maximum of:

$$\frac{q}{\sqrt{gH_{mo}^3}} = 0.2\exp(-2.6\frac{R_c}{H_{m0}}\frac{1}{\gamma_f\gamma_\beta})$$ (3.28)

The equation in EurOtop Manual (2018) has coefficients that are slightly changed compared to the equation in EurOtop Manual (2007). Also a new coefficient c is added, which has a value of 1.3. The study of Van der Meer and Bruce (2013) stated that the previous equation overestimated the amount of overtopping. The change in coefficients improves the equation especially for situations with very low freeboards, $R_c/H_{mo}<0.5$. This results in the following equations.

$$\frac{q}{\sqrt{gH_{mo}^3}} = \frac{0.023}{\sqrt{\tan(\alpha)}}\gamma_b\xi_{m-1,0}\exp(-2.7\frac{R_c}{H_{m0}}\frac{1}{\xi_{m-1,0}\gamma_b\gamma_f\gamma_\beta\gamma_v})^{1.3}$$ (3.29)

With a maximum of:

$$\frac{q}{\sqrt{gH_{mo}^3}} = 0.09\exp(-1.5\frac{R_c}{H_{m0}}\frac{1}{\gamma_f\gamma_\beta})^{1.3}$$ (3.30)

Looking at figure 3.12 shows that the relative freeboard for the tested cases in both wave flumes is around 1. The difference between the two equations will become visible for low freeboards, Rc/Hm0 < 0.5. Since the differences between the two equations will be negligible for the tested range is chosen to use the most recent equation of the EurOtop Manual. To this method will be referred as EurOtop Manual (2018).
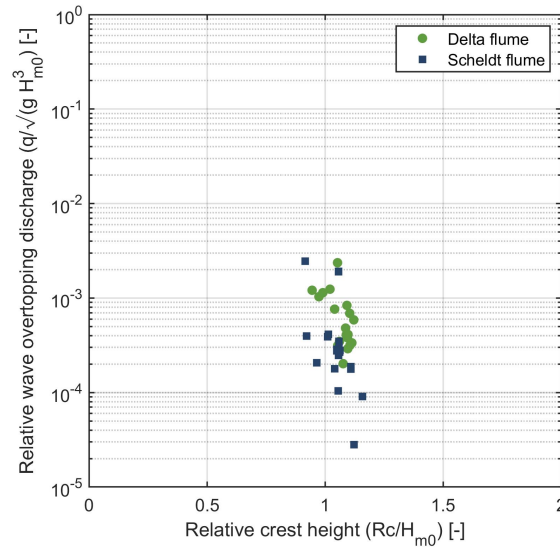
Figure 3.12: Relative free board and relative average wave overtopping discharge, based on the measured wave conditions at deep water and the measured average wave overtopping discharge

Capel (2015)

The study of Capel (2015) derived a slightly different equation to estimate the overtopping as the equation in the EurOtop Manual (2007). The study focused on the wave overtopping discharge and run-up reduction by the increased roughness caused by the ribs constructed in a block revetment. The equation is shown below, in section 3.3 a thorough explanation of the different parameters is given. This is the other method that will be used to predict the wave overtopping discharge. It can be used for both breaking and non-breaking waves.

$$\frac{q}{\sqrt{g \cdot H_s^3}} = \frac{0.027}{\sqrt{\tan(\alpha)}} \cdot \xi_{m-1,0} \cdot \exp(-6.5 \cdot \frac{R_c}{3.45 \cdot \tanh(0.65 \cdot \xi_{m-1,0}) \gamma_f \cdot H_s}) \tag{3.31}$$

3.4.4. Physical model tests

Another way to estimate the amount of wave overtopping is by executing physical tests. Those tests are most of the time executed on a smaller scale than the prototype, because of economical and practical reasons. The results of these tests might not give very accurate results of the wave overtopping discharge, due to scaling effects and model effects.

Scale effects

Scale effects occur when the applied scaling laws do not present the physical processes between the model and prototype accurately. A distinction between large scale model (> 1:10) and small scale models (< 1:10) is made in this report. Small scale tests may result in scale effects, because the interaction between the prototype structure and water can not be reproduced correctly on the model scale. Therefore it might be necessary to execute large scale model tests.Kirkegaard et al. (2011)

Between the prototype and the scale model there are three types of similarity.

- Geometric ($n_l = L_p / L_m$)
- Kinematic ($n_t = t_p / t_m$)
- Dynamic ($n_l = F_p / F_m$)

Geometric similarity of a model is given when all geometric lengths in the prototype have a constant relation to the corresponding lengths in the model. Kinematic similarity means that time dependent processes in the model have a constant relation to the processes in the prototype. Dynamic similarity means that the forces in the model have a constant relation to the processes in the prototype.

There are four scaling laws that are important for coastal structures, but these scaling rules can not be fulfilled at the same time.

- Froude - ratio between inertia and gravity
- Reynolds - ratio between inertia and viscosity
- Weber - ratio between inertia and surface tension
- Cauchy - ratio between inertia and elasticity

$$Fr = \frac{u}{\sqrt{g \times L}} \tag{3.32}$$

$$Re = \frac{u \times L}{v_k} \tag{3.33}$$

$$We = \frac{\rho_w \times u^2 \times L}{\sigma} \tag{3.34}$$

$$Ca = \frac{\rho_w \times u^2}{E} \tag{3.35}$$

The importance of each of these scaling laws depends on the force. Froude law is important for flows with a free surface. Reynolds scaling is important when viscous forces are dominant. Weber becomes important in case of air entrainment and breaking waves. Cauchy is important when elastic deformation of the structure is expected. In figure 3.13 is shown which scaling laws are important for the different flow regimes during the wave run-up on a rubble mound structure.
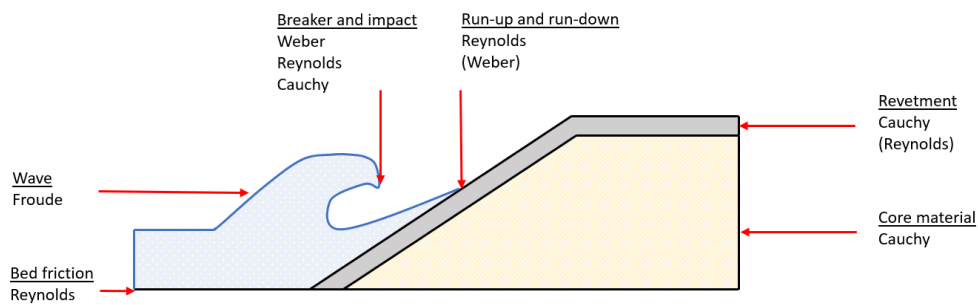

Figure 3.13: Characterisation of flow regimes during run-up on a rubble mound structure based on Kirkegaard et al. (2011)

There have been several studies about scale effects, combining the results of these studies led to a set of generic rules that should be applied for physical model studies. Water depths in the model should be larger than 2.0 centimeter, wave periods should be larger than 0.35 seconds, wave heights should be larger than 5.0 centimeter, the Reynolds number should be larger than 1000 for overtopping. The diameter of the core material should be scaled based on the velocities, not geometrically.

Table 3.6: Critical limits for processes related to run-up on a rubble mound structure, Schüttrumpf and Oumeraci (2005)

Process	Critical limits
Wave propagation	$Re_w > Re_{w,critical} = 1 \times 10^4$ $T > 0.35$ s $h > 2.0$ cm
Wave breaking	$Re_w > Re_{w,critical} = 1 \times 10^4$ $T > 0.35$ s $h > 2.0$ cm
Wave run-up	$Re_q > Re_{q,critical} = 1 \times 10^3$ $We > We_{critical} = 10$
Wave overtopping	$Re_q > Re_{q,critical} = 1 \times 10^3$ $We > We_{critical} = 10$ $q > 1$ l/m/s

Model effects

Model effects arise from an incorrect reproduction of the prototype. In this research model effects might occur between tests on large scale and small scale. Model effects in this study can be separated in two categories. The first category are the model effects related to the modelled waves and their generation. The second category are the model effects due to the modelled structure.

Model effects regarding the waves can occur due to differences in the boundary conditions and the generation of the waves. Also the measurements of the wave conditions can result in differences between the flumes. For the wave conditions the damping of the reflected waves is important in wave flumes.

The second category, model effects regarding the modelled structure might occur due to differences in the geometry and material properties. In case of wave overtopping discharge the friction of the material is important to model correctly between the different models.

4
Model setup

This chapter explains the setup of the wave overtopping tests executed in the wave flumes and the setup of the computational model to model waves. The first part considers the physical modelling. In this section information about the wave flumes, scaling parameters, modelled structure and measurements is given. Next, the setup and output of the computational wave model are explained. Here the link between the physical tests and the computational model is made.

4.1. Physical model

4.1.1. Test facilities

To test different designs of the Afsluitdijk regarding the wave overtopping discharge, tests are performed in two wave flumes. These wave flumes are located at Deltares and called Scheldt flume and Delta flume. They are respectively on scale 1:19.8 and 1:2.95. Both wave flumes make use of a piston-type spectral wavemaker. Other characteristics of these wave flumes are described in table 4.1.

Table 4.1: Comparison characteristics flume Van Gent (2017) Van Gent

Characteristics	Scheldt flume	Delta flume
Scale	1:19.8	1:2.95
Length	55 m	291 m
Width	1,0 m	5,0 m
Height	1,2	9,5
$H_{max,r}$	0.4 m	3.3 m
$H_{max,f}$	0.55 m	4.5 m
H_{m0}	0.25 m	2.2 m
Wave period	$0.5\,s < T < 100\,s$	$1\,s < T < 20\,s$
Active Reflection Compensation	✓	✓

In these wave flumes, various foreshores with different structures and wave conditions are tested. Figure 4.1 gives a schematic overview of the test setup. It should be mentioned that the slopes of the foreshore are in this schematization much steeper presented than is the case in reality. Table 4.4 gives the location and the number of installed wave gauges. The wave gauges are placed in a longitudinal direction and the distance between the wave gauges is not equally spaced. The different foreshores are shown in figure 4.5.

4.1.2. Modelled structure

The model setup and tested cross-sections are designed by Levvel. Figure 4.1 shows a schematization of the foreshore and structure that is constructed in the wave flume. Different foreshores are tested, but they all have the same geometry. Starting with a 1:10 slope, then a flat transition zone and the foreshore continues with a slope till the structure. Between the different foreshores, the height and length of the transition zone and the slope from the transition towards the structure vary.
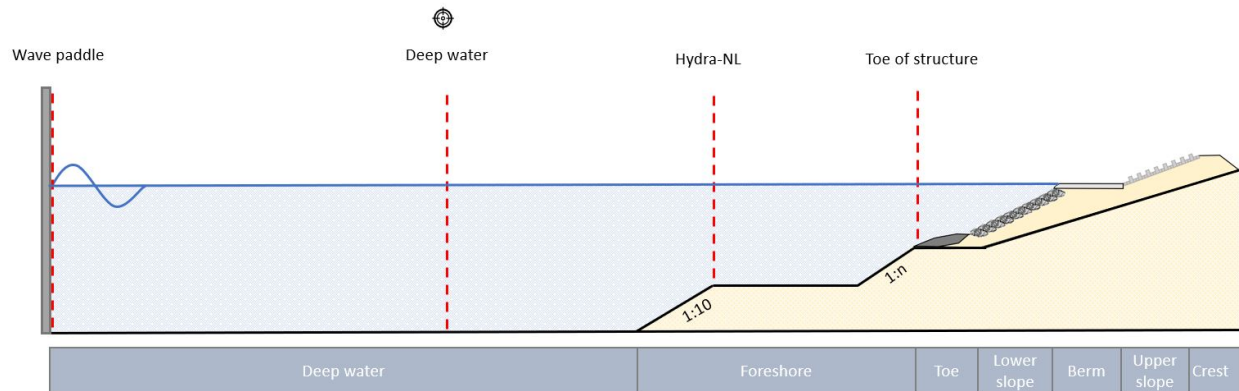
Figure 4.1: Schematization of the bottom profiles in the wave flume, not to scale

In figure 4.2 the modelled structure in the Delta flume and Scheldt flume is shown. Many variations are applied to the modelled structure to optimize the design. The table below gives an overview of the variations that can be applied to the different elements in the design. Between the different tests, in most cases more than one parameter is changed at the same time.

Figure 4.2: Modelled structure in Delta flume (left) and Scheldt flume (right)

Table 4.2: Possible parameters to vary in structures

Element	Possible variations
Toe	Height
Lower slope	Slope
	Type of elements
Berm	Width
	Height
Upper slope	Slope
	Length
	Number of ribs
	Height of ribs
	Configuration of ribs
Crest	Height

Model effects

In ideal test conditions, to be able to compare the results in wave overtopping between the Delta flume and Scheldt flume, both modelled structures should have the same material properties. However, looking at the elements of the modelled structure separately there are differences between the Delta flume and the Scheldt flume. These differences are causing model effects and might be the reason for the difference in wave overtopping between the different wave flumes.

Table 4.3: Comparison modelled structure

Element	Scheldt flume	Delta flume
Side walls flume	Glass	Concrete
Foreshore	Sand-cement	Sand-cement
Toe	Quarry run	Quarry run
Lower slope	Concrete Xbloc^{plus}	Concrete Xbloc^{plus}
Berm	Timber or PVC	Concrete
Upper slope	Milled PVC plate	Quattroblocks

The main differences in the structure can be found in the upper slope. In the Scheldt flume, the upper slope with ribs is modelled with a PVC plate with ribs milled in it. In the case of the Delta flume, the upper slope is modelled with Quattroblocks on a smaller scale. The main difference between these upper slopes is the open space that is present between the Quattroblocks in the Delta flume which is not present in the PVC plate. Also, the ribs in the Delta flume have rounded corners, where the ribs in the Scheldt flume are modelled as perfect rectangles. In figure 4.3 the left figure shows the ribs as modelled in the Delta flume and the right figure the ribs as modelled in the Scheldt flume.

Figure 4.3: Different shape of ribs in Delta flume (left) and Scheldt flume (right)

4.1.3. Scaling parameters

In the Scheldt flume and the Delta flume, the scaling law of Froud is applied. This means the ratio between inertia and gravity stays equal between the prototype and the model. According to this scaling law, the following hydraulic and structural parameters should be scaled as shown below.

$$n_L = \frac{L_{prototype}}{L_{model}} \tag{4.1}$$

Wave height H	$n_H = n_L$
Wave period T	$n_T = n_L^{0.5}$
Wave overtopping discharge q	$n_q = n_L^{1.5}$
Weight M	$n_M = n_L^3$
Time t	$n_t = n_L^{0.5}$
Leakage length Λ	$n_\Lambda = n_L$
Manning friction constant cf	$n_{cf} = n_L^{1/6}$

The toe of the structure is made of quarry rock. The toe armour is scaled down with the stability number. The quarried rock needs to be modelled 10% weaker since the density of rock can not be changed, the diameter is corrected.

The scaling of the Xbloc^{plus} in the Delta flume and Scheldt flume is based on the non-dimensional stability number as defined in equation 4.2. The relative density of the blocks is 10% lower than on the prototype scale. This is decided to reach a more conservative design.

$$N = \frac{H_s}{\Delta D_n} \tag{4.2}$$

The Quattroblocks in the structure in the Delta flume are also scaled-down concerning the stability number, as stated in equation 4.2. Here again, the density of the blocks is 10% lower than on the prototype scale. The Quattroblocks in the Scheldt flume are modelled as ribs in a PVC plate. These ribs are scaled-down geometrically, but the stability number is not taken into account during the downscaling.

The scaling of the filter layers in the Delta flume is based on the leakage length which is also a dimensionless number given by equation 4.3. In the Scheldt flume the filters are not scaled, but modelled with timber and sand-cement.

$$\Lambda = \sqrt{\frac{kbD}{k'}} \tag{4.3}$$

4.1.4. Test programs
Different types of tests are executed to assess the safety of the various designs. These different tests are executed to examine the wave overtopping discharge, the stability of the structure and the stability of the toe. This research focuses on the cases with reasonable overtopping. For this reason is decided to only take into account the cases with an average wave overtopping discharge of at least 1 l/m/s.

The wave paddle generates irregular waves according to the standard JONSWAP spectrum with a peak enhancement factor of 3.3. At deep water wave conditions are prescribed for the various test cases. The wave conditions that are prescribed are the peak period and the significant wave height. Also, the still water level is specified for the test cases.

4.1.5. Measurements
Wave conditions
To measure the wave conditions at fixed locations wave gauges are installed in the flumes. Table 4.4 gives an overview of the locations and the number of installed wave gauges. From the measurements of the wave gauges, the significant wave height, peak period and the spectral mean energy wave period are determined.

In the Delta flume, three wave gauges are installed at deep water. Later, when wave overtopping tests are performed, another set of three wave gauges is installed at the flat part of the foreshore. The majority of the tests in the Delta flume are executed with only wave gauges at deep water. In the Scheldt flume, two sets of four wave gauges are installed to measure the wave conditions at deep water and the flat part of the foreshore. The wave conditions at the Hydra-NL location are prescribed. To obtain these wave conditions, the wave conditions at the Hydra-NL location are calculated to deep water wave conditions using SWAN. The waves conditions generated by the wave paddle are adapted iteratively until the same wave conditions are measured at deep water as calculated in SWAN. The wave conditions at deep water are called the target wave conditions.

Table 4.4: Location wave gauges, distance from structure model scale

Flume	Bottom profile	Deep water [m]				Foreshore [m]			
Delta	All	131.4	128.4	122.4	-	20.6	12.8	11.2	-
Scheldt	6b-179	14.1	13.5	13.1	12.8	3.8	1.8	1.4	1.2
	8a-179	14.1	13.5	13.1	12.8	3.1	1.8	1.4	1.2
	8b-208	14.1	13.5	13.1	12.8	2.6	1.8	1.4	1.2

Overtopping discharge

Also, the average wave overtopping discharge is measured. At the rear side of the cross-section of the dike an overtopping tank is installed. In this way, all the water that passes the crest of the dike will flow into the overtopping tank. The volume in the tank is measured. The overtopping tank is divided into two sections, so the amount of overtopping can be measured more accurately. If the amount of overtopping is larger than 8.5 l/m/s the first tank flows over in the second tank. The average wave overtopping discharge is calculated by dividing the total volume of water in the tank by the duration of the experiment. The individual wave overtopping volumes are not measured.

4.2. Computational model

4.2.1. Geometry

The geometry of the model setup between the wave flumes and SWASH is different regarding two aspects. The bottom profile in SWASH is longer, to prevent that non-linearities at the boundary occur in the area of interest. The other difference between the wave flume and the SWASH model is the absence of the structure in SWASH. The purpose is to determine the incoming wave conditions at the toe of the structure. To prevent the system from reflected waves the structure is removed and a sponge layer is added to absorb the wave energy. The remainder of the geometry corresponds to the applied bottom profiles in the flume experiment. A schematization of the geometry in SWASH can be seen in figure 4.4.
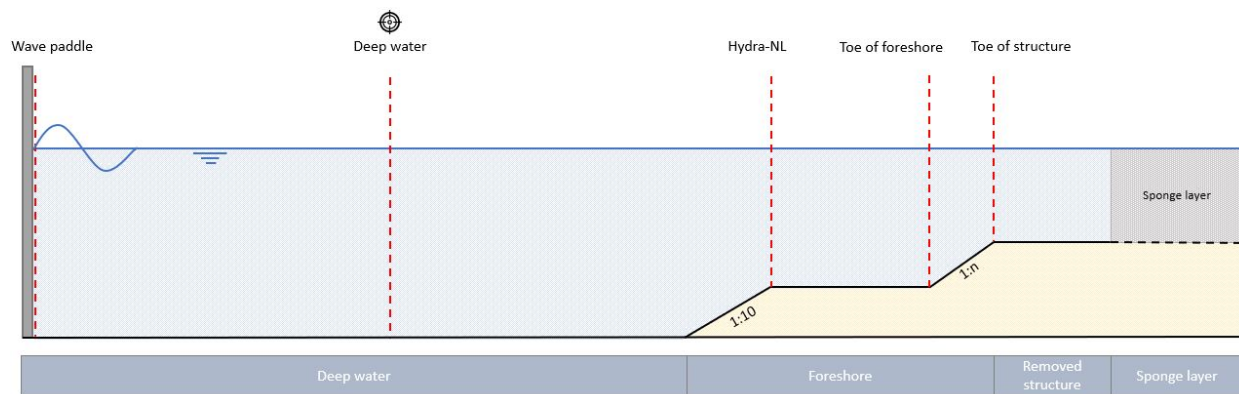
Figure 4.4: Geometry of SWASH model, not to scale

4.2.2. Output

SWASH has two options to return the output of the simulation. The 'block' option, which returns a parameter over the entire spatial domain. Here is decided to return the surface elevation, water depth and the significant wave height. The other option is the 'table' option. This option returns the surface elevation and the water depth for chosen output locations. These output locations are at the same position as the wave gauges in the wave flume, with respect to the toe of the structure. There are also other variables that can be returned as the output on these locations. The exact output locations for the different bottoms profiles are shown in table 4.4.

Based on the output information it is possible to determine the following parameters:

- Significant wave height [m]
- Two percent highest waves [m]
- Peak wave period [s]
- Spectral mean wave energy period [s]

In Appendix A it is explained how the data is processed to obtain the results of the wave conditions in section 5.2.

4.2.3. Scaling

The simulations are scaled with the Froude law. Since different parameters are important between the physical test and the computational tests. The following parameters are scaled as shown below.

Wave height H $\quad n_H = n_L$
Wave period T $\quad n_T = n_L^{0.5}$
Test duration t $\quad n_t = n_L^{0.5}$

To attain the same accuracy between the different scales the following parameters are scaled as well. The amount is kept constant.

- Time step
- Grid size

The Manning friction constant between the two scales is kept at the same value of 0.018. Since it is expected that this value corresponds best to the characteristics of both flumes.

4.2.4. Test programs

To simulate the tests from the wave flumes as accurately as possible in SWASH, the model is calibrated at the same target conditions at deep water as in the wave flume. Although, not the exact same wave signal can be imposed at the wave generating boundary in SWASH, presumed is that the wave conditions correspond to those in the wave flume. This is assumed since the JONSWAP spectrum with a peak enhancement factor of 3.3 is applied. This generates an irregular wave field, the paper of Verhaeghe et al. (2008) supports that wave conditions over 1000 waves are constant. This corresponds to a test duration of approximately two hours on the prototype scale.

The separate runs in SWASH that are performed are based on the scale, foreshore, still water level and target significant wave height and peak period at deep water. The results of the executed runs are shown in table 5.1.
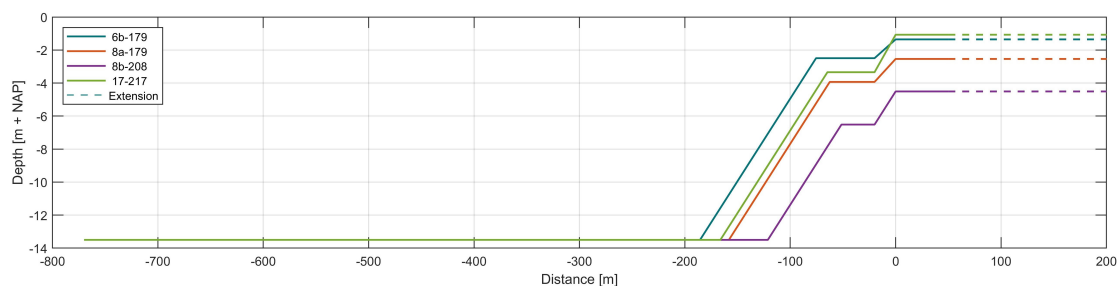
Figure 4.5: Different tested foreshores, prototype scale

Results and analysis: Computational wave model

In this chapter, the results of the wave model in SWASH are presented. The wave conditions from the wave flumes and the wave model in SWASH are compared to the target conditions to verify the calibration of the model. Also, the results of the wave model in SWASH are compared to the measurements in the wave flumes to validate the wave model. Furthermore, the evolution of the wave conditions from deep water to the toe of the structure is considered.

5.1. Calibration and validation wave model

To calibrate the wave model in SWASH the target conditions at deep water should be met. The calibration method of the model is described in Appendix A. The prescribed target conditions at deep water are the peak period and the significant wave height. In the figures below the dots indicate the measurements in the wave flume and the stars indicate the results from SWASH. From these results can be seen that SWASH is capable of reproducing the target wave conditions at deep water within the same accuracy as the wave flume.
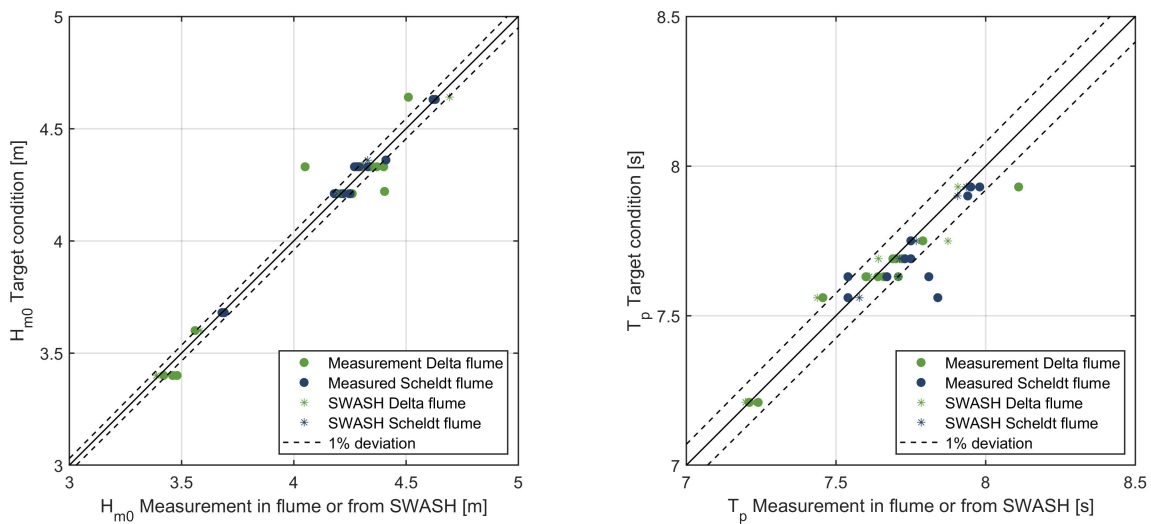
Figure 5.1: Calibration of H_{m0} and T_p on deep water

To see if SWASH correctly reproduces the wave processes using the target conditions at deep water, the measurements taken by the wave gauges in the wave flume at the foreshore can be compared to the results gathered from SWASH at the foreshore. For this reason, only the test cases from the wave flume with wave gauges on the foreshore are involved. Not all the test cases of the Delta flume are taken into account, because in the Delta flume only during a small number of tests wave gauges were installed at the foreshore. This gives the results as shown in the figure below.
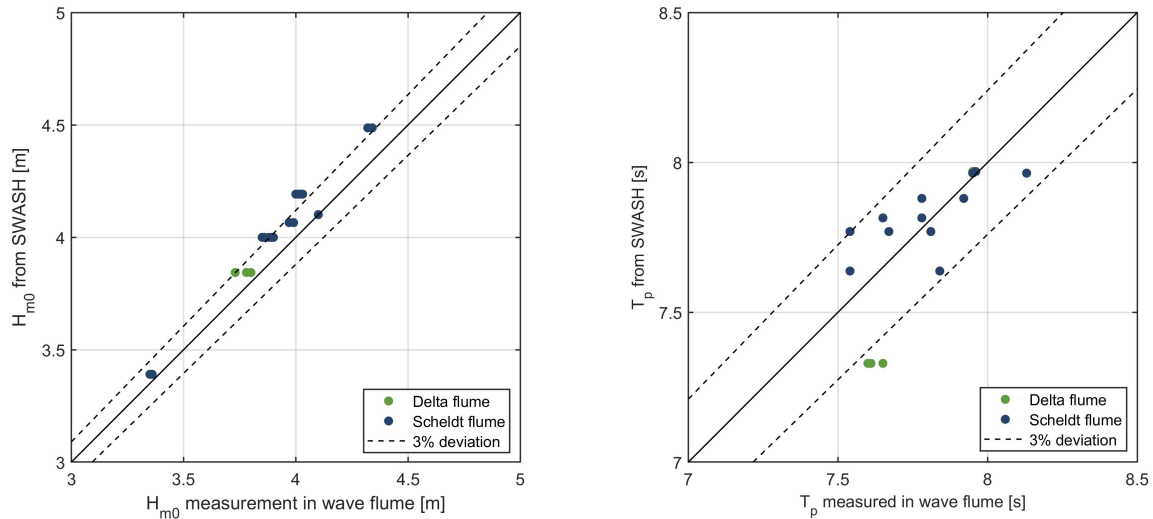
Figure 5.2: Validation of H_{m0} and T_p on the foreshore

From the results in figure 5.2 it can be seen that SWASH is able to predict the significant wave height with a deviation of approximately 3% and the peak period with a deviation of also 3%. The deviation of 3% in the peak period can be accounted to the spectral resolution of 0.02 Hz, which might cause the peak to 'jump' to another frequency. To decrease this effect the peak frequency is already smoothed, but that can not entirely eliminate this effect.

To check if the wave conditions provided by SWASH can be used as the incident wave conditions the method of Zelt and Skjelbreia (1992) is used to separate the total wave height in the reflected wave height and the incoming wave height. The results show a reflection coefficient of 7% to 8%, despite the sponge layer. In terms of energy, this affects the significant wave height by only 1% and is considered to be insignificant. During the rest of the research it will be assumed that total wave height is equal to the incoming wave height. In Appendix A an example of the total wave height, reflected wave height and the incident wave height are presented.

5.2. Wave conditions

As elaborated in the problem statement, section 1.2, for the most of the tests in the Delta flume only data of the wave conditions at deep water are available. In the Scheldt flume data of the wave conditions at deep water and at the flat part of the foreshore are available. The exact locations of the wave gauges in both flumes are given in table 4.4.

To get more insight into the wave conditions the structure is exposed to, the wave model in SWASH is used. From this model the significant wave height, the peak period and the spectral mean wave energy period, respectively H_{m0}, T_p and $T_{m-1,0}$ are determined based on the energy density spectrum. Also, the height of the two percent highest waves is calculated, $H_{2\%}$. This value is derived from the time domain analysis. The complete analysis of the individual tests can be found in Appendix B. Here the significant wave height over the length of the flume, the Rayleigh distribution and the frequency energy density spectrum are shown for every test. The analysis of the tests results in the following wave conditions.

5.2.1. Wave height

H_{m0}

The significant wave height shows a slight, linear decrease over the spatial domain as can be seen in figure 5.3. This decrease is most likely caused by bottom friction and breaking of waves. The significant wave height decreases from deep water to the toe of the structure with approximately 5%, as showed in figure 5.4. However, a decreasing water depth on the foreshore causes an even further decrease in the significant wave height. These are the markers below the dashed line of 5% deviation in the left figure of figure 5.4. These markers correspond among others to bottom profiles 6b-179 and 8a-179. The other markers from the Scheldt flume correspond to bottom profile 8b-208. Bottom profile 17-217 is also very shallow and only tested in the Delta flume.

The results of this dike section are the three green squares with the lowest significant wave height. Despite, bottom profile 17-217 is the shallowest foreshore, it does not show the largest decrease in significant wave height. This indicates that the relation between h/H_{m0} is an important parameter for the decrease in the significant wave height. The decrease in energy between deep water and the toe of the structure for the dike sections is also visible in the frequency energy density spectrum in the left figure of figure 5.6, the full results are shown in Appendix B. Bottom profile 8b-208, results in a smaller decrease in significant wave height, due to the larger water depth.
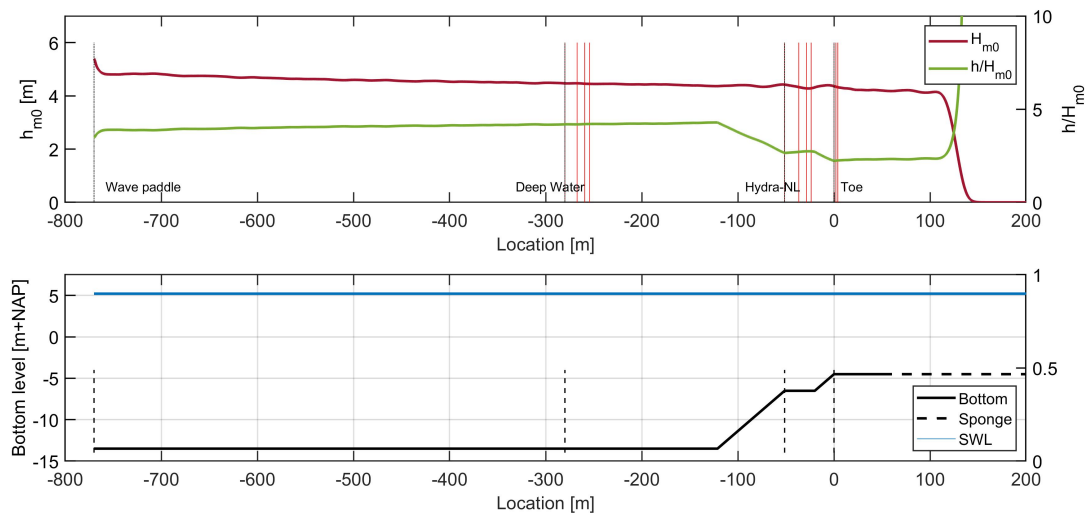
Figure 5.3: Example of variations in significant wave height, wave gauges are indicated by the vertical red lines.

From a relative depth of $h/H_{m0} \approx 3$, variations in the significant wave height occur. An example of these variations is shown in figure 5.3. A list of the various possible causes for these variations is given below. These causes are discussed in section 7.1, but none of these seems to cause this variation in significant wave height. Examples of significant wave height over the spatial domain can be found in Appendix B. The amplitude of these variations can be up to 5% of the total significant wave height. Possible reasons are for the variations are:

- Reflection of primary waves
- Seiches
- Trapped infragravity waves
- Shoaling and breaking

$H_{2\%}$

Although the significant wave height is not decreasing substantially, the decrease of the highest waves over the spatial domain becomes very clear for bottom profiles with small water depth. An example of the decrease in the two percent highest waves is given in Appendix A. Here first an increase is visible in the two percent highest waves. This increase might be caused by shoaling. When the waves enter shallower water the highest waves start breaking. This is caused by depth induced wave breaking. The breaking of these waves is very important since the overtopping is generally caused by the few highest waves.

The right figure in figure 5.4 shows the relation between the two percent highest waves at deep water and at the toe of the structure. Here a similar pattern is visible as in the significant wave height. A stronger decrease in the two percent highest waves for the shallower bottom profiles, 6b-179 and 8a-179 can be distinguished. Again the wave height of bottom profile 17-217 decreases between deep water and the toe of the structure with approximately 5%. These are the three lower squares in figure 5.4. The other markers that do not show a decrease at the toe or are even slightly larger than the two percent highest waves at deep water all correspond to dike section 8b-208. Also, here it can be seen that the ratio between water depth and wave height is an important parameter for the wave height.
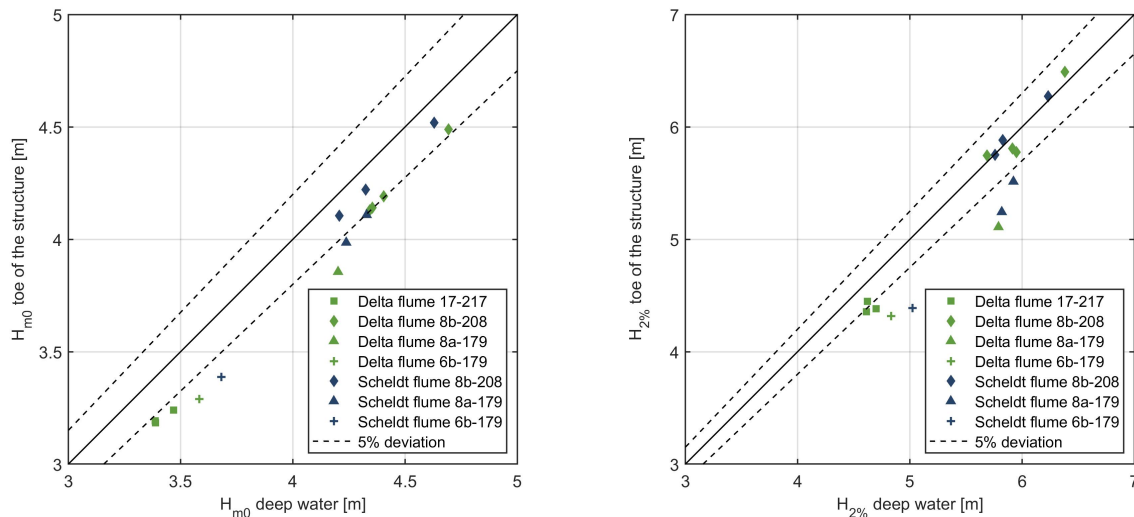
Figure 5.4: Change in wave height between deep water and toe of the structure

$H_{2\%}/H_{m0}$

The wave height distribution does not follow a Rayleigh distribution anymore for some of the cases. The highest waves are breaking and the relation between $H_{2\%}/H_{m0}$ is not 1.4 anymore but is around 1.3. A clear example of this is presented in the right graph of figure 5.6, which belongs to dike section 6b-179.

5.2.2. Wave period

T_p

The peak period shows in some cases small variations. These variations occur due to the chosen settings of the energy density spectrum and not to physical processes. The accuracy of the peak period depends on the duration of the tests and the frequency resolution.

$T_{m-1,0}$

The frequency energy density spectrum shows that energy is redistributed from the peak frequency to lower and higher frequencies at shallower water. From the left figure in figure 5.6 can be seen that a secondary peak occurs at twice the peak frequency. Which happens due to triad wave-wave interaction. The redistribution of energy affects the spectral mean wave energy period. Since this period gives more weight to the lower frequencies and thus the longer wave periods, the spectral mean wave energy period approaches or becomes even larger than the peak period in shallow water. For the integration of the frequency energy density the lower limit is chosen as 1/5th of the peak frequency and the upper limit is 3 times the peak frequency. This parameter is very important in the overtopping calculation because it determines among others the breaker parameter and the local steepness of the waves.

For a single-peaked spectrum, like the JONSWAP spectrum, $T_{m-1,0}$ is often estimated from the peak period at deep water. The ratio between $T_p/T_{m-1,0} = 1.1$ is often assumed to be constant. Looking at figure 5.5 it can be seen that at deep water $T_p/T_{m-1,0} \approx 1.05$. At the toe of the structure, the relation between $T_p/T_{m-1,0}$ differs for the different test cases. These differences occur because of the water depth. For some test conditions with bottom profile 8b-208 and 17-217, $T_p/T_{m-1,0} \approx 1$.
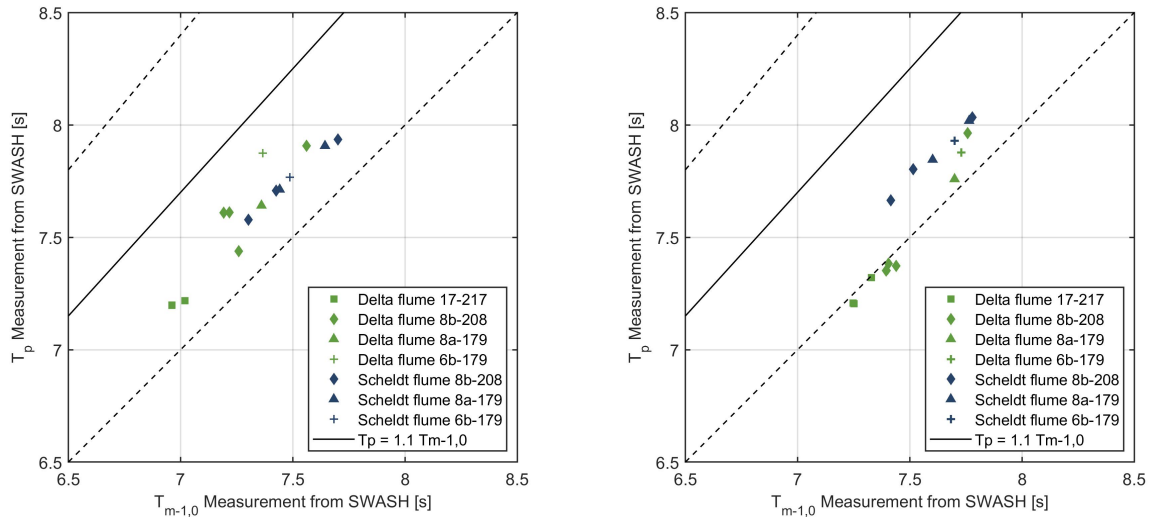
Figure 5.5: Relation between T_p and $T_{m-1,0}$ for deep water (left) and toe of the structure (right)
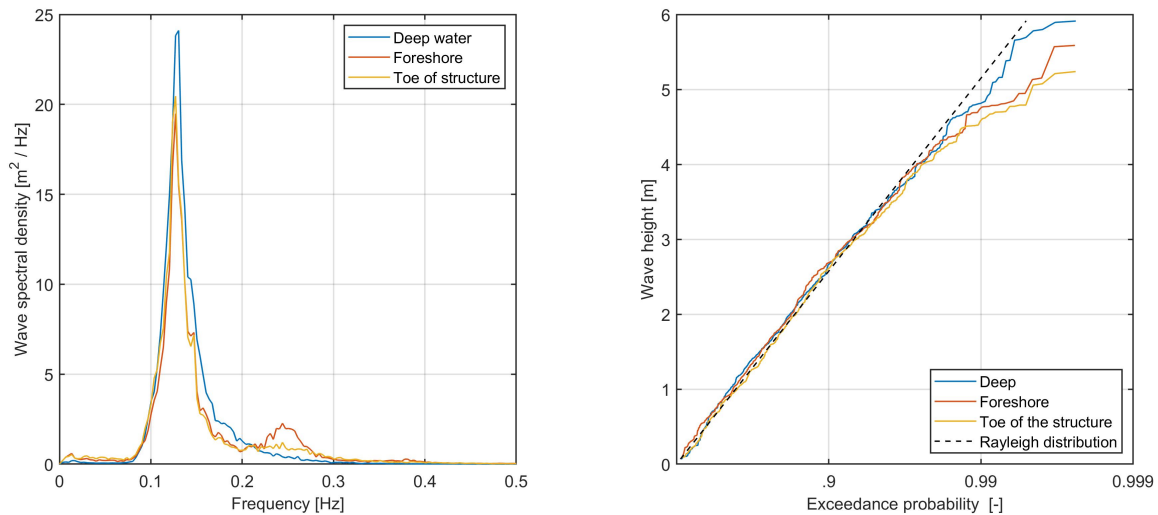
Figure 5.6: Differences between deep water, foreshore and toe of the structure from bottom profile 6b-179. Left figure shows the energy density spectrum the right figure shows the exceedance probability of the incoming wave height in SWASH.

5.3. Conclusion wave conditions

SWASH is capable in reproducing the target wave conditions within a 1% deviation at deep water, based on the target peak period and the target significant wave height. The results of SWASH are validated based on the measurements in the wave flume at the foreshore. This proves that SWASH can reproduce the wave conditions quite accurately. The deviation between the results of the wave flume and the wave model is approximately 3%. Also, the reflection of the waves by the foreshore in the wave model is examined. However, this effect seems negligible. Based on this validation it is decided that the wave results from SWASH can be used as the incident waves during the research. The wave conditions in table 5.1 are used as a starting point for the next chapter.

From the results of SWASH can be concluded that the water depth is an important parameter for the wave conditions. It affects both the significant wave height and the two percent highest waves. The relation between the significant wave height and the two percent highest waves is not 1.4 anymore in some of the cases. This indicates that the waves are not in deep water anymore when they approach the structure. Notable is the stronger decrease of the significant wave height than the decrease of the two percent highest waves at the toe in some cases.

Currently, the variations in the significant wave height can not be explained. This results in an uncertainty of the significant wave height. The uncertainty is equal to the amplitude of the variation in the significant wave height, which is approximately 5% of the significant wave height.

The spectral mean wave energy period becomes larger and approaches the peak period for shallow water. A possible reason for this is triad wave-wave interaction redistributing the wave energy to lower frequencies. This also indicates that deep water conditions are no longer valid at the toe of the structure. Resulting in changes in the wavelength and wave steepness.

Table 5.1: Results wave conditions at different locations from SWASH

Flume	Dike section	SWL	Target deep		SWASH deep				SWASH Hydra-NL				SWASH toe			
			H_{m0}	T_p	H_{m0}	$H_{2\%}$	T_p	$T_{m-1,0}$	H_{m0}	$H_{2\%}$	T_p	$T_{m-1,0}$	H_{m0}	$H_{2\%}$	T_p	$T_{m-1,0}$
		[m+NAP]	[m]	[s]	[m]	[m]	[s]	[s]	[m]	[m]	[s]	[s]	[m]	[m]	[s]	[s]
Scheldt	6b-179	5.13	3.68	7.75	3.68	5.02	7.77	7.49	3.39	4.67	7.88	7.35	3.39	4.39	7.93	7.70
Scheldt	8a-179	5.57	4.36	7.90	4.33	5.92	7.91	7.64	4.10	5.81	7.97	7.53	4.11	5.51	8.02	7.76
Scheldt	8a-179	5.13	4.21	7.56	4.24	5.82	7.71	7.44	4.00	5.59	7.81	7.34	3.99	5.24	7.85	7.60
Scheldt	8b-208	5.07	4.21	7.56	4.21	5.76	7.58	7.30	4.07	5.76	7.64	7.30	4.10	5.75	7.66	7.41
Scheldt	8b-208	5.21	4.33	7.63	4.32	5.83	7.71	7.43	4.19	5.98	7.77	7.42	4.22	5.88	7.80	7.52
Scheldt	8b-208	5.07	4.63	7.93	4.63	6.23	7.93	7.70	4.49	6.49	7.96	7.65	4.52	6.27	8.03	7.78
Delta	8b-208	5.59	4.22	7.56	4.20	5.69	7.52	7.20	4.02	5.83	7.47	7.30	4.01	5.75	7.38	7.40
Delta	8b-208	5.30	4.33	7.63	4.34	5.95	7.61	7.19	4.16	6.02	7.33	7.28	4.13	5.77	7.35	7.39
Delta	8b-208	5.61	4.64	7.93	4.69	6.38	7.91	7.56	4.51	6.43	7.97	7.61	4.49	6.43	7.96	7.76
Delta	8b-208	5.22	4.33	7.63	4.35	5.91	7.61	7.22	4.14	6.07	7.47	7.30	4.14	5.81	7.37	7.44
Delta	17-217	5.47	3.40	7.21	3.39	4.62	7.20	6.96	3.28	4.96	7.21	6.99	3.19	4.45	7.21	7.25
Delta	17-217	5.20	3.40	7.21	3.47	4.70	7.22	7.02	3.33	4.98	7.27	7.05	3.24	4.38	7.32	7.33
Delta	17-217	5.32	3.40	7.21	3.39	4.61	7.20	6.96	3.27	4.93	7.21	6.99	3.18	4.36	7.20	7.25
Delta	6b-179	5.12	3.60	7.75	3.58	4.83	7.87	7.37	3.32	4.68	7.87	7.36	3.29	4.32	7.88	7.73
Delta	8a-179	5.13	4.21	7.69	4.15	5.62	7.45	7.14	3.84	5.22	7.33	7.24	3.75	4.96	7.35	7.47

Results and analysis: Overtopping

In this chapter, the results of the overtopping tests are analyzed. Particularly the effect of the enhanced roughness due to ribs on the wave overtopping is investigated. First, the parameters that influence the wave overtopping discharge are considered. Then the theory of Capel (2015) and EurOtop Manual (2018) are used to predict the wave overtopping discharge. These values are compared to the measured wave overtopping discharge from the wave flumes. Afterward, methods to predict the wave overtopping more accurately are investigated. This information will be used to adjust the empirical relation to predict wave overtopping more accurate. Then possible scale and model effects are investigated. Finally, the uncertainty and sensitivity of the equation including several adjustments are calculated.

6.1. Mechanisms influencing overtopping

To assess the effect of different structural parameters on the wave overtopping discharge, test cases with the same hydraulic loading and the same structural parameters, except for one structural parameter, are compared. The parameters of the compared cases are shown in table 6.2. Based on the Test-ID the different considered cases can be distinguished. In figure 6.2 to figure 6.5, two compared cases are indicated with a colored line. This does not show the relation between the considered parameter and the average wave overtopping discharge.

6.1.1. Water depth at toe of the structure

Chapter 5 showed that the significant wave height and the two percent highest waves at the toe of the structure deviate from the wave conditions at deep water. In the Rayleigh distribution, which corresponds to deep water conditions, the relation between the significant wave height and the two percent highest waves is 1.4. However, at shallow water conditions this relation changes. In the left figure of figure 6.1, the effect of the relative water depth at the toe of the structure on the relation between the significant wave height and the two percent highest waves is shown. A flattened Rayleigh distribution will result in a lower average wave overtopping discharge, because the highest waves are reduced in wave height and thus the overtopping volume per wave is smaller. Also, the relation between the peak period and spectral mean wave energy period is smaller than 1.1. The increase of the wave period results in longer waves.
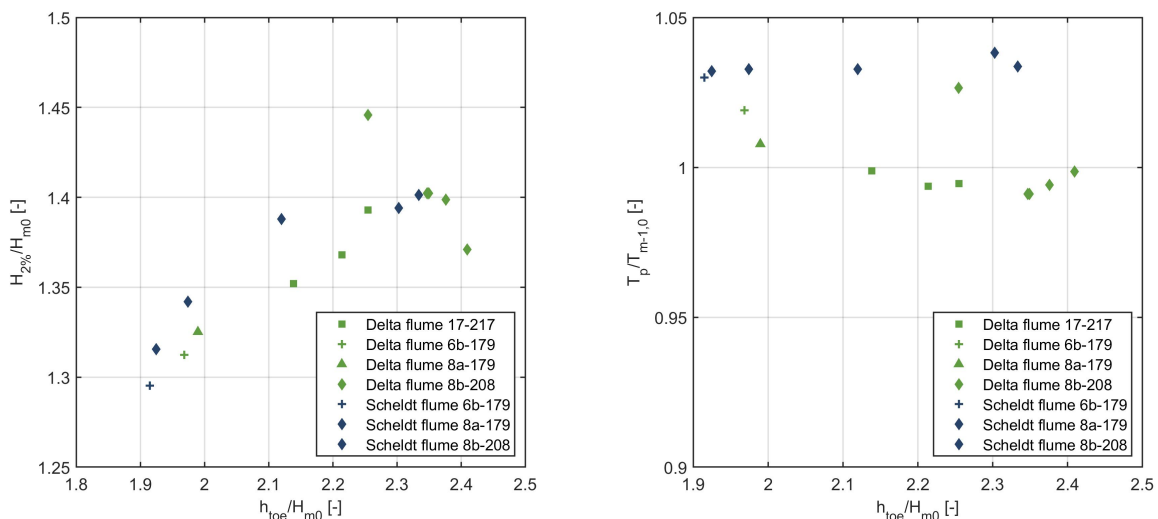
Figure 6.1: Effect of relative water depth at the toe on the wave conditions

6.1.2. Berm width

The berm width is one of the parameters that reduces the wave overtopping discharge, according to the studies of Ahrens and Ward (1991) and Van der Meer and Janssen (1994). To show the effect of the berm width on the reduction of the wave overtopping discharge, test cases that are loaded hydraulic equally and with the same structural parameters, except the berm width, are compared. In this way, the berm is isolated from all the other factors that might affect the wave overtopping. In figure 6.2 the comparable cases are plotted. Looking at the results in figure 6.2 confirms that the width of the berm influences the wave overtopping discharge. An increase in berm width results in a reduction of the wave overtopping discharge.
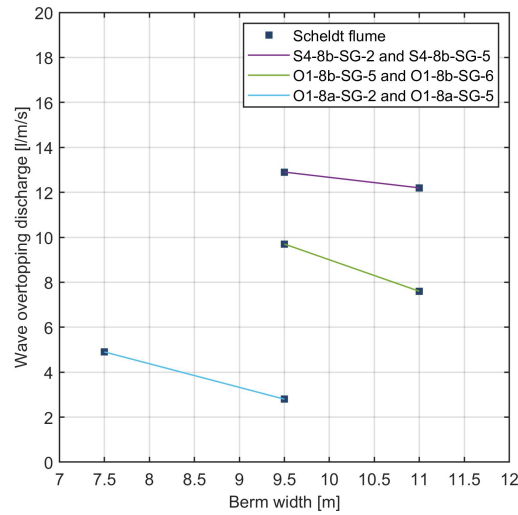
Figure 6.2: Effect of increasing berm width on the overtopping discharge

If the roughness influence factor between two test cases is kept constant, the behaviour of equation 3.11 can be verified. From the comparison in table 6.1, it is visible that this works quite well.

Test ID	$\gamma_{berm\ fit}$	$\gamma_{berm\ calculated}$
S4-8b-SG-2	0.71	0.71
S4-8b-SG-2	0.74	0.72
O1-8b-SG-5	0.69	0.71
O1-8b-SG-6	0.72	0.74
O1-8a-SG-2	0.72	0.73
O1-8a-SG-5	0.76	0.79

Table 6.1: Fitted gamma berm and calculated gamma berm

6.1.3. Ribs on upper slope

There are various options to change the configuration of the ribs on the upper slope. To express the effect of different modifications of the rib profile on the wave overtopping discharge, other structural and hydraulic parameters will be constant. Variations in the following parameters that will be considered are:

- Presence of ribs
- Exposed area of ribs
- Protrusion of ribs
- Density of ribs

Presence of ribs

From figure 6.3 it becomes clear that constructing ribs on the upper slope of a dike is a very effective method to decrease the wave overtopping discharge. In this graph no characteristics of the ribs are taken into account, only the presence of ribs on the upper slope is considered.
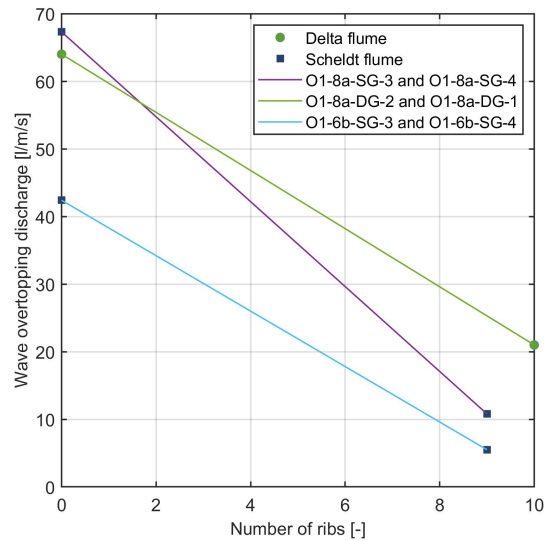
Figure 6.3: Effect of ribs on the wave overtopping discharge

Exposed area of ribs

From figure 6.3 can be concluded that the presence of ribs reduces the wave overtopping discharge. Now other parameters will be investigated. First, the exposed area of the ribs is considered. The exposed area of the ribs is described as the area of the ribs per meter dike length. This is calculated by multiplying the number of ribs times the protrusion of the ribs times the density of the ribs.
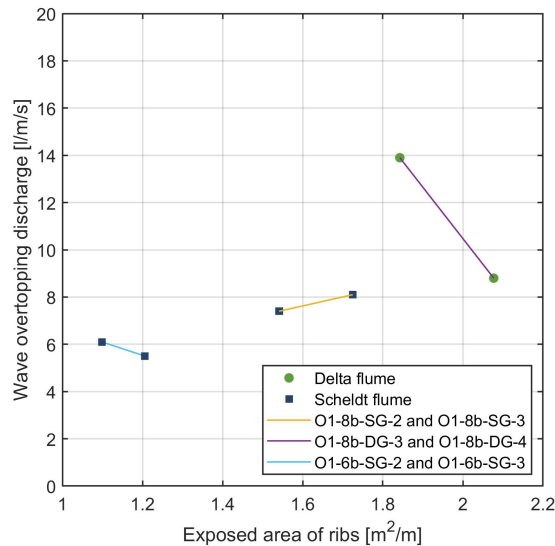
Figure 6.4: Influence wave overtopping discharge by exposed area of ribs

From figure 6.4 there is no clear trend visible between the exposed area of ribs and the wave overtopping discharge. Therefore other characteristics of the ribs will be investigated. The influence of the protrusion, the number of ribs and the density of the ribs on the wave overtopping discharge will be treated one by one.

Protrusion of ribs

One of the main parameters of the ribs is the protrusion. In figure 6.5 the relation between rib height and the average wave overtopping discharge becomes clear. Increasing the rib height reduces the wave overtopping discharge significantly. From table 6.2 can be seen that the crest height for case O1-8b-DG-4, with a protrusion of 0.28 meter, has a slightly lower crest height than case O1-8b-DG-3. The difference in crest height between the two cases is 0.05 meter. Nevertheless, the wave overtopping discharge is still significantly smaller. For case O1-6b-SG-2 and O1-6b-SG-3 this is the other way around, the case with a higher protrusion also has a larger crest height. The difference in crest height is 0.04 meter. The case with a larger protrusion also results here in a slightly smaller average wave overtopping discharge.
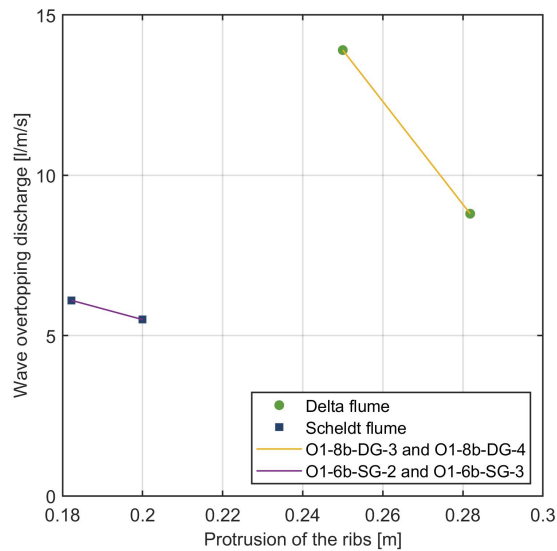
Figure 6.5: Effect protrusion of ribs on the average wave overtopping discharge

Density of the ribs

The dataset does not contain cases where only the density of the ribs is varied. The density of the ribs is only varied in combination with the number of ribs. See the cases with Test-ID O1-8b-SG-2 and O1-8b-SG-3 in table 6.2 From this combination can be seen that a decrease in the number of ribs can be compensated by the density of the ribs. Based on this it is assumed that an increase in density of the ribs reduces the average wave overtopping and that an increase of the number of ribs reduces the average wave overtopping discharge as well.

Table 6.2: Structural and hydraulic parameters comparison tests

Comparison	Flume	Test-ID	q [l/m/s]	H_{m0} at toe [m]	T_p at toe [s]	$T_{m-1,0}$ at toe [s]	SWL [m+NAP]	Toe height [m+NAP]	Berm height [m+NAP]	Crest height [m+NAP]	Berm width [m]	α lower slope [-]	α upper slope [-]	Number of ribs [-]	Protrusion ribs [m]	Density ribs [-]
Berm width	Scheldt	S4-8b-SG-2	12.2	4.52	8.03	7.78	5.07	-0.55	5.20	9.75	11.0	2.0	4.0	10	0.25	0.67
	Scheldt	S4-8b-SG-5	12.9	4.52	8.03	7.78	5.07	-0.55	5.20	9.75	9.5	2.0	4.0	10	0.25	0.67
	Scheldt	O1-8b-SG-5	7.6	4.15	7.80	7.52	5.21	-0.55	5.20	9.75	11.0	2.0	4.0	10	0.25	0.67
	Scheldt	O1-8b-SG-6	9.7	4.15	7.80	7.52	5.21	-0.55	5.20	9.75	9.5	2.0	4.0	10	0.25	0.67
	Scheldt	O1-8a-SG-2	2.8	3.99	7.85	7.60	5.13	-0.25	5.20	9.55	9.5	2.0	4.0	10	0.26	0.76
	Scheldt	O1-8a-SG-5	4.9	3.99	7.85	7.60	5.13	-0.50	5.20	9.55	7.5	2.0	4.0	10	0.26	0.77
Rib parameters	Scheldt	O1-8a-SG-3	10.8	3.99	7.85	7.60	5.13	-0.25	5.20	9.02	9.5	2.0	4.0	9	0.26	0.78
	Scheldt	O1-8a-SG-4	67.3	3.99	7.85	7.60	5.13	-0.25	5.20	9.02	9.5	2.0	4.0	0	0.00	0.00
	Delta	O1-8a-DG-1	21.0	3.76	7.35	7.47	5.13	-0.46	5.20	9.56	7.5	2.0	4.0	10	0.20	0.67
	Delta	O1-8a-DG-2	64.0	3.76	7.35	7.47	5.13	-0.46	5.20	9.56	7.5	2.0	4.0	0	0.00	0.00
	Scheldt	O1-6b-SG-2	6.1	3.39	7.93	7.70	5.13	0.19	5.20	8.99	7.5	2.0	4.0	9	0.18	0.67
	Scheldt	O1-6b-SG-3	5.5	3.39	7.93	7.70	5.13	0.19	5.20	9.03	7.5	2.0	4.0	9	0.20	0.67
	Scheldt	O1-6b-SG-4	42.4	3.93	7.93	7.70	5.13	0.19	5.20	9.03	7.5	2.0	4.0	0	0.00	0.00
	Delta	O1-8b-DG-3	13.9	4.14	7.37	7.44	5.22	-0.80	5.20	10.00	9.5	2.0	4.0	11	0.25	0.67
	Delta	O1-8b-DG-4	8.8	4.14	7.37	7.44	5.21	-0.80	5.20	9.95	9.5	2.0	4.0	11	0.28	0.67
	Scheldt	O1-8b-SG-2	8.1	4.22	7.80	7.52	5.21	-0.89	5.20	9.75	12.0	2.0	4.0	15	0.23	0.50
	Scheldt	O1-8b-SG-3	7.4	4.22	7.80	7.52	5.21	-0.89	5.20	9.75	12.0	2.0	4.0	10	0.23	0.67
Uncertainty	Delta	O1-8b-DG-6	10.8	4.15	7.47	7.44	5.22	-0.80	5.20	9.98	9.5	2	4	11	0.23	0.67

6.2. Performance EurOtop Manual (2018) and Capel (2015)

In section 3.4 the methods of Capel (2015) and EurOtop Manual (2018) are described. Both theories explain how the average wave overtopping discharge can be predicted. They make use of different equations to predict the roughness influence factor of ribs, respectively equation 3.25 and equation 3.19 for Capel (2015) and EurOtop Manual (2018). To predict the average wave overtopping discharge equation 3.26. is used for Capel (2015) and equation 3.29 is used for EurOtop Manual (2018). For the area over which the roughness should be taken into account the lengths as given in table 3.4 are used. The combined influence factor for the structure is calculated with equation 3.16. The influence factor of the berm is calculated with equation 3.11.

6.2.1. Capel (2015)

In order to validate the performance of the method of Capel (2015) to predict the average wave overtopping discharge and estimate the roughness influence factor of the ribs on the upper slope based on the provided hydraulic conditions and structural parameters, the following approach is used. First, the wave overtopping discharge and the roughness influence factor are calculated according to the method of Capel (2015). The results of this calculation are indicated hereafter with respectively q_{theory} and $\gamma_{rib\,theory}$. The next step is to fit the roughness influence factor of the ribs on the upper slope in the equation of Capel (2015) until it meets the measured overtopping discharge. The parameters are called $\gamma_{rib,fit}$ and $q_{measured}$. This method enables the verification of the performance of the equation.
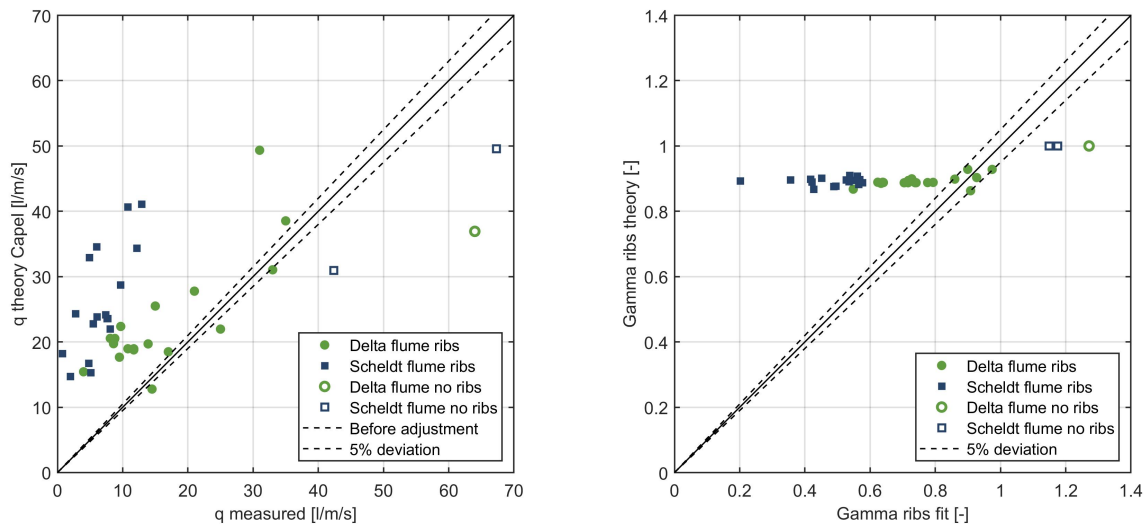
Figure 6.6: Comparison between theory and measurement of the overtopping discharge and the roughness of the upper slope based on the method of Capel (2015), using the wave conditions at the toe of the structure

Table 6.3: Root mean square error of the wave overtopping discharge and the roughness influence factor between the measured and the theoretical values using the method of Capel (2015)

Delta flume			Scheldt flume		
q	log(q)	γ_f	q	log(q)	γ_f
9.13	0.61	0.17	19.85	1.55	0.41

6.2.2. EurOtop Manual (2018)

To assess the performance of the method in EurOtop Manual (2018) to predict the wave overtopping discharge and the roughness of the ribs on the upper slope, the same method as above is followed. The roughness influence factor of the ribs is determined according to the method in EurOtop Manual (2018). Based on this value the overtopping discharge is calculated. The measured overtopping discharge is compared to the predicted wave overtopping discharge. Furthermore, the calculated roughness influence factor of the ribs is compared to the fitted roughness influence factor belonging to the measured wave overtopping discharge. These comparisons are shown in figure 6.7.
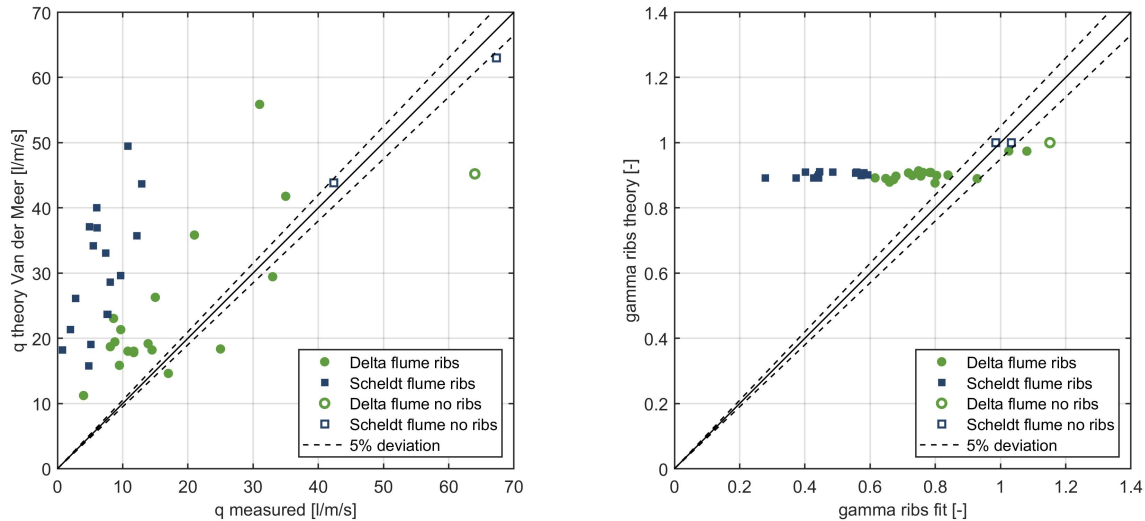
Figure 6.7: Comparison between theory and measurement of the overtopping discharge and the roughness of the upper slope based on the method in EurOtop Manual (2018), using the wave conditions at the toe of the structure

Table 6.4: Root mean square error of the wave overtopping discharge and the roughness influence factor between the measured and the theoretical values using the method in EurOtop Manual (2018)

Delta flume			Scheldt flume		
q	log(q)	γ_f	q	log(q)	γ_f
10.29	0.58	0.16	24.62	1.71	0.42

6.3. Predict average wave overtoppping discharge and roughness influence factor

From the figures above large differences between the measured values and the predicted values of the wave overtopping discharge and the roughness influence factor of the ribs are visible. Also, the difference between the Delta flume and the Scheldt flume, respectively large scale and small scale, become clear in the scatter as two separate groups of points.

In figure 6.6 and figure 6.7 the roughness influence factors of the ribs are fitted until they correspond to the measured wave overtopping discharge. However, this factor contains all other effects that are not taken into account by the method of Capel (2015) and EurOtop Manual (2018). Thus gamma fit is a more appropriate term. For example the effect of shallow water conditions and the effect of a berm on the roughness influence of the ribs are also in this factor. Several adjustments are implemented so that the theoretical value of the roughness influence factor of the ribs better approaches gamma fit. How the equations are adjusted is shown in Appendix C. The effect of the adjustments is demonstrated by the difference between the gray markers and the colored markers in the different graphs.

The method of Capel (2015) is specially designed to predict the wave overtopping discharge for structures with ribs on the upper slope. Also, the root mean square errors are slightly lower than those of the EurOtop Manual (2018) method. Therefore it is decided to continue with the method of Capel (2015) and it is tried to adjust this method to predict the wave overtopping discharge more accurately.

6.3.1. Combined roughness influence factor

Regarding the method of the combined roughness influence factor, two objections can be made. The first objection is the fact that the amount of tests including berm and roughness on the upper slope is very limited in the CLASH database, where this equation is based on. The equation is not validated systematically. Therefore it is unknown if the weighting of the different parts (lower slope, berm and upper slope) should be based on the length of each section or that an extra location-weighting factor should be implemented as described in the paper by Kriebel (2019).

The other objection is that the effect of the roughness influence of the lower slope and the berm is questionable. Since one of the major observations during the flume tests was that wave overtopping was most often caused by the second wave in a wave group, when waves were travelling close to each other. The run-down of the first wave from the wave group was not entirely completed, still some water was in-between the ribs and on the berm. The Xbloc^{plus} was fully submerged during these events. Then already the second wave hits the structure. Since the Xbloc^{plus} was submerged and the berm was covered by a water layer, the roughness of these elements was reduced. The ribs are not entirely drained and therefore the roughness was possibly lower than predicted. It seems that in the equation of the weighted roughness too much weight is assigned to the berm and the lower slope since almost all the roughness is generated by the ribs.

Based on the first objection it is decided to include an extra location-weighting factor for the location as described in the study by Kriebel (2019). This method uses equation 3.18 with location-weighting factors of 0.13, 0.22 and 0.65 for respectively the lower slope, berm and upper slope. This gives the results shown in figure 6.8.
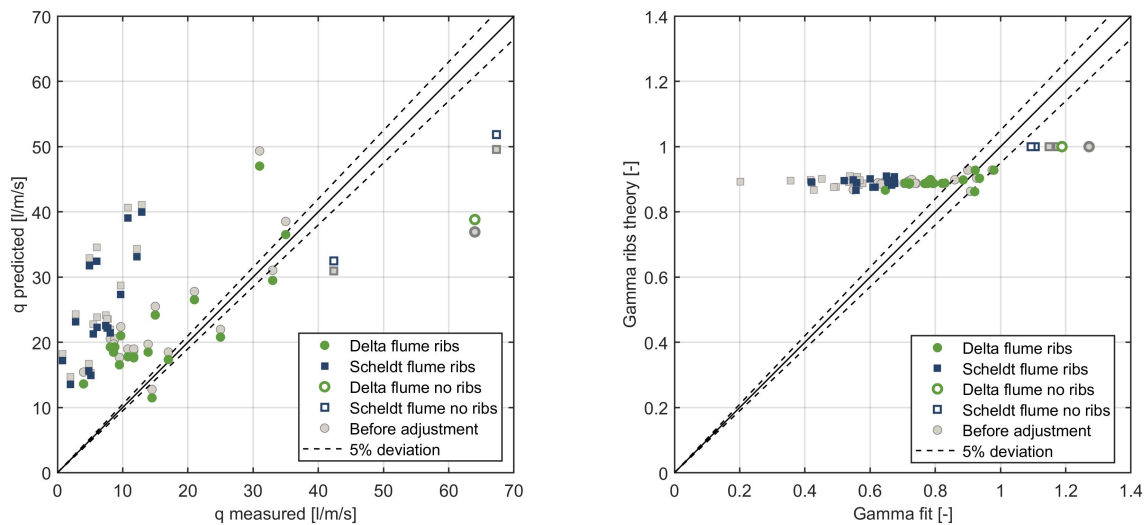
Figure 6.8: Comparison of theoretical gamma of the ribs to the fitted gamma roughness according the study of Kriebel (2019)

Table 6.5: Root mean square error of the wave overtopping discharge and the roughness influence factor between the measured and the theoretical values using the method of Kriebel method

Delta flume			Scheldt flume		
q	log(q)	γ_f	q	log(q)	γ_f
8.43	0.58	0.12	17.34	1.45	0.28

Based on the second objection it is decided to compare the gamma fit to the theoretical roughness influence factor of the ribs. The measured wave overtopping is compared to the theoretical wave overtopping. In the calculation of the theoretical wave overtopping discharge the roughness influence factor is formed only by the ribs of the upper slope.

The root mean square error shows the largest decrease if the roughness influence factor is only formed by the theoretical roughness influence factor of the ribs. This adjustment is implemented in the next step.
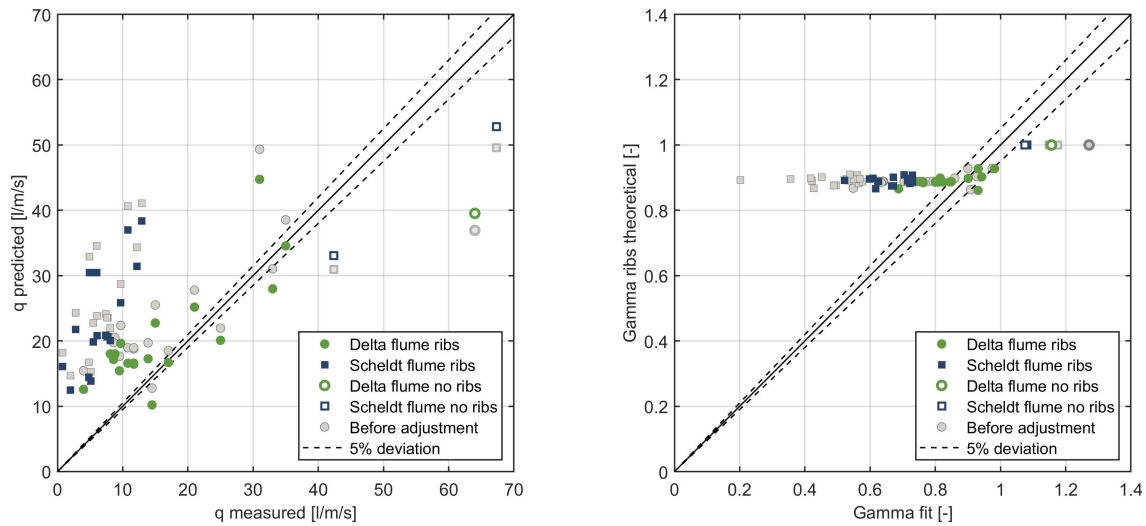
Figure 6.9: Comparison of theoretical gamma of the ribs to the fitted gamma roughness of the entire structure

Table 6.6: Root mean square error of the wave overtopping discharge and the roughness influence factor between the measured and the theoretical values using the method of Capel (2015)

Delta flume			Scheldt flume		
q	log(q)	γ_f	q	log(q)	γ_f
7.03	0.51	0.09	17.18	1.44	0.22

6.3.2. Rayleigh distribution

In the previous chapter, the results show that in most test cases the wave conditions at the toe of the structure are influenced by the bottom profile and the shallow foreshore. Since waves in shallow water conditions do not follow the Rayleigh distribution, more waves are needed to reach the same amount of wave overtopping. The average overtopping volume per wave is lower for the flattened Rayleigh distribution because the average wave height resulting in overtopping is decreased. This is shown in the left figure of figure 6.1. The two percent run-up equation which is used in the method of Capel (2015) is based on the constant relation between $H_{m0}/H_{2\%}=1.4$. However, this is not the case here, see figure 6.1. Therefore an influence factor for a shallow foreshore is implied in the run-up equation, equation 3.10. The run-up is directly implemented in the overtopping equation, to take the effect of the shallow water conditions at the toe of the structure into account. This will mainly affect tests with bottom profile 6b-179 and 8a-179 because these have the shallowest foreshores.

Imposing an extra influence factor for the shallow foreshore results in lower root mean square errors. Therefore this adjustment in combination with the roughness influence factor which is only formed by the ribs will be used.
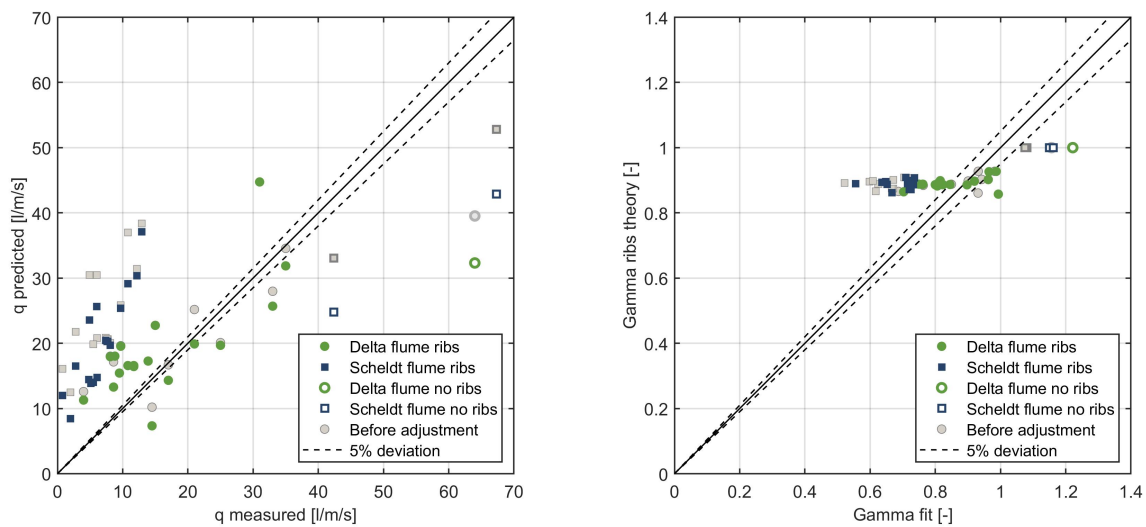
Figure 6.10: Comparison of theoretical gamma to the fitted gamma roughness of the entire structure including a foreshore factor

Table 6.7: Root mean square error of the wave overtopping discharge and the roughness influence factor between the measured and the theoretical values using the method of Capel (2015) including an influence factor for the shallow foreshore

Delta flume			Scheldt flume		
q	log(q)	γ_f	q	log(q)	γ_f
6.99	0.51	0.09	14.26	1.28	0.20

6.3.3. Wave steepness

The local wave steepness based on the wavelength calculated by the dispersion relation, equation 3.4, results in very steep waves. During the tests in the study by Capel (2015) no foreshore was present and the water depth at the toe of the structure was around four times the significant wave height. This corresponds to a deep foreshore according to table 3.2. Since it is expected that the waves can not adapt so quick to the water depth at the foreshore the deep water wave steepness will be used instead of the local wave steepness. To calculate the deep water wave steepness, the significant wave height at the toe of the structure and the deep water wavelength, equation 3.5, based on the wave period at the toe of the structure, are used. This gives the following results as shown in figure 6.11. Here the previous adjustments are also taken into account. So the roughness influence factor of the rib is used and the influence factor for the shallow water conditions at the toe imposed.

The combination of the roughness influence factor formed by the ribs only, the influence factor of the shallow foreshore and the use of the deep water wave steepness results in an even lower root mean square error. Therefore is continued with this adjusted equation.
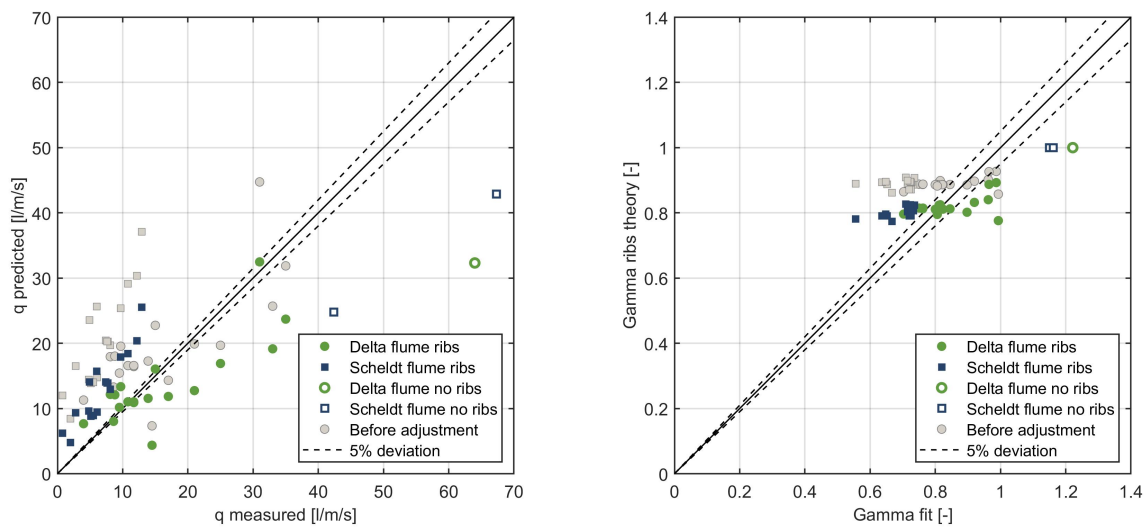
Figure 6.11: Comparison between the predicted and measured average wave overtopping discharge and the comparison between the theoretical gamma ribs and the fitted gamma of the ribs if the deep water wave steepness is used

Table 6.8: Root mean square error of the wave overtopping discharge and the roughness influence factor between the measured and the theoretical values using the Capel (2015) method taking only the roughness influence factor of the ribs, an influence factor for the shallow foreshore and the deep water wave steepness into account.

Delta flume			Scheldt flume		
q	log(q)	γ_f	q	log(q)	γ_f
5.99	0.43	0.08	6.83	0.85	0.11

6.3.4. Flow depth run-up

Since in all tested cases the flow depth of the run-up is larger than the rib height, the full height of the ribs is taken into account in the determination of the roughness influence factor. This causes the theoretical roughness influence factor to have a value around 0.8. However, the values of $\gamma_{f,rib,fitted}$ are distributed between 0.5 and 0.9. Perhaps the effect of the ribs is not limited to the height of the ribs only, but affects the water layer above the ribs as well.

Looking at the results between the fitted roughness influence factor including an influence factor for the shallow water effects at the foreshore and the measured wave overtopping discharge in figure 6.12, a relation is visible. For wave overtopping discharges larger than 20 liter per meter per seond the effect of the roughness is negligible. It seems that the method of Capel (2015) does not capture the full effect of ribs on the wave overtopping discharge. Probably, besides the roughness of the ribs, the ribs also block a part of the water layer, which leads to a larger reduction of the wave overtopping discharge for an average wave overtopping discharge smaller than 20 liter per meter per second.
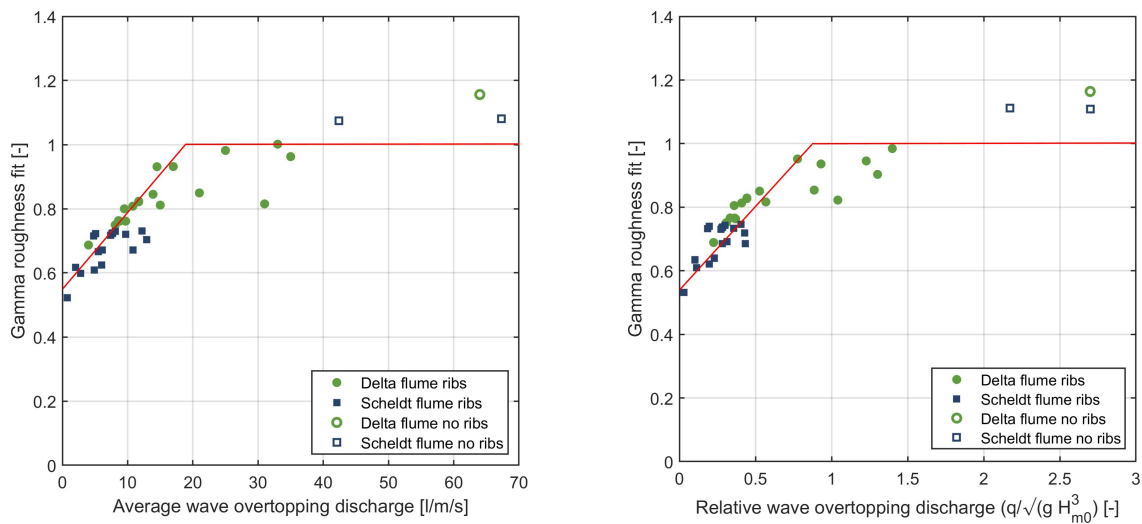
Figure 6.12: Relation between the wave overtopping discharge and the fitted roughness reduction factor in the equation of Capel including foreshore influence factor

To relate the roughness of the upper slope to the flow depth of the run-up, a new influence factor is introduced. This influence factor replaces the roughness influence factor in the overtopping equation. This influence factor expresses the relative height of the ribs compared to the flow depth of the run-up. As can be seen in figure 6.13 the rib height (δ) of each rib is divided by the flow depth (h) at that rib. Since it is not investigated if the effect of the rib depends on the location on the upper slope, the average over all ribs is taken. This results in equation 6.1. The flow depth is calculated by equation 3.23 from the study by Schüttrumpf and Oumeraci (2005).

$$\gamma_{rib} = 1 - \frac{1}{\frac{\sum h(z)}{\sum \delta(z)}} \tag{6.1}$$

Equation 6.1 is formulated in such a way that the influence factor decreases for a smaller flow depth and/or a larger rib height. The run-up is still calculated based on the roughness influence factor of Capel (2015).
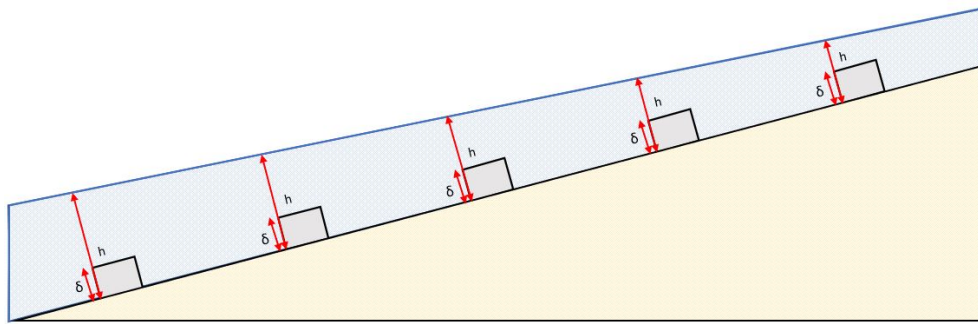
Figure 6.13: Flow depth and rib height

In the overtopping equation of Capel (2015), the roughness influence factor is now replaced by 6.1. Also, the influence factor for a shallow foreshore is used. In the calculation of the run-up, still the roughness influence factor is formed by the ribs only. The roughness influence factor of the ribs is calculated with the deep water wave conditions. Using this method the following results are obtained, as shown in figure 6.14.

The root mean square error for the average wave overtopping discharge increases for the Delta flume. In contrast to the Scheldt flume, which results in a very small root mean square error. Yet, the prediction of the wave overtopping discharge on a large scale is in our interest and so this adjustment will not be taken into account since it results in a worse prediction for the Delta flume. Nevertheless, this adjustment results in a spread in the theoretical gamma similar to that of the fitted gamma. This was not visible in the previous adjustments and is therefore worth to have a look at.
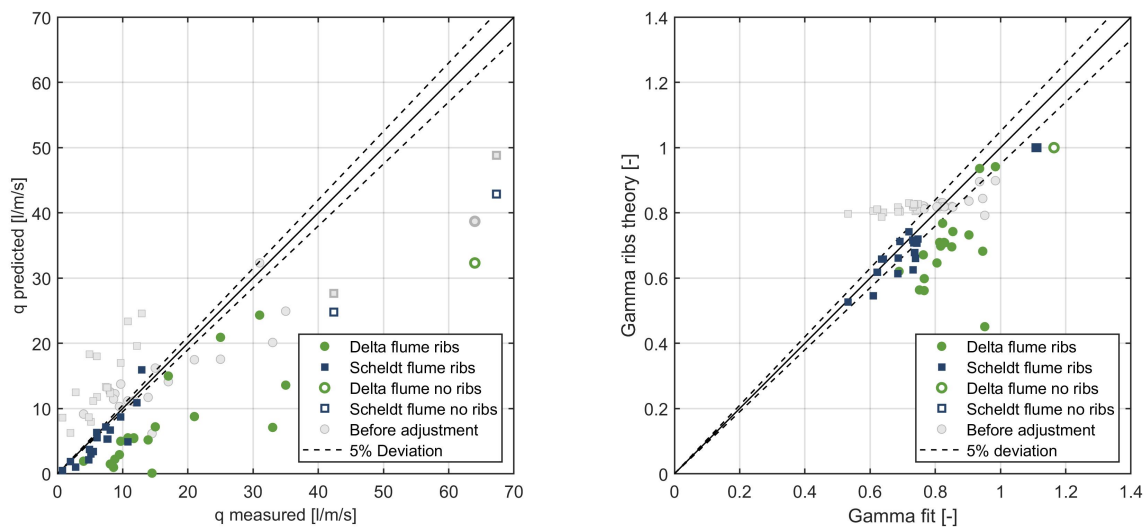
Figure 6.14: Comparison between measured overtopping including the extra reduction factor due to the blocking of the ribs

Table 6.9: Root mean square error of the wave overtopping discharge and the roughness influence factor between the measured and the theoretical values using the Capel (2015) method. Using the influence factor of equation 6.1 instead of the roughness influence factor of the ribs. It also includes an influence factor for the shallow foreshore and the deep water wave steepness.

Delta flume			Scheldt flume		
q	log(q)	γ_f	q	log(q)	γ_f
10.57	1.60	0.21	2.15	0.45	0.05

The previous method showed a spread in the calculated theoretical gamma, similar to the spread in the fitted gamma. The shape of the ribs between the Scheldt flume and the Delta flume is different, see figure 4.3. The top of the ribs in the Delta flume is more rounded and thus the blocking of the water is mainly caused by the straight part of the ribs. This is untill the part where the rounding of the ribs starts. This effect is schematized by decreasing the height of the ribs of the Delta flume in this equation by 3 centimetres.

The results show that the calculated roughness of the ribs in the Delta flume is now lower and results in a larger average wave overtopping discharge.
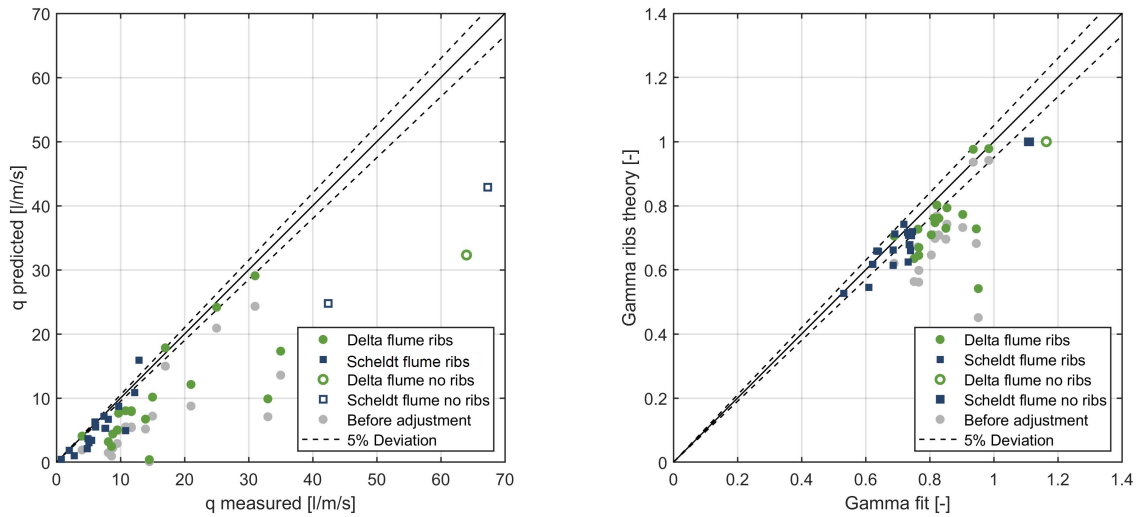
Figure 6.15: Comparison between measured overtopping including the extra reduction factor due to the blocking of the ribs. The ribs in the Delta flume are schematized 3 centimetres shorter.

Table 6.10: Root mean square error of the wave overtopping discharge and the roughness influence factor between the measured and the theoretical values using the Capel (2015) method. Using the influence factor of equation 6.1 instead of the roughness influence factor of the ribs. It also includes an influence factor for the shallow foreshore and the deep water wave steepness. The protrusion of the ribs is decreased by 3 centimetres for the Delta flume.

Delta flume			Scheldt flume		
q	log(q)	γ_f	q	log(q)	γ_f
8.65	1.05	0.13	2.15	0.45	0.05

Instead of the deep water wave steepness, the local wave steepness is used to predict the average wave overtopping discharge. In this case also the protrusion of the ribs in the Delta flume are schematized 3 centimetre shorter.

Using the local wave steepness instead of the deep water wave steepness, decreases the spread. For the Delta flume this results in smaller root mean square errors. For the Scheldt flume the root mean square errors increase. This is presented in table 6.11.
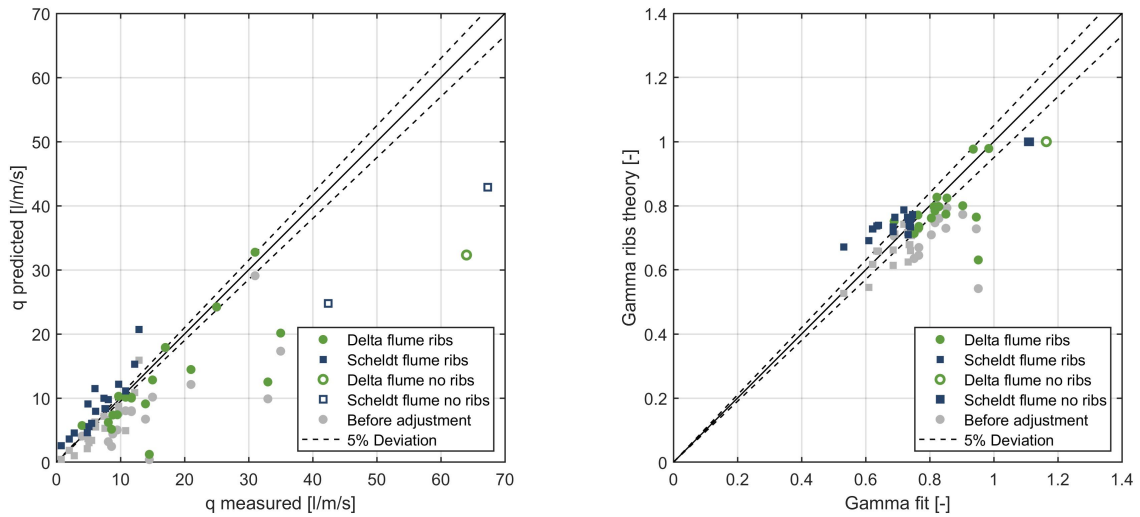
Figure 6.16: Comparison between measured overtopping including the extra reduction factor due to the blocking of the ribs. The ribs in the Delta flume are schematized 3 centimetres shorter. The local wave steepness is used.

Table 6.11: Root mean square error of the wave overtopping discharge and the roughness influence factor between the measured and the theoretical values using the Capel (2015) method. Using the influence factor of equation 6.1 instead of the roughness influence factor of the ribs. It also includes an influence factor for the shallow foreshore and the local wave steepness. The protrusion of the ribs is decreased by 3 centimeter for the Delta flume.

Delta flume			Scheldt flume		
q	log(q)	γ_f	q	log(q)	γ_f
7.15	0.68	0.10	2.89	0.44	0.06

6.3.5. Effect of location wave conditions

In the previous chapter the wave conditions at deep water, the foreshore and at the toe of the structure are determined. From these results was concluded that the shallow foreshore affects the wave conditions. The wave conditions of the different locations are used to predict the wave overtopping discharge. This chapter showed that the wave overtopping discharge is predicted best by using only the roughness influence of the ribs on the upper slope, imposing an extra influence factor for the shallow foreshore and making use of the deep water wave steepness. This method is used with the wave conditions from different locations to predict the average wave overtopping discharge.

From these figures it seems that the wave conditions at the toe are best to use for the prediction of the wave overtopping discharge in case of shallow foreshores. The results of the Delta flume and Scheldt flume follow the trend.
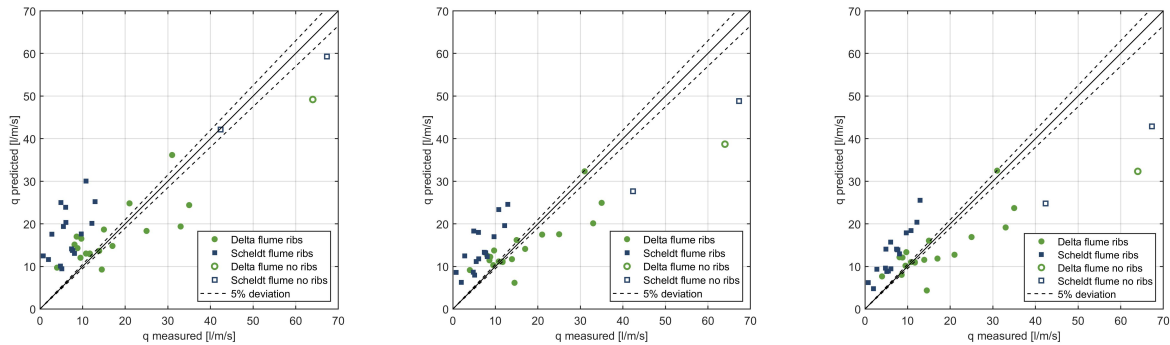
Figure 6.17: From left to right, wave overtopping discharge based on wave conditions deep water, foreshore and toe of structure

Table 6.12: Root mean square error using the wave conditions from different locations. The overtopping is calculated using the method of Capel including a foreshore influence factor, the roughness influence factor is formed by the upper slope and the deep water wave steepness is used.

	Delta flume			Scheldt flume		
Location	q	log(q)	γ_f	q	log(q)	γ_f
Deep water	6.11	0.45	0.09	11.62	1.22	0.18
Foreshore	5.61	0.41	0.07	7.88	0.97	0.13
Toe of structure	5.99	0.43	0.08	6.83	0.85	0.11

6.4. Scale and model effects

6.4.1. Hydraulic conditions

Scale effects are not expected to occur in the hydraulic conditions since a wave model is used. Still the differences between the wave conditions on large and small scale are considered. The following test cases are selected, see table 6.13, which have exactly the same bottom profile and target wave conditions.

From the results in table 6.13 can be seen that the significant wave height and the two percent highest waves at the foreshore and the toe of the structure are slightly larger in the Scheldt flume than in the Delta flume. These differences are still within the deviation of 3%, as described in section 5.3.

Table 6.13: Comparison wave conditions Scheldt flume and Delta flume, scaled to prototype

Test-ID	SWL [m+NAP]	Deep water				Foreshore				Toe of structure			
		H_{m0} [m]	$H_{2\%}$ [m]	T_p [s]	$T_{m-1,0}$ [s]	H_{m0} [m]	$H_{2\%}$ [m]	T_p [s]	$T_{m-1,0}$ [s]	H_{m0} [m]	$H_{2\%}$ [m]	T_p [s]	$T_{m-1,0}$ [s]
O1-8a-SG	5.13	4.24	5.92	7.71	7.44	4.00	5.69	7.81	7.34	3.99	5.24	7.85	7.60
O1-8a-DG	5.13	4.20	5.79	7.64	7.41	3.93	5.56	7.67	7.41	3.86	5.11	7.76	7.70
O1-8b-SG	5.21	4.32	5.83	7.71	7.43	4.19	5.98	7.77	7.42	4.22	5.88	7.80	7.52
O1-8b-DG	5.21	4.35	6.07	7.61	7.22	4.17	6.07	7.47	7.30	4.14	5.81	7.37	7.44
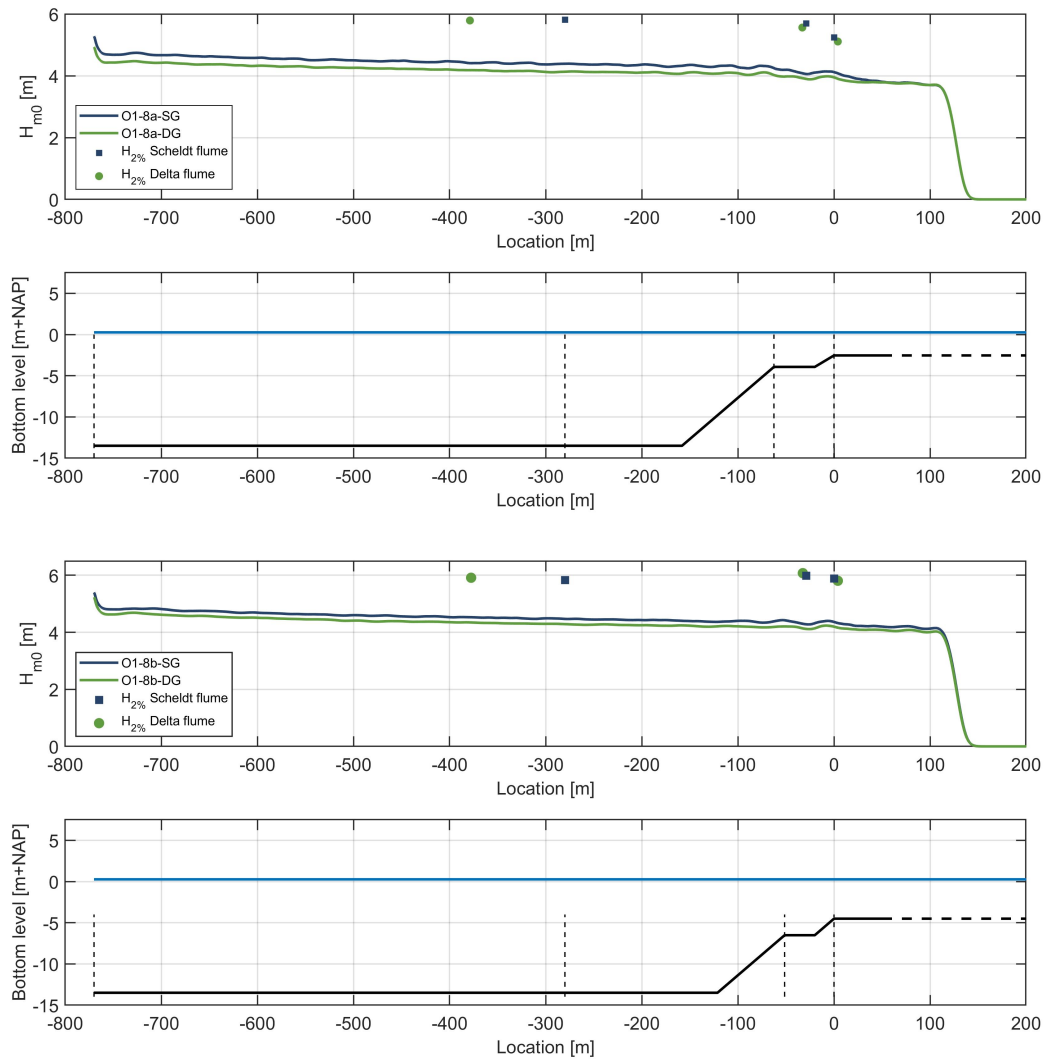
Figure 6.18: Comparison significant wave height between large and small scale

Model effects

One of the model effects in hydraulic loading, that might result in differences in the wave conditions between large and small scale is the Manning friction coefficient. This coefficient has a constant value of 0.018 in both models. However, if this parameter would be scaled correctly, see subsection 4.2.3, the Manning friction would be approximately a factor 1.35 larger for the Delta flume than the Scheldt flume. This indicates that the roughness of the bottom profile in the Delta flume is modelled smoother than the Scheldt flume, which should result in larger wave heights. Although this can not be derived from the results in table 6.13.

It should be noted that the wave gauges in the Delta flume and Scheldt flume differ in number and locations. So averaging the wave conditions might result in slightly different results of the wave conditions between the two

wave flumes.

From figure 6.18 can be seen that the differences in significant wave height occur already at the wave paddle and seem not to increase over the change of the wave flume.

Critical limits scale effects
Scale effects in wave propagation can be avoided by staying above some critical limits according to Schüttrumpf and Oumeraci (2005), see table 3.6. The Reynolds number should be larger than 1x10^4. To validate this limit, equation 6.2 is used with the deep water wave conditions. Both scales results in Reynolds number much larger than the critical limit. The Reynolds numbers for the Delta flume and the Scheldt flume are respectively 11x10^7 and 6x10^7.

$$Re = \frac{u \cdot L}{v_k} = \frac{\sqrt{\frac{g \cdot L}{2\pi}} \cdot L}{v_k} \tag{6.2}$$

Also, the critical conditions regarding the minimum water depth and wave period, see table 3.6, are exceeded for both scales. Based on this, it is expected that during the physical tests in the wave flumes scale effects in the wave conditions did not play an important role.

6.4.2. Wave overtopping discharge
The target wave conditions and the structural parameters are exactly the same between the test cases with Test-ID O1-8b-SG-6 and O1-8b-DG-1. The parameters of the test cases can be found in table 6.2. Nevertheless, the wave overtopping discharge between the two cases differs with a factor 1.5. The large scale test results in a higher average wave overtopping discharge. This difference in wave overtopping discharge might be caused by model effects or by scale effects. Both will be evaluated below.

Model effects
As described in section 4.1 the shape of the ribs between the Delta flume and the Scheldt flume differ. To express the effect of the different shape of the ribs on the wave overtopping discharge the ribs are compared to two types of broad crested weirs. The rounded ribs formed by the Quattroblocs in the Delta flume show similarities to the round-nosed broad crested weir and the rectangular ribs of the Scheldt flume can be compared to square-edged broad crested weirs. Several studies, Azimi and Rajaratnam (2009), Amruthure et al. (1988) showed that rounding the upstream corner of broad crested weirs increases the discharge coefficient compared to the square-edged broad crested weirs. A larger discharge coefficient means that the ribs are less effective in reducing the wave overtopping discharge. The rounded corner prevents the flow to separate when it approaches the rib. Figure 6.19 shows the schematization of the flow over a round-nosed broad crested weir, and a rectangular broad crested weir. The flow separation and thus the energy loss is indicated with the circular arrow in the right figure, the blue straight arrow indicates the flow direction.
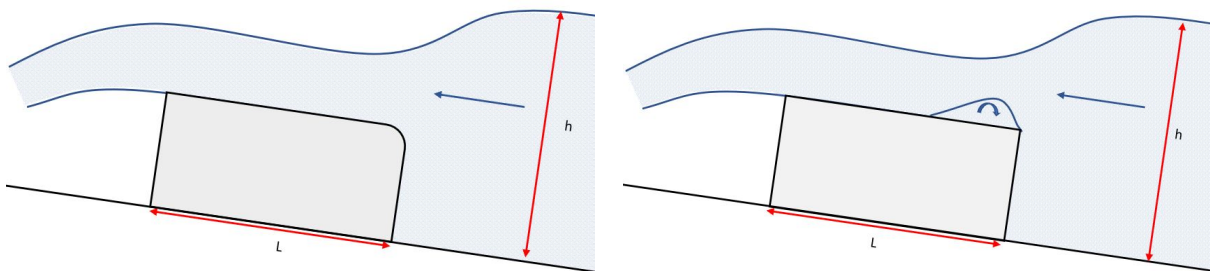
Figure 6.19: Round-nosed broad crested weir (left) and rectangular broad crested weir (right)

The study of Azimi and Rajaratnam (2009) developed the following two empirical correlations, equation 6.3 and equation 6.4, to describe the discharge coefficient for respectively a round crested weir and a squared crested. Both equations can be used in the range of 0.4 < h/L < 2.0.

$$C_d = 0.90 + 0.176 \cdot (\frac{h}{L}) \tag{6.3}$$

$$C_d = 0.767 + 0.215 \cdot (\frac{h}{L})$$ (6.4)

The effect of a rounded downstream corner on the discharge coefficient for a broad crested weir is not investigated yet. However, the study by Gong et al. (2019) shows that the discharge coefficient for round crested weirs (not broad crested) is higher than for rectangular crested weirs, but the effect of the rounded downstream corner is negligible compared to the effect of the upstream rounded corner on the discharge coefficient.

Critical limits scale effects

The critical limits regarding wave run-up and wave overtopping are the same. The Reynolds number should be larger than $1\text{x}10^3$ and the Weber number should be larger than 10.

The Reynolds number indicates the type of flow of a fluid and thus the relative significance of the viscous effect compared to the inertia effect. The flow can be separated in roughly three categories:

- Laminar Re < 2300
- Transitional 2300 < Re < 4000
- Turbulent Re > 4000

To have an idea about the order of magnitude of the Reynolds number on both scales, equation 6.5 is used. The velocity is based on the propagation speed of the significant wave and the length in the equation is based on the protrusion of the ribs, see equation 3.4. This gives us the Reynolds as described below.

$$Re = \frac{u \cdot L}{v_k} = \frac{\sqrt{g(h + H_{m0})} \cdot h_k}{v_k}$$ (6.5)

With a kinematic viscosity of $1.3\text{x}10^{-6}\text{m}^2/\text{s}$ for water, results in Reynolds numbers of $4\text{x}10^5$ and $2\text{x}10^4$ for respectively the Delta flume and the Scheldt flume. The Scheldt flume behaves more viscous than the Delta flume, but they are both turbulent.

The value of Weber can be calculated with equation 6.6. It describes the ratio between inertia and surface tension.

$$We = \frac{\rho_w \cdot u^2 \cdot L}{\sigma} = \frac{\rho_w \cdot (g(h + H_{m0})) \cdot h_k}{\sigma}$$ (6.6)

With a surface tension of $75\text{x}10^{-3}\text{N/m}$ for water with a temperature of 10 degrees Celsius the Weber number for the Delta flume and the Scheldt flume is respectively $5\text{x}10^5$ and $1\text{x}10^3$. This is much larger than the critical limit.

6.5. Uncertainty and sensitivity

In the prediction of the wave overtopping discharge using the equation of Capel (2015), where only the roughness influence factor of the ribs is taken into account, an extra influence factor for the shallow water effects at the toe is considered. Secondly, the deep water wave steepness is used instead of the local wave steepness, several parameters are involved. From some of these parameters the uncertainty is estimated. The mean average deviation in these parameters will be used, to form an opinion about the uncertainty of the prediction of the average wave overtopping discharge. From this follows the sensitivity of the empirical equation of the wave overtopping discharge to different parameters as well. The case with Test-ID O1-8b-DG-6 is used for this calculation, using the geometry as described in table 6.2. This case is chosen since the measured wave overtopping discharge and the estimated wave overtopping discharge were very close to each other. From the different considered parameters the mean average deviation is added and subtracted, resulting in the predicted lower and upper average wave overtopping discharge.

6.5.1. Incoming significant wave height

The incoming significant wave height derived from the SWASH wave model shows variations on both scales, starting at a relative water depth of three times the significant wave height, see figure 5.3. These variations occur also at the toe of the structure. Since the wave gauges at the toe of structure are placed close to each other the maximum

amplitude of the variations is taken into account as uncertainty. The amplitude of these variations is around 5% of the significant wave height.

Using the method Capel (2015) to predict the wave overtopping discharge a maximum deviation of 5% in the significant wave height results in a deviation of 25% in the predicted wave overtopping discharge. This is shown in table 6.14.

Table 6.14: Sensitivity of wave overtopping discharge by significant wave height

Deviation of H_{m0}	$q_{measured}$ [l/m/s]	$q_{predicted,lower}$ [l/m/s]	$q_{predicted,upper}$ [l/m/s]	Deviation q
5%	10.8	7.3	12.4	25%

6.5.2. Wave period
The peak period and the spectral mean wave energy period show both a deviation of at most 3% between the measured values in the wave flume and the results from SWASH. The spectral mean wave energy period affects the wave length and thus the steepness of the waves and the breaker parameter. This deviation in the wave period results in a deviation of 6% in the average wave overtopping discharge.

Table 6.15: Sensitivity wave overtopping discharge to spectral mean wave period

Deviation of $T_{m-1,0}$	$q_{measured}$ [l/m/s]	$q_{predicted,lower}$ [l/m/s]	$q_{predicted,upper}$ [l/m/s]	Deviation q
3%	10.8	10.35	11.6	6%

6.5.3. Roughness influence factor
To get an idea of the mean average deviation of the roughness influence factor, the Delta flume and the Scheldt flume are separated. The deviation in the roughness reduction factor is defined by the difference between the calculated roughness influence factor and the fitted roughness influence factor. The mean average deviation of the roughness influence factor for the Delta flume is 0.06. In the Scheldt flume the mean average deviation is larger and is 0.10. Which is a deviation of respectively 6.8% and 12.2 % in the roughness influence factor .

Table 6.16: Sensitivity of wave overtopping discharge by roughness influence factor

Deviation of γ_f	$q_{measured}$ [l/m/s]	$q_{predicted,lower}$ [l/m/s]	$q_{predicted,upper}$ [l/m/s]	Deviation q
6.8%	10.8	8.1	15.8	35%
12.2%	10.8	5.97	19.46	62%

6.5.4. Berm influence factor
The accuracy of the influence factor of the berm is based on the cases with a smooth upper slope. From these cases is known that the influence factor of the roughness is equal to 1, since earlier is stated that the roughness influence factor is best described in these cases by the roughness influence factor of the upper slope only. The deviation between the calculated influence factor of the berm and the fitted influence factor is determined. For the Delta flume the deviation in the influence factor was 0.04 and for the Scheldt flume this was 0.08. Which is a deviation of respectively 5% and 11% in the berm influence factor for the Delta flume and the Scheldt flume respectively.

Table 6.17: Sensitivity of wave overtopping discharge by berm influence factor

Deviation in γ_b	$q_{measured}$ [l/m/s]	$q_{predicted,lower}$ [l/m/s]	$q_{predicted,upper}$ [l/m/s]	Deviation q
5%	10.8	7.5	15.3	35%
11%	10.8	4.9	20.6	73%

6.5.5. Geometry of ribs

The different shape of the ribs might be the reason for the difference in the measured overtopping discharge between the Delta flume and the Scheldt flume for the same structure. For that reason a simplified example between the test cases with Test-ID O1-8b-SG-6 and O1-8b-DG-1, as in table 6.2, is used to show the difference in discharge coefficient and thus in the average wave overtopping discharge.

In both cases 10 ribs are constructed on the upper slope. The equations to calculate the discharge coefficient of the two types of weirs can be used in the range of $0.4 < h/L < 2.0$. Using the equation of Schüttrumpf and Oumeraci (2005) the flow depth can be calculated. This shows over which ribs the equation for the discharge coefficient of weirs can be used. It shows that the equations can be applied over the upper 6 ribs. The ribs have a width of 0.55 meter. The calculated discharge coefficients are presented in table 6.18.

Table 6.18: Discharge coefficient for ribs with different geometry

Rib	Water layer thickness [m]	C_d squared [-]	C_d rounded [-]	Percentage difference [%]
1	1.10	1.20	1.25	4.3
2	1.01	1.16	1.22	5.0
3	0.93	1.13	1.20	5.6
4	0.84	1.09	1.17	6.3
5	0.75	1.06	1.14	7.0
6	0.66	1.03	1.11	7.7

Taking into account the difference of the discharge coefficient over the width of the ribs, results in a 20% lower discharge for the situation with the squared ribs than the rounded ribs. This simplified calculation is shown below.

Simplified calculation

First, the discharge reduction over the ribs is calculated.

(1-0.043)x(1-0.05)x(1-0.056)x(1-0.063)x(1-0.07)x(1-0.077) = 0.69

Over the ribs the discharge is decreased by 31%. However, the ribs only cover 2/3 of the length. Between the ribs the discharge coefficient does not change between the squared and rounded ribs.

The difference in wave overtopping discharge is calculated by multiplying the change in discharge coefficient over the corresponding length.

(0.69 x 0.67) + (1 x 0.33) = 0.80

<div align="right">

7

Discussion

</div>

In this chapter first the results of the hydraulic loading are discussed. Attention is paid to different wave parameters and the difference between the wave flume and the computational wave model. Then the results of the model setup are discussed. Here the model and scale effects, test cases and test setup are considered. Finally the independency of influence factors, the theory in the EurOtop manual (2018), the theory of Capel (2015) are discussed.

7.1. Hydraulic loading

Using the results of the computational wave model as input for the wave conditions at the toe of the structure to predict the average wave overtopping discharge gives rise to new uncertainties. The uncertainties in the used wave parameters will be discussed. Afterwards, the differences between the physical model and the computational model are evaluated.

7.1.1. Variations in H_{m0}

The variations in the significant wave height look like wiggles. Different causes for the variations in the significant wave height have been studied. As already mentioned, these are reflection of primary waves, seiches, trapped infragravity waves and shoaling. They will be discussed separately.

Reflection of primary waves

The variation in the significant wave height look like wiggles with a length of approximately 30 to 35 meter. The length of a wiggle corresponds to half a wavelength of the reflected primary wave, which is 60 to 70 meter. With equation 3.5 the corresponding wave period can be calculated. The wave period of the primary wave is between 6.2 and 6.7 seconds. Looking at the frequency energy density spectrum of the reflected wave signal at deep water, there is no energy at the corresponding frequencies. Also, based on the method of Zelt and Skjelbreia (1992) it was concluded that only 1% of the wave energy belongs to the reflected waves.

Seiches

Seiches occur if the system is not able to absorb long wave energy of a certain frequency, which is in resonance with the length of the wave flume. A long period standing wave occurs, which is called a seiche, according to Kamphuis (2015).

$$T_n = \frac{2L}{n\sqrt{gh}} \tag{7.1}$$

The seiche might result in variations in the significant wave height. The antinodes of the seiches will correspond to the peak of the wiggles in the significant wave height. The significant wave height will be larger at the antinodes of the seiche, because the seiche results in fluctuating 'water levels' at these positions. At the moment the seiche has a peak at the antinode, the waves are less likely to break due to the larger water depth. This results in a higher significant wave height. When the seiche is at its through at the antinode, more waves will break. This will not affect the significant wave height, since the significant wave height is calculated as the average of the one-third of the highest waves. Thus only the highest waves affect his parameter.

Based on the natural frequencies of the basin is expected that seiches are not the cause of the wiggles in the significant wave height.

Trapped infragravity waves

Trapped infragravity waves might be caused by a sudden decrease in water depth. On the flat part of the foreshore, the incoming waves that are not dissipated by breaking or bottom friction might be reflected by the slope at the end of the flat part causing outgoing waves. Waves can be trapped when the outgoing wave is reflected by the depth change of the foreshore, redirecting it back to the foreshore. The flat part of the foreshore acts like a semi-enclosed basin. If the incoming wave and the outgoing wave have the same frequency a standing wave pattern

occurs. The frequencies for which these standing waves occur can be determined with equation 7.2. If in the energy density spectrum also a peak occurs at this frequency, it might be caused by the standing wave. At the natural frequencies of the flat part resonant amplification might occur. Buckley and Lowe (2018)

$$f_{node} = \frac{1}{4}(2n-1)(\frac{L}{\sqrt{gh}})^{-1} \qquad (7.2)$$

Shoaling and breaking

It is not expected that shoaling and breaking results in these wiggles. Shoaling increases the significant wave height when the water depth decreases. Breaking might reduce the significant wave height again. This combination of shoaling and breaking can result in wiggles, however in this case also an increase in significant wave height is visible for the flat part on the foreshore. This is can not be caused due to shoaling. Therefore it is expected that this is not the reason for the wiggles in the significant wave height.

7.1.2. $H_{2\%}$

From the tests in the wave flumes appeared that approximately the 30 largest waves of the roughly 1000 produced waves resulted in the measured average wave overtopping discharge. This means that the few largest waves are important for the wave overtopping discharge and $H_{2\%}$ is thus an important parameter. Since the value of this parameter is only formed by approximately 20 waves this parameter is more sensitive to the imposed wave signal. To increase the reliability of this parameter, more tests can be executed with the same JONSWAP spectrum and the average $H_{2\%}$ over those tests should be taken. Another option to increase the reliability of this parameter, is increasing the test duration,.

7.1.3. Wave period

The peak wave period is based on the frequency energy density spectrum. This energy density spectrum has a spectral resolution of 0.02 Hz. Due to this spectral resolution it might be the case that the peak period jumps from one frequency bin to another frequency bin.

The spectral mean wave energy period, $T_{m-1,0}$, is based on the frequency energy density spectrum. Based on the measurements in the wave flumes and the corresponding frequency energy density spectrum is decided to cut off the spectrum from SWASH at 3 times the peak frequency and at 1/5 of the peak frequency. This might slightly affect the spectral mean wave energy period, since this parameter allocates more weight to the lower frequencies. A similar procedure is performed with the measurements from the wave flumes. Also, the amount of energy is very small at these frequencies and thus the effect will be limited.

7.1.4. Difference between wave flume and computational model

To estimate the wave overtopping discharge the wave conditions at the toe of the structure are important. At this location are no wave gauges installed in both wave flumes. This is the reason to use the computational wave model SWASH to model the wave conditions at this location. The main difference between the physical model and the computational model is the absence of the structure. The waves that are reflected by the structure in the wave flume, might result in a different type of wave breaking. This effect is not taken into account in the computational model. The reflected wave in the wave flume is filtered out at the wave paddle, where in the computational model almost no reflection occurs due to the sponge layer.

Another difference between the wave flume and the computational model is the imposed wave signal. The wave signal of both, the wave flume and SWASH, are based on a JONSWAP spectrum with a peak enhancement factor of 3.3 and the same peak period and significant wave height. However, this does not mean the surface elevation signal is equal. Based on the assumption that over 1000 waves, corresponding to a time duration of two hours on prototype scale, the wave parameters are constant is expected that this does not influence the measurements much.

For the Manning friction coefficient a value of 0.018 is taken in SWASH. From the results of the wave parameters at the flat part of the foreshore it seems that SWASH returns slightly larger values for the significant wave height than the measurements in the wave flumes. This might indicate that the roughness in SWASH is thus too low.

7.2. Model setup and test cases

There are several points of discussion regarding the comparison of the two model setups on a different scale. The differences between the modelled structures may lead to model effects. Also, the scale effects are here considered since it is hard to quantify these two effects. Furthermore, different test cases are considered.

7.2.1. Model effects

The main difference in the modelled structure is found at the upper slope. The upper slope in the Delta flume is modelled like the prototype, with concrete Quattroblocks. The upper slope of the Scheldt flume is modelled with a PVC plate with ribs milled in it. These ribs are perfect rectangular blocks. Where the ribs in the Delta flume have rounded corners, the ribs in the Scheldt flume have sharp corners. These differences in material properties and shape results in a different behaviour of the water flowing over the ribs. The flow over the ribs in the Scheldt flume will detach. Accordingly the discharge coefficient decreases and the wave overtopping discharge decreases. Regarding the example calculation, see section 6.4, some remarks can be made. The main remark is the comparison between the Quattroblocks and the round-nosed broad crested weirs. Moreover, the effect of the ribs on the estimated water flow depth is not examined. Finally, only the effect of the run-up is considered. Expected is that the run-down also takes less time, resulting in better drainage of the upper slope and thus in more roughness compared to the case where the ribs are undrained.

Other differences between the model setup of the Delta flume and the Scheldt flume can be found in the berm. In the Delta flume the berm is made of concrete, but in the Scheldt flume the berm is made of timber or PVC. Also, the side walls are different. In the Delta flume these are from concrete and in the Scheldt flume these are of glass. Expected is that both, the berm and the sidewalls, do not influence the wave overtopping discharge, because the used materials are all smooth and impermeable.

Another difference in the model setup is the location of the wave gauges. This does not affect the wave overtopping discharge, but it makes a comparison between the different wave flumes more difficult. The wave gauges in the Delta flume are at fixed locations, namely at deep water and at the flat part of the foreshore. The wave gauges in the Scheldt flume are fixed at deep water, but the locations of the wave gauges at the foreshore are changing for different foreshores. Also, the amount of wave gauges between the Delta flume and the Scheldt flume differs.

7.2.2. Scale effects

Scale effects can distort the modelling results. They occur when the employed scaling law does not correctly reproduce the physical conditions between the different scales. The models are scaled according to the Froude law, therefore other physical processes might not be scaled correctly. Two important processes are the Reynolds number and air entrainment. The Reynolds number is not correctly scaled, because the kinematic viscosity of the water is the same between the two model scales. This might result in different flow regimes. If the Reynolds number is calculated for both scales, it can be concluded that on both scales the flow will be turbulent, Re > 4000. Further is expected is that the viscous forces are small compared to other forces. The Scheldt flume behaves more viscous and therefore the ribs might act rougher. It is not clear if this effect can be neglected.

The study of Blenkinsopp and Chaplin (2011) and Blenkinsopp and Chaplin (2007) considers the effect of scale on air entrainment by breaking waves. There are differences between the total volume of entrained air due to the rising time of the bubbles between the different scale. The volume of entrained air in breaking waves and thus in the run-up is lower on a small scale than on large. The flow depth of the run-up is therefore expected to be larger on a large scale than on a small scale. Expected is that the thicker water layer experiences less of the ribs on the upper slope, resulting in less roughness and thus larger wave overtopping discharges are measured.

7.2.3. Test cases and measurements

To assess the effect of different structural parameters on the wave overtopping discharge, structural parameter should be isolated. With the structural parameter of interest, various tests should be performed to find out what the actual relation is between that specific structural parameter and the wave overtopping discharge. During the performed test cases only a limited amount of tests are executed with only one parameter being varied. This makes it hard to decide which processes are important for the wave overtopping discharge. The isolation of structural parameters allows the determination of the scale effects.

Increasing the reliability of the test results can be reached by executing the same tests multiple times or by a longer test duration. However, expected is that this will not have much effect on the wave overtopping discharge,

because the wave parameters are expected to be constant over 1000 waves.

The location of the wave gauges at the foreshore is not optimal in the Scheldt flume. The wave gauges are located close to the slope of the foreshore, so the effects of shoaling are playing parts in the measurements of the wave conditions. This gives somewhat distorted results of the wave conditions. Better is to locate the wave gauges further away from the slope.

The best method to determine the wave conditions at the toe of the structure from SWASH is not evident. In this study is chosen for three wave gauges with a distance of 6 meters, on the prototype scale, from each other. This distance is not large enough to capture the full effect of the wiggle that occurs there. It is uncertain if the wave conditions at the toe of the structure can be determined best by only one wave gauge at the location of the toe or by the average overseveral wave gauges. Also, the distance to use between the wave gauges is undecided.

The average wave overtopping discharge is calculated by dividing the volume in the overtopping tank divided by the duration of the test. This volume is based on the area of the overtopping tank times the water level in the tank. The reliability of this parameter is thus dependent on the area of the tank and the measuring device.

7.3. Current theories wave overtopping

7.3.1. Independence of influence factors

The study of Chen et al. (2019) investigated the combined effect of roughness elements and berm on wave overtopping by executing physical model tests. This research suggests that the combined effect of the roughness elements and a smooth impermeable berm are not static, but are influenced by the breaker parameter and the relative freeboard. If the relative freeboard increases, the roughness influence factor increases because the flow depth decreases. The wave steepness affects the influence of the berm. If the wave steepness increases the berm influence decreases. Also, the effect of the berm and the roughness elements are not independent according to the research of Chen et al. (2019) since the berm reduces the wave overtopping discharge which causes the roughness elements to act rougher. The roughness elements on the upper slope will also affect the berm. Due to the extra roughness, less water will overtop resulting in a larger run-down volume and thus a water layer might be presented on the berm. Resulting in a different influence of the berm on the run-up.

7.3.2. Combined roughness influence factor

Equation 3.16 results in a roughness influence factor for the entire slope. Since the length of the berm is large compared to the length of the lower slope and upper slope, it seems that too much weight is assigned to the berm. Which results in too high roughness influence factors, since the berm is smooth. The principle that the weight of the roughness influence factor is only dependent on the length over which it is applied is questionable. Therefore the paper of Kriebel (2019) makes use of an extra location factor, which states that the effect of the roughness elements on the lower slope is less effective than roughness elements on the berm, which are less effective than roughness elements on the upper slope.

Also, the area over which the roughness should be taken into account might be discussed. Capel takes the entire upper slope into account over which the ribs are applied, whereas Van der Meer only takes part of the roughness of the upper slope into account. Furthermore, throughout the tests was observed that during the wave overtopping events the lower slope with the Xbloc^{plus} and the berm were covered by a water layer and thus the roughness influence was arguable.

7.3.3. EurOtop Manual (2018)

The method in the EurOtop Manual (2018) can predict the wave overtopping discharge accurately for the cases with a smooth upper slope. The method of Van der Meer takes constant values into account based on an interpolation between the height of the rib and the significant wave height, as described in equation 3.19. But the roughness of the ribs depends on more parameters.

This method takes the roughness elements on the upper slope into account until a height of 0.5 $R_{u2\%\ smooth}$ above the still water level. However, the two percent run-up height is larger than this value. Thus using $R_{u2\%\ smooth}$ over which the roughness is effective, causes that not the full roughness of all ribs is taken into account.

7.3.4. Capel (2015)

The equation of Capel (2015) is used outside of its tested range. During the tests where the equation of Capel (2015) is based on, no berm and no roughness elements on the lower slope where applied. The roughness reduction factor was only formed by the ribs. The theory of Capel (2015) results in higher values of the roughness reduction factor than the measurements showed on a large scale. It is likely that the ribs behave rougher in practice due to the presence of the berm, as described by Chen et al. (2019). The wave overtopping discharge is even harder to predict for the Scheldt flume. The wave overtopping discharge is overestimated in all cases.

Another difference between the tested cases and the tests in the study of Capel is the relative freeboard. The relative freeboard in the tested cases is much lower. In the tests, the relative freeboard was between 0.95 and 1.3, compared to Capel 1.2 - 2.7. The paper of Chen et al. (2019) also mentioned the effect of the relative freeboard on the wave overtopping discharge. Larger freeboards, result in smaller flow depths and thus the roughness elements are more effective.

Also, the water depth at the toe of the structure was at least four times the significant wave height, corresponding to deep water, in the study of Capel (2015). Where in the tested cases of this study the water depth was often smaller than four times the significant wave height, resulting in a flattened Rayleigh distribution and higher local wave steepness. The roughness of the ribs depends among others on the local wave steepness. Expected is that the waves can not adapt so fast to the foreshore and that the wave steepness is more like the deep water wave steepness.

During the wave overtopping events, all the ribs are submerged. The equation of Capel (2015) uses the wave overtopping discharge as a parameter in the roughness factor. However, the flow depth is probably a better parameter.

Deviation in average wave overtopping discharge

Often the dimensionless wave overtopping discharge is presented on a logaritmic scale. In the EurOtop manual (2018) equation 3.29 with a part of the CLASH database is plotted. This plot shows that in the 90% confidence interval there might still be a factor 10 difference in the wave overtopping discharge.

Also, in the study of Capel (2015) there is a spread in the wave overtopping discharge of approximately factor 5.

In the adjusted equation, presented in this report, the spread is smaller. However, also the variation in hydraulic and structural parameters is small. Therefore the equation works good for this case.

<div align="right">

8
Conclusion

</div>

The objective of this research was to find a method to accurately predict the average wave overtopping discharge for a composite slope on large scale. To answer this a set of research questions is formulated. By answering these five research questions the objective should be fulfilled as described in the research objective, section 1.3.

8.1. Subquestions

Can deep water wave conditions be used to predict the average wave overtopping discharge?

In the case of the Afsluitdijk, the foreshore appears to be important for the wave transformation towards the dike. Therefore the wave conditions measured at deep water and at the flat part of the foreshore can not be used to predict the wave overtopping discharge accurately. The wave conditions at the toe of the structure should be determined for an accurate prediction of the wave overtopping discharge.

When the wave conditions are not provided from the flume tests, the wave conditions can be simulated with the wave model SWASH. The validation of the measurements between the wave flume and the computational model showed that SWASH is able to reproduce the significant wave height and the peak period with a deviation of 3% at the flat part of the foreshore. The results of the wave conditions are averaged over the wave gauges, so the spacing between the wave gauges is important.

Which mechanisms influence the average wave overtopping discharge?

Comparing the cases where only one structural parameter was changed at the same time, showed that the water depth at the toe, the berm width, the presence of ribs and the characteristics of the ribs are important for the wave overtopping discharge. Since the dataset that was provided does not have many cases where only one parameter is isolated at the same time, only a trend is visible. The exact relation between the isolated parameter and the wave overtopping discharge was not clear.

The results showed that the presence of ribs has the largest influence on the wave overtopping discharge. The average wave overtopping discharge decreases with a factor 3 to 6 due to the ribs. The foreshore, berm and characteristics of the ribs have a smaller influence on the wave overtopping discharge.

How can the roughness of the rib profile accurately be determined?

From the executed flume tests the influence of the rib profile on the average wave overtopping discharge can not be determined accurately, from the available data. There are too many uncertainties involved and the variations in the geometry of the structure have not been systematically verified as the tests had a different objective.

The results of SWASH show variations in the significant wave height starting at a relative water depth of three times the significant wave height. This means that for an accurate prediction of the wave conditions several wave gauges should be installed. The spacing between these wave gauges is important to capture the wiggles. The wave conditions can be determined by taking the average over the wave gauges. Nevertheless, the uncertainty of the variation in the significant wave height remains.

From the different geometries, some important parameters of the rib profile can be distinguished for the roughness. These are the protrusion of the ribs, density of the ribs and the number of the ribs. Also, the average wave overtopping discharge was an important parameter. The effect of the ribs was negligible for wave overtopping discharges larger than 20 l/m/s on prototype scale.

From the different geometries, it was not possible to isolate the effect of the upper slope from other influential factors of the structure. A systematic test program is required to determine the roughness influence of the upper slope accurately.

How can existing methods be adapted to better predict the average wave overtopping discharge?

The considered methods are the theory in EurOtop manual (2018) and Capel (2015). The method described in EurOtop manual (2018) was able to predict the average wave overtopping discharge very accurately for a composite slope with Xbloc[plus] on the lower slope, a berm and a smooth upper slope. On a small scale, the predicted wave overtopping discharge shows an average deviation of 6% to the measured wave overtopping discharge. On a large scale, this deviation is 30%.

On a small scale, the average wave overtopping discharge for a composite slope with roughness elements on the upper slope, a berm and a lower slope consisting of Xbloc^{plus}, is overestimated by both methods.

On a large scale, the average wave overtopping discharge for a composite slope with roughness elements on the upper slope, a berm and lower slope consisting of Xbloc^{plus}, the wave overtopping discharge is overestimated by both methods till 17.5 l/m/s. For larger overtopping volumes both methods show a spread.

To predict the wave overtopping discharge more accurate, three modifications to the existing method of Capel (2015) are applied.

- Include an influence factor for shallow water effects at the toe of the structure in the calculation of the run-up. This factor should be implemented to take into account the breaking of the highest two percent of the waves on the foreshore.
- The roughness influence factor is only formed by the ribs, so it is not a combined influence factor composed of the roughness located on the lower slope, berm and upper slope.
- Instead of the local wave steepness, the deep water wave steepness should be used. The waves can not adapt so fast to foreshore and thus the local wave steepness results in too steep waves.

For the cases with ribs on the upper slope, applying these three modifications results in a prediction of the average wave overtopping discharge with an average deviation of 30% on a large scale and 170% on a small scale. The root mean square error decreases from 9.13 to 5.99 for the Delta flume and from 19.85 to 6.83 for the Scheldt flume.

A fourth modification might be a limit to the influence of the ribs related to the wave overtopping discharge. The influence of the ribs on the wave overtopping discharge becomes negligible if the wave overtopping discharge is larger than 20 l/m/s.

What causes the difference in wave overtopping discharge between large scale and small scale?

Based on existing literature scale effects in the average wave overtopping discharge should be negligible if certain critical limits are exceeded. During the considered tests these limits are all exceeded. However, from the results of the wave overtopping discharge measurements differences between the Delta flume and Scheldt flume are clearly visible. The Delta flume results in higher wave overtopping discharges than the Scheldt flume.Two expected phenomena to cause this difference are:

- The rougher behaviour of the ribs on the upper slope in the Scheldt flume might be caused by scale effects in the air entrainment. The water layer thickness of the run-up does not correctly scale from large to small scale. Resulting in smaller water layer thickness and thus on a rougher behaviour of the ribs in the Scheldt flume. Also, water acts more viscous on a small scale, resulting in rougher behaviour of the ribs and thus lower average wave overtopping discharges.

- Differences between the setup are mainly found in the upper slope, these are model effects. The squared edges of the ribs in the Scheldt flume result in detachment of the flow. This leads to energy reduction. Causing the upper slope in the Scheldt flume to act rougher.

8.2. Research question

How can the average wave overtopping discharge for a composite slope as designed for the Afsluitdijk rehabilitation project accurately be predicted?

The average wave overtopping discharge can best be predicted with tests in the wave flume on the largest scales as possible.

If the average wave overtopping discharge should be predicted based on smaller scale wave flume tests, the ribs should be rounded. This results in a more realistic shape and a lower roughness of the upper slope.

In the specific case of the Afsluitdijk, two subjects are very important in the prediction of the average wave overtopping discharge. This is the shallow foreshore and the composite slope including a berm. The shallow foreshore affects the wave conditions, the highest waves will break and the wave period increases. For the case of a composite slope including a berm and water level around berm height only the roughness on the upper slope seems to influence the wave overtopping discharge. The effect of the roughness elements shows a strong relation to the wave overtopping discharge. For large wave overtopping discharges, the influence becomes negligible.

For more general cases, with a shallow foreshore (h/H$_{m0}$ < 4) and a composite slope including a berm, is suggested to adjust the equation of Capel (2015) to predict the average wave overtopping discharge. The adaptations are the

area over which the roughness influence factor is taken into account, the wave steepness and an extra influence factor for the wave conditions on a shallow foreshore.

<div align="right">

9

Recommendations

</div>

This chapter is divided into two parts. The first part will explain how the modelling with SWASH can be improved. The second part will focus on the improvement of the model setup to obtain better data which can be used to understand the physical processes during run-up and wave overtopping better. This knowledge can be used to predict the wave overtopping more accurate in the future.

9.1. Recommendations wave model in SWASH

In SWASH there are some uncertainties regarding the wave parameters that might be interesting for further research. Also, regarding the repeatability of the tests and the application of the computational model to simulate the wave flumes some recommendations are presented in the next section.

9.1.1. Further research wave parameters

The results of the significant wave height from SWASH showed variations. It is not clear if these variations are real or if they are a numerical effect. In the discussion already some causes are discussed. However, for the trapped infragravity waves and the combination of shoaling and breaking, extra SWASH simulations might give more insight. From these SWASH runs it could be possible to exclude or confirm the cause of these variations. These extra simulations are therefore recommended for further research.

Trapped infragravity waves

Waves can be trapped when the outgoing wave is reflected by a sudden depth change of the foreshore, redirecting it back to the foreshore. The flat part of the foreshore will act like a semi-enclosed basin. If the wiggles are caused by trapped infragravity waves, the wiggles will not occur if the flat part of the foreshore is removed since the waves will not be reflected by the foreshore and there is no sudden decrease in water depth. For that reason is suggested to perform extra tests with a bottom profile as shown in figure 9.1.
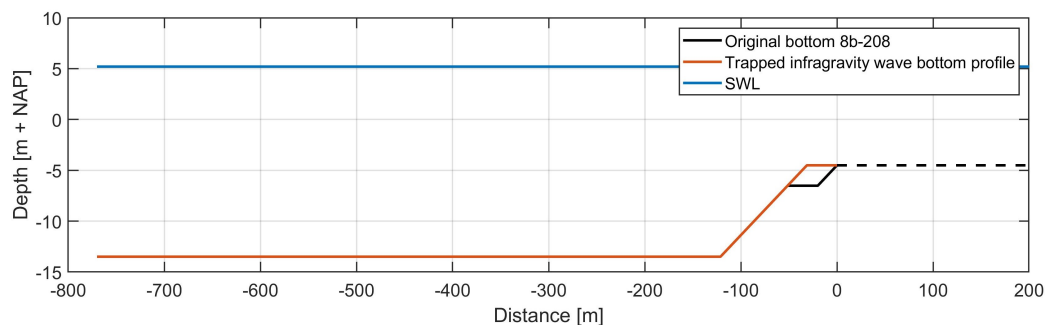
Figure 9.1: Check cause of variations in significant wave height by adjusting bottom profile

Shoaling and breaking

Since the relative water depth seems to be an important parameter for the existence of the wiggles. The wiggles might be related to the effect of shoaling and breaking of the waves. Turning off the breaking function in SWASH, shows which part of the wiggle is caused by breaking of the waves.

Wave period

The peak period of the JONSWAP spectrum is expected to remain constant. However, the spectral analysis shows that the peak of the frequency energy density spectrum jumps to another frequency. Smoothing the peak wave period can not eliminate this effect. To increase the resolution of the frequency energy density spectrum, the time duration of the tests can be increased. This increases the accuracy of the wave period.

9.1.2. Bottom friction

In the test cases of SWASH the bottom friction between the two scales is kept constant. For further research it is recommended to modify this parameter. By changing the bottom friction in the wave model the deviation between the measurements in the wave flume and the computational wave model might decrease. Furthermore, keeping the bottom friction constant between the two scales might result in scale effects.

9.1.3. Repeatability of the tests

The average wave overtopping discharge depends mainly on the few highest waves of the imposed wave signal. This makes it interesting to impose the same scale down wave signal between the two flumes for the comparison of the average wave overtopping discharge. Also, it would be interesting to impose the same wave signal in SWASH to derive $H_{2\%}$ at different locations. Expected is that $H_{2\%}$ is more sensitive to the wave signal since it only depends on the highest few waves.

9.2. Recommendations model setup wave flume

Based on the executed tests in the wave flume it is very hard to determine the effect of different elements of the structure on the average wave overtopping discharge. Based on this test setup it is impossible to determine the roughness of the upper slope. To get more insight into the effect of the different elements a systematic approach is described below. If the following test cases are executed, the influence of different parameters on the wave overtopping discharge can be investigated. Furthermore, recommendations regarding the locations of the wave gauges are provided and additional measurements are proposed. Finally, recommendations regarding scale effects and model effects are given.

9.2.1. Structural parameters

From the test cases the effect of the following combinations will be investigated.

- Effect of the berm width
- Effect of roughness elements on the upper slope
- Effect of roughness elements on the lower slope
- Combined roughness
- Effect of combination of berm and roughness elements
- Effect of foreshore

The first step is to assign the effect of the berm width on the wave overtopping discharge. This would be a case without foreshore, no roughness elements on the lower slope and upper slope. Different berm widths will be tested under the same hydraulic conditions. In this way the berm influence factor can be estimated.

The next step will be the investigation of the ribs on the wave overtopping discharge. In this case there is no foreshore, no roughness elements on the lower slope, no berm and only ribs on the upper slope. Test can be executed with different protrusion, number of ribs and density of the ribs. This is similar as the study of Capel (2015). Added value can be created by testing ribs with different shapes.

Then the effect of the Xbloc^{plus} at the lower slope on the average wave overtopping discharge will be investigated. During these tests the effect of the foreshore will again be excluded, the upper slope will be smooth and there will be no berm in the structure.

The combined roughness influence will be investigated by applying the Xbloc^{plus} on the lower slope and ribs on the upper slope. In this way can be tested if the equation of the combined roughness take the correct area over which the roughness is effective into account. Also, the location weighting factor can be fitted.

Since it is still unknown if the reduction factor of the berm and the roughness reduction are independent of each other, tests will be performed including a berm and roughness elements on the lower slope and upper slope. This results in the combined effect of a berm and roughness on the wave overtopping discharge.

Finally, foreshores can be added to the test cases to validate the importance of the water depth at the foreshore in reducing the average wave overtopping discharge. Also, the effect of the local wave steepness on the average wave overtopping discharge can be determined.

It is very important that one structural parameter is isolated between the different tests. Otherwise it is impossible to appoint the effect of one parameter to wave overtopping discharge.

9.2.2. Relation wave overtopping discharge and roughness elements
Yet the roughness influence factor of roughness elements is assumed to be constant. This originated from the wave overtopping limits that were maintained for flood protection of the Netherlands. The average wave overtopping discharge was limited to 1 l/m/s. In these situations, the roughness elements act very rough and the roughness influence factor is almost constant. From figure 6.12 is evident that the roughness influence factor of the roughness elements depends on the wave overtopping discharge until 20 l/m/s. Since the limits for the wave overtopping discharge are less strict, more research is needed to the relation between the average wave overtopping discharge and the roughness influence factor.

9.2.3. Relation between blocking influence factor and wave overtopping discharge
Several adjustments have been applied to the method of Capel (2015) to predict the average wave overtopping discharge more accurately. The method which replaced the roughness influence factor by the blocking factor did not achieve the smallest root mean square error. However, the results looked promising since the spread in the calculated influence factor shows the same spread as the fitted influence factor.

More research might be done to this blocking influence factor. Also, research should be done to, the height of the rib that actually blocks the run-up.

9.2.4. Measurements
Using the wave conditions at the toe of the structure should result in a better prediction of the wave overtopping discharge. The results of SWASH showed 3% deviation compared to the measurements in the wave flume on the foreshore. However as described in the discussion, the effect of the reflected wave on the wave breaking in front of the structure is not known. The best option to include all these processes is to install an array of three wave gauges at the toe and in front of the toe of the structure.

Expected is that the flow depth of the run-up is a very important parameter in the roughness influence of the ribs. Therefore it is recommended to perform during these tests extra measurements to the flow depth of the run-up.

Besides the average wave overtopping discharge, the individual wave overtopping volume is an interesting parameter. Since the limited water depth on the foreshore affects the Rayleigh distribution, more waves are required to arrive at the same overtopping volume in shallow water than at deep water conditions at the foreshore. Therefore it might be interesting to relate the individual wave overtopping volumes to the distribution of the wave height.

9.2.5. Model and scale effects
Regarding the model effects, the upper slope is the main uncertainty. It is recommended to use on a small scale Quattroblocks as well. The shape of these blocks with the rounded corners is expected to give a very different flow pattern over the ribs compared to the squared corners of the rectangular ribs. It might also be interesting to investigate the effect of the shape of the ribs on the wave overtopping discharge and relate this to a discharge coefficient like with the weirs.

One of the scale effects that could not be investigated with the used test setup, was the air entrainment in the run-up. Hence it might be interesting to make slow-motion videos of the wave breaking. So the volume of air in the run-up can be determined and the influence of the flow depth of the run-up on the average wave overtopping discharge can be investigated.

Bibliography

Ahrens, J. and Ward, D. (1991). Performance of Bermed Revetments. *Journal*, 117(5).

Amruthure, S., Udoyara, S., and Rao, M. (1988). Characteristics of Square-Edged and Round-Nosed Broad-Crested Weirs. *Journal of Irrigation and Drainage Engineering*, 114(1):61–73.

Azimi, A. H. and Rajaratnam, N. (2009). Discharge characteristics of weirs of finite crest length. *Journal of Hydraulic Engineering*, 135(12):1081–1085.

Battjes, J. (1974). Surf Similarity. In *Proceeding 14th International Conference on Coastal Engineering*, pages 466–480, Copenhagen.

Battjes, J. A. and Groenendijk, H. W. (2000). Wave height distributions on shallow foreshores. *Coastal Engineering*, 40(3):161–182.

Blenkinsopp, C. E. and Chaplin, J. (2007). Validity of small-scale physical models involving breaking waves. *22nd International workshop on water waves and floating bodies*, (April):13–16.

Blenkinsopp, C. E. and Chaplin, J. R. (2011). Void fraction measurements and scale effects in breaking waves in freshwater and seawater. *Coastal Engineering*, 58(5):417–428.

Buckley, M. L. and Lowe, R. (2018). Mechanisms of Wave-Driven Water Level Variability on Reef- Fringed Coastlines. *Journal of Geophysical research: Oceans*, (May).

Capel, A. (2015). Wave run-up and overtopping reduction by block revetments with enhanced roughness. *Coastal Engineering*, 104:76–92.

Capel, A. and Klein Breteler, M. (2016). Vergelijkend onderzoek zetstenen voor dijken: Ruwheid ten aanzien van golfoverslag van steenzetting met dambordpatroon en ribbenpatroon. Technical report, Deltares.

Chen, W., Van Gent, M., Warmink, J., and Hulscher, S. (2019). The influence of a berm and roughness on the wave overtopping at dikes. *(submitted to Coastal Engineering)*, pages 1–34.

Chen, W., Warmink, J., Van Gent, M. R. A., and Hulscher, S. Experimental study on the influence of berms and roughness on wave overtopping over dikes.

Gong, J., Deng, J., and Wei, W. (2019). Discharge Coefficient of a Round-Crested Weir. 2(1).

Haringman Beton. Haringman beton Zeewering Hydroblocks.

Hasselmann, K. (1974). On the spectral dissipation of ocean waves due to white capping. *Boundary-Layer Meteorology*, 6:107–127.

Hasselmann, K., Barnett, T., Bouws, E., Carlson, H., Cartwright, D., Enke, K., Ewing, J., Gienapp, H., Hasselmann, D., Kruseman, P., Meerburg, A., Muller, P., Olbers, D., Richter, K., Sell, W., and Walden, H. (1973). Measurements of Wind-Wave Growth and Swell Decay during the Joint North Sea Wave Project (JONSWAP). *Erganzungsheft zur Deutschen Hydrographischen Zeitschrift. Reihe A(8)*, 12(8 0).

Hofland, B., Chen, X., Altomare, C., and Oosterlo, P. (2017). Prediction formula for the spectral wave period T m-1,0 on mildly sloping shallow foreshores. *Coastal Engineering*, 123:21–28.

Holcim Coastal B.V. Basalton Quattroblock.

Holthuijsen, L. H. (2007). *Waves in Oceanic and Coastal Waters*. Cambridge.

Huppes, N. (2019). *Wave overtopping and scale effects Experimental case study New Afsluitdijk. MSc thesis*. University of Technology Delft.

Kamphuis, J. W. (2015). Long Waves in Flume Experiments. 1(1):1154–1167.

Kirkegaard, J., Wolters, G., Sutherland, J., Soulsby, R., Frostick, L., McLelland, S., Mercer, T., and Gerritsen, H. (2011). Users Guide to Physical Modelling and Experimentation Experience of the HYDRALAB Network. Technical report, IAHR.

Kriebel, M. (2019). *Quantification of Grass Erosion Due to Wave Overtopping at the Afsluitdijk. MSc thesis.* Number July. Universtity of Twente.

Landa, P. M. (2014). *Wave Overtopping Resilient 'Afsluitdijk' Design Procedures for Landward Slope Erosion Stability during Large Overtopping Volume Events. MSc thesis.* University of Technology Delft.

Madsen, O. and Rosengaus, M. (1988). Spectral wave attenuation by bottom friction: Experiments. In *21ste International Conference on Coastal Engineering*, pages 492–504.

Mansard, E. P. D. and Funke, E. R. (1980). The Measurement of Incident and Reflected Spectra Using a least Squares Method. pages 154–172.

Ministerie van Infrastructuur en Milieu (2016a). Natura 2000-beheerplan Waddenzee. Technical report, Ministerie van Infrastructuur en Milieu Rijkswaterstaat Noord-Nederland.

Ministerie van Infrastructuur en Milieu (2016b). Rijksinpassingsplan Afsluitdijk Toelichting en regels. Technical report, Rijkswaterstaat.

Moreno, A. J. (2017). *Experimental study on the wave overtopping performance of Xbloc+ armour unit. MSc thesis.* University of Technology Delft.

Owen, M. (1980). Design of seawalls allowing for wave overtopping. *Hydraulic Research Wallingford, UK.*

Reedijk, B., Eggeling, T., Bakker, P., Jacobs, R., and Muttray, M. (2018). Hydraulic Stability and Overtopping Performance of a New Type of Regular Placed Armor Unit. *International Conference on Coastal Engineering*, 1(36):54.

Reedijk, B., Eggeling, T., Muttray, M., Bakker, P., and Jacobs, R. (2019). Hydraulic Stability and Overtopping Performance of a New Type of Regular Placed Armor Unit. *Coastal Engineering Proceedings*, 1(36):54.

Schüttrumpf, H. and Oumeraci, H. (2005). Layer thicknesses and velocities of wave overtopping flow at seadikes. *Coastal Engineering*, 52:473–495.

Steendam, G. J., Van der Meer, J. W., Verhaeghe, H., Besley, P., Franco, L., and Van Gent, M. R. (2004). The international database on wave overtopping. In *International Conference on Coastal Engineering*, number 29.

The SWASH team (2014). User Manual SWASH version 2.00A. Technical report.

UNESCO Centre (2019). Wadden Sea World Heritage.

Van der Meer, J. (2002). Technisch rapport Gofloploop en golfoverslag bij dijken. Technical report, Technische Adviescommissie voor de Waterkeringen.

Van der Meer, J., Allsop, N., Bruce, T., Kortenhaus, A., Pullen, T., Schüttrumpf, H., Troch, P., and Zanuttigh, B. (2018). EurOtop Manual on wave overtopping of sea defences and related structures An overtopping manual largely based on European research, but for worldwide application Second Edition 2018. Technical report.

Van der Meer, J. and Bruce, T. (2013). New Physical Insights and Design Formulas on Wave Overtopping at Sloping and Vertical Structures. *Journal of Waterway, Port, Coastal, and Ocean Engineering.*

Van der Meer, J. and Janssen, J. (1994). Wave run-up and wave overtopping at dikes and revetments. Technical Report 485, Delft Hydraulics.

Van der Meer, J. W. (1998). *Wave run-up and overtopping.*

Van Gent, M. Delta flume / Deltagoot.

Van Gent, M. (2017). Scheldt flume / Scheldegoot.

Verhaeghe, H., De Rouck, J., and Van der Meer, J. (2008). Combined classifier-quantifier model: A 2-phases neural model for prediction of wave overtopping at coastal structures. *Coastal Engineering*.

Vrouwenvelderk, A. and Struik, P. (1990). Dike design safety philosophy. In *Coastal Engineering*, pages 1254–1267.

Zelt, J. A. and Skjelbreia, J. E. (1992). Estimating Incident and Reflected Wave Fields Using an Arbitrary Number of Wave Gauges. *Coastal Engineering*, pages 777–789.

Zijlema, M., Stelling, G., and Smit, P. (2011). SWASH: An operational public domain code for simulating wave fields and rapidly varied flows in coastal waters. *Coastal Engineering*, 58(10):992–1012.

Zijlema, M. and Stelling, G. S. (2005). Further experiences with computing non-hydrostatic free-surface flows involving water waves. *International Journal for Numerical Methods in Fluids*, 48(2):169–197.

List of Figures

List of Tables

A
SWASH

A.1. Settings model

SWASH makes use of a command file. This command file should include all the input parameters to run the simulation and return the desired results. In this section the choice for different settings and input parameters the SWASH command file is explained. Also the processing of the SWASH results to the results which are showed in the report is explained. The standard SWASH input file can be found in section A.3.

A.1.1. Bottom profile and boundary conditions

The SWASH model is configured in 1D-modus and makes use of three vertical layers which are equally distributed over depth. The used scheme receives good linear dispersion up to kd is approximately 16 at 1 % error in phase velocity of the primary waves. With a water depth of approximately 19 meter and a mean wave period of 6.75 seconds gives a kd of approximately 1.7. The bottom profiles that are applied for the different cases are presented in figure 4.5. Beyond the toe the bottom profile continuous horizontally and a sponge layer of 150 meter is added to prevent reflection of waves. This sponge layer is indicated with a dashed line and a grey square in figure 4.4. The reflection caused by the foreshore is checked with the method of Zelt and Skjelbreia. This is explained in section A.2.2. On the other side a wave generating boundary condition is present. The area of interest, located between the deep water location and the toe of the construction, should be located two wave lengths away from the boundary conditions. For this case the deep water wave length is roughly 75 meter, for a mean wave period of 7 seconds. So the area of interest should be located 150 meter of the boundaries.

A.1.2. Wave conditions and calibration

To express the irregular wave field by means of a wave spectrum the JONSWAP spectrum with a peak enhancement of 3.3 is used. The peak enhancement factor of 3.3 is often applied for young sea state which means that the sea is in a developing state. This is the case for storm conditions according the research of Hasselmann et al. (1973).

The wave conditions at the deep water are calculated with SWAN using the prescribed wave conditions at the Hydra-NL point. The wave conditions at deep water are called the target wave conditions. In order to attain the deep water wave conditions a calibration step is performed, so that the wave conditions imposed at the wave paddle in SWASH result in the target wave conditions at deep water. The deviation between the simulated and the target values of the significant wave height and the peak period at deep water are maximum 1%. The calibration step returns a larger significant wave height and peak period at the wave paddle than the deep water wave conditions. The calibration makes use of an underrelaxation factor α. The equations to calculate the new input conditions at the wave paddle used in the calibration are presented below.

$$H_{m0,wavepaddle,new} = H_{m0,wavepaddle} \cdot (\frac{(H_{m0,target} - H_{m0,deepwater})}{H_{m0,target}} \cdot (1 - \alpha) + 1) \tag{A.1}$$

$$T_{p,wavepaddle,new} = T_{p,wavepaddle} \cdot (\frac{(T_{p,target} - T_{p,deepwater})}{T_{p,target}} \cdot (1 - \alpha) + 1) \tag{A.2}$$

An example of the decrease in significant wave height from the wave paddle to deep water is presented in figure 5.3.

A.1.3. Space and time

SWASH makes use of a Cartesian coordinate system. The spatial resolution is 0.5 meter on prototype scale. According to The SWASH team (2014) for low waves ($H_{m0}/d \ll 1$) at least 50 grid cells per peak wave length are needed to achieve a sufficient spatial resolution. For the tested cases there are approximately 150 to 200 grid points per peak wave length provided. The grid size is linear scaled to the model scale of the flumes. Initially SWASH makes use of a time step of 0.00025 second. This time step increases automatically when possible to satisfy the CFL condition. The duration of the model is based on the time it takes to generate approximately 1000 waves. On prototype scale this means a simulation duration of 2 hours. The output parameters are calculated over the total duration of the simulation minus the time of the spin up effect. According to the SWASH manual a spin up time

of 10 to 15 % of the total simulation duration is suggested. However, looking at the surface elevation in figure A.1 a spin up time of approximately 5 minutes would be appropriate.

A.1.4. Other settings

Wave breaking uses the default settings with an α value of 0.6, which indicates the maximum local surface steepness and determines the onset of the breaking process. To simulate breaking waves a numerical method that conserves momentum is preferred, so the properties under breaking waves are modelled correctly. The momentum equations use the upwind discretization method. The threshold parameter at which wave breaking stops is indicated with β and has a a default value of 0.3. The bottom friction is kept constant between the models and has a Manning value of 0.018.

A.2. Processing output

The purpose of using SWASH is to determine the incident wave conditions at different locations in the spatial domain. The following steps are carried out to achieve these conditions. First, the spin up of the model is checked, afterward the reflection coefficient is calculated. After that the parameters for the spectral analysis and the time domain analysis are defined.

A.2.1. Surface elevation signal

The surface elevation produced by SWASH is used for the time domain analysis, spectral analysis and for the determination of the reflection coefficient. Therefore some important characteristics will be showed below.
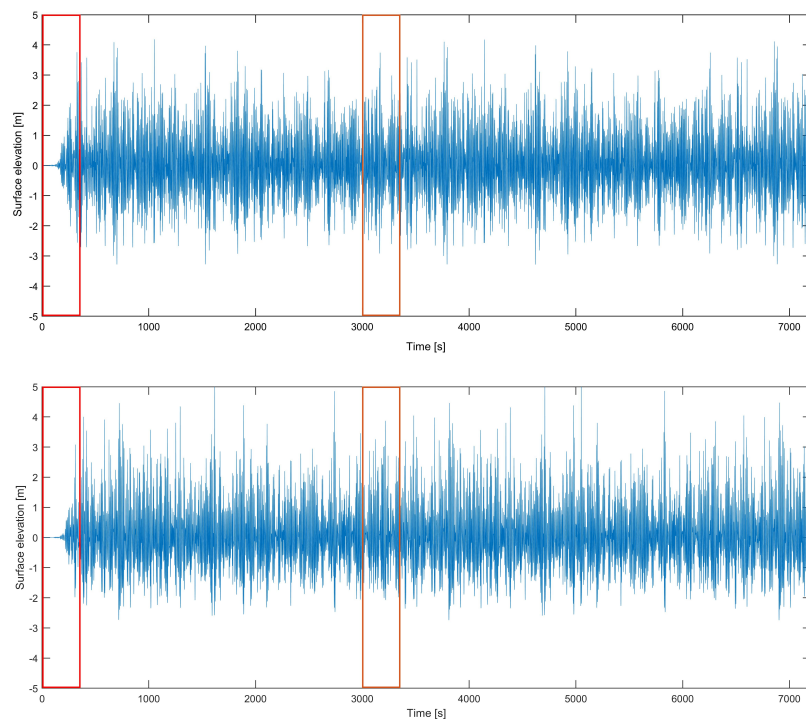
Figure A.1: Surface elevation signal at deep water (upper) and at the foreshore (lower). Spin up of the model indicated with the red box and detail of surface elevation in the orange box.

Spin up

Looking at the surface elevation signal at one of the wave gauges on the foreshore, it becomes visible the system needs some time to spin up. The spin up time is estimated to be approximately 5 minutes on the prototype scale. The spin up time is cut off from the surface elevation signal to achieve better results.

Non-linearities

If a closer look is taken at the surface elevation signal, it becomes visible that the waves at the foreshore are no longer sinusoidal. The waves are non-linear and cnoidal. Figure A.2 shows the comparison between waves at deep water and at the foreshore. The waves at the foreshore have wider troughs and steeper crests than the waves at the deep water.
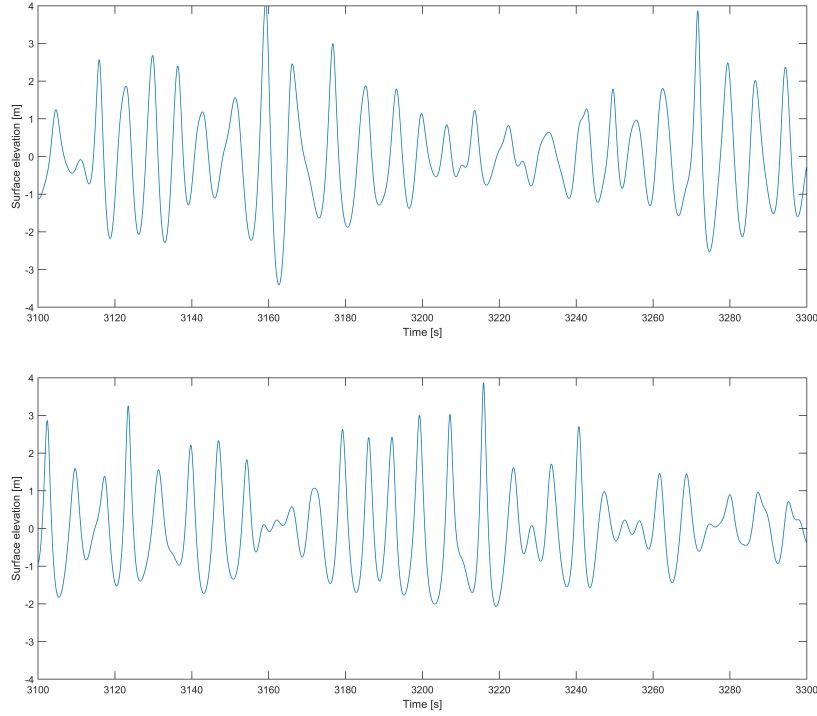

Figure A.2: Detail of the surface elevation at deep water (upper) and foreshore (lower)

A.2.2. Reflection

Waves propagating over the foreshore might be reflected to some degree by the slopes that are present in the bottom profile, although the presence of the sponge layer. The wave motion is the sum of the incoming wave and the reflected wave. The method by Zelt and Skjelbreia (1992) describes a mehtod to split the incoming wave height and the reflected wave height. This method is based on linear wave theory, but waves approaching shallow water deviate from the linear wave theory. As waves enter shallow water the wave profile evolves from sinusoidal to a profile with flatter troughs and sharper crests. The waves are symmetrical about their vertical axis and non-symmetrical about the horizontal axis. Consequently the used method is not able to describe the measured wave profile in shallow water (Hydra-NL and the toe of the structure) accurately. Based on the wave conditions on deep water an estimate of the reflection coefficient can be made, see equation A.3.

$$c_{reflection} = \frac{\sqrt{m_{0r}}}{\sqrt{m_{0i}}} = \frac{H_r}{H_i} \tag{A.3}$$

The use of equation 3.2 resulted in a reflection coefficient between 7% to 8% for the different bottom profiles. The effect of the reflection between the total wave height and the incoming wave height is smaller than 1%. This difference is considered to be insignificant and therefore during the rest of the research will be assumed that $H_{m0,T} = H_{m0,i}$.

$$H_{m0,T} = \sqrt{H_{m0,i}^2 + H_{m0,r}^2} \tag{A.4}$$
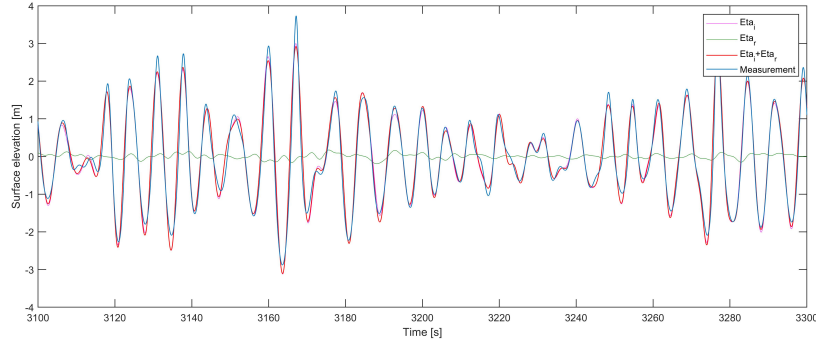
Figure A.3: Detail of surface elevation split in incoming and reflected

A.2.3. Spectral analysis

Only one wave record of two hours is simulated in SWASH for each of the different tested cases. If this record is used in the spectral analysis to estimate the variance density. The variance density is based on only one amplitude. This results in large errors, order 100 %. The error can be decreased, but this is at the cost of the spectral resolution. To decrease the error, the time record is divided into a number of blocks (p). On these blocks a Fourier transformation is performed and the density variance is determined. According Holthuijsen (2007) the duration of the blocks should be 15-30 minutes and the wave record should be divided in 20-30 blocks for typical observations at sea. However, the used signal has only a duration of 2 hours, and a high sampling frequency of 10 Hz. Therefore the decision is made to make 12 non-overlapping blocks of 10 minutes. Which is approximately an average over 80 waves per block. This gives a compromise between an acceptable spectral resolution and an acceptable reliability. The resolution will be 0.02 Hz and the error is decreased to 29 percent, calculated with respectively equation A.5 and equation A.6.

$$\delta f = p \Delta f \tag{A.5}$$

$$error = \frac{100\%}{\sqrt{p}} \tag{A.6}$$

Another phenomenon that should be considered is the Nyquist frequency. Around the Nyquist frequency the energy of the high frequency is added to the energy density of the low frequency. The energy of the high frequency appears at the wrong frequency. If the Nyquist frequency is chosen correctly it will not effect the main part of the frequency spectrum. Recommended is to have a Nyquist frequency larger than 4 to 5 times the mean frequency. In the tested cases the Nyquist frequency is around 5 and the mean wave frequency is approximately 0.15. Assumed is that main part of the frequency spectrum is not effected.

$$f_{Nyquist} = \frac{1}{2\Delta t} \tag{A.7}$$

Based on the variance density spectrum the significant wave height, spectral mean wave energy period and the peak period are determined. The moments of the variance density spectrum are determined with equation A.8.

$$m_n = \int_{1/5 \cdot f_p}^{3 \cdot f_p} f^n E_f df \tag{A.8}$$

The significant wave height and the spectral mean wave energy period are determined on these moments, respectively equation A.9 and equation 3.3.

$$H_{m0} = 4\sqrt{m_0} \tag{A.9}$$

$$T_{m-1,0} = \frac{m_{-1}}{m_0} \tag{A.10}$$

A.2.4. Time domain analysis

The time domain analysis is based on the time series of the surface elevation signal. In the time domain analysis a time step is used as threshold, to eliminate very small waves from the results. The time domain analysis is performed at the location of the wave gauges. The time domain analysis searches for zero up-crossings to determine the individual waves. From the time domain analysis $H_{2\%}$ is derived, which is the wave height that is only exceeded by 2% of the waves.

A.3. Input file

Below an example of one of the used input files is showed. In *Italic* the function of the settings of the input file is explained.

```
$***********HEADING***********************************
$
$ Project name
PROJ 'AFSLUITDIJK' 'DELTA'
$
$***********MODEL INPUT********************************
$
$ Error level, above this value calculation will not start
SET MAXERR=10000
$
$ One dimensional mode
MODE DYN ONED
$
$ Still water level
SET LEVEL 1.8949
$
$ Discretization computational grid
CGRID -261.0169 0.  0.  345.7627 0.  2040 0
$
$ Number of vertical layers
VERTICAL 3
$
$ Address bottom input grid
INPGRID BOTTOM -261.0169 0.  0.  2040 0 0.1695 0.
$
$ Reads bottom input file
READINP BOTTOM -1.  'bottom_8b_208sc2.bot' 1 0 FREE
$
$ Initial velocity component set to zero
INIT zero
$
$ Define boundary conditions
BOU SHAPE JONSWAP PEAK
$
$ Define JONSWAP spectrum BOU SIDE W CCW BTYPE WEAK SMOO 30 SEC CON SPECT 1.75
4.32 0 0 30 MIN
$
$ Sommerfeld radiation boundary
BOU SIDE E CCW BTYPE RADIATION
$
$ Add sponge layer
SPONG EAST 50.8475
$
$Bottom friction using Manning
FRIC MANNING 0.018
$
$ Control wave breaking
BREAK 0.6 0.3
$
$ Include non-hydrostatic pressure in shallow water equations
NONHYDROSTATIC BOX PREC ILU
$
```

```
$ Space discretization
DISCRET UPW MOM
$
$ Time integration
TIMEI 0.1 0.5
$
$************ OUTPUT REQUESTS *************************
$
$ Influence the output quantities
QUANT XP HEXP 100.QUANT DIST HEXP 10.
QUANT HS DUR 29.9334 MIN
$
$ Reads output locations
POINTS 'GAUGE' FILE 'points xp_8b_208sc2_refl.pnt'
$
$ Write information of parameters at certain locations to table file
TABLE 'GAUGE' HEAD 'table 8b_208_O1_24_sc2.tbl'SEC TIME XP BOTL WATL & OUTPUT 000000.000
0.058222 SEC
$
$ Write spatial distribution of specific parameters to block file
FRAME 'GRID' -261.0169 0.  0.  345.7627 0.  2040 0
BLOCK 'GRID' NOHEAD 'block 8b_208_O1_24_sc2.mat' LAY 3 TSEC TIME XP BOTL WATL &
OUTPUT 000500.000 0.11644 SEC
BLOCK 'GRID' NOHEAD 'block 8b_208_O1_24_sc2_HS.mat' LAY 3 Xp Hsig $
$ Write intermediate results
TEST 1 0
$
$ Start computation
COMPUTE 000000.000 0.000146 SEC 012000.000
STOP
```

B
Results SWASH

Here the results from SWASH are presented. The significant wave height over the spatial domain, the wave height exceedance probability of different locations and the frequency energy density spectrum of different locations is presented. In the table, the still water level and the target wave conditions are given. All the results are scaled to the prototype scale. First the results of the Scheldt flume are shown. Afterward the results of the Delta flume are shown.

B.1. Scheldt flume
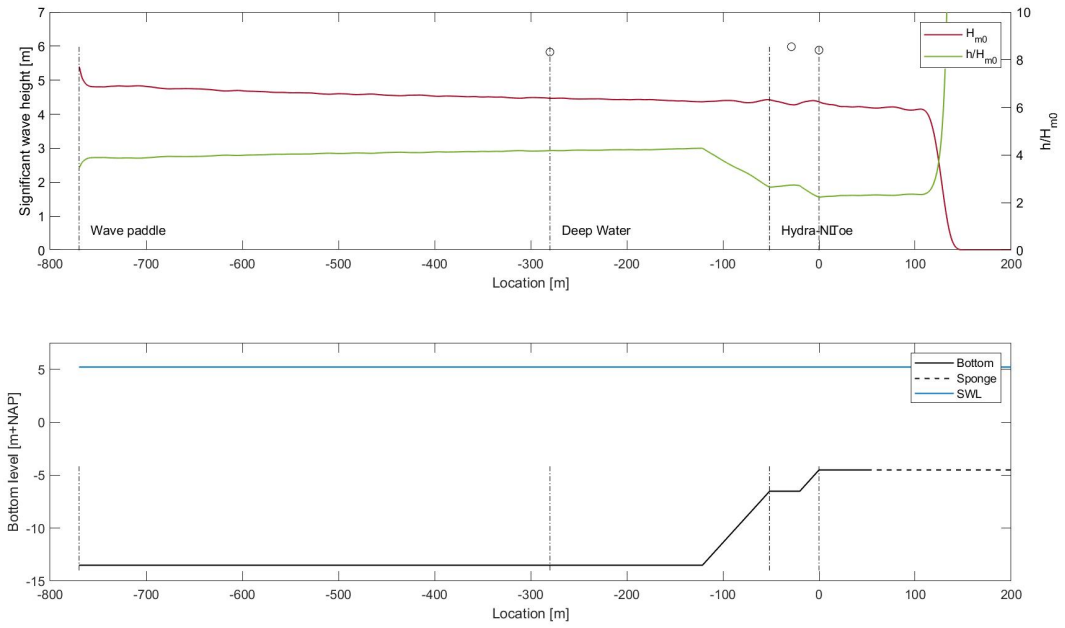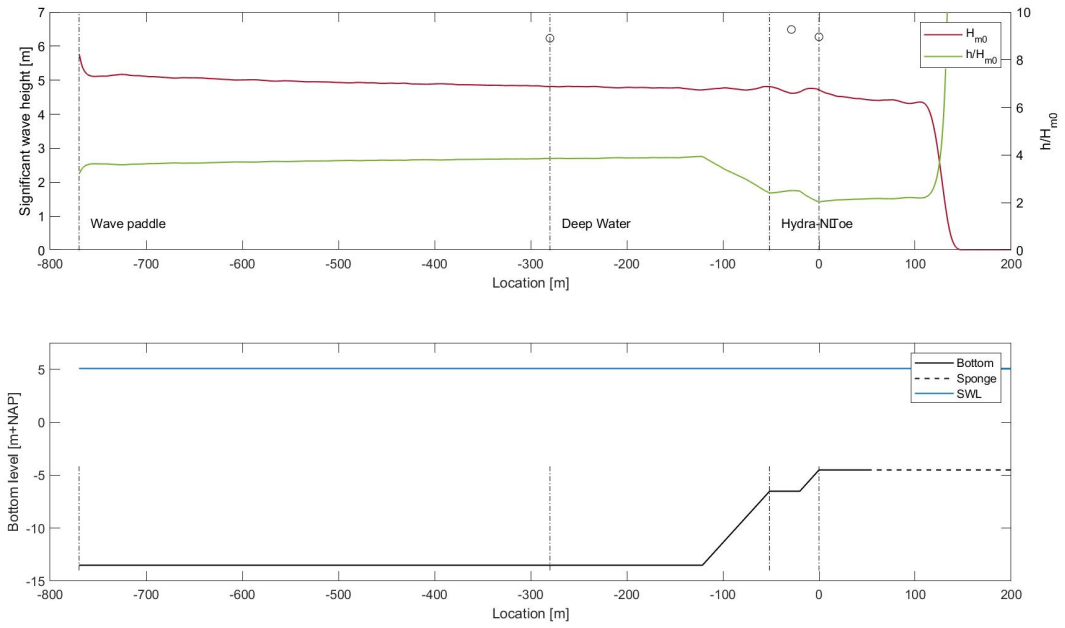## B.1.1. Bottom profile 6b-179
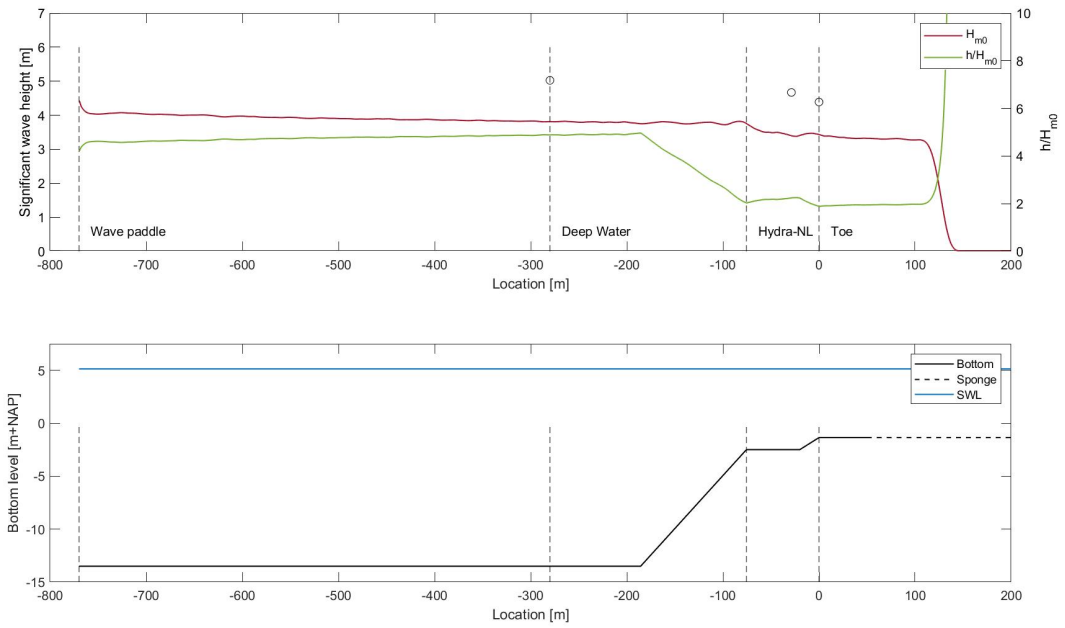
Figure B.1: Significant wave height over spatial domain
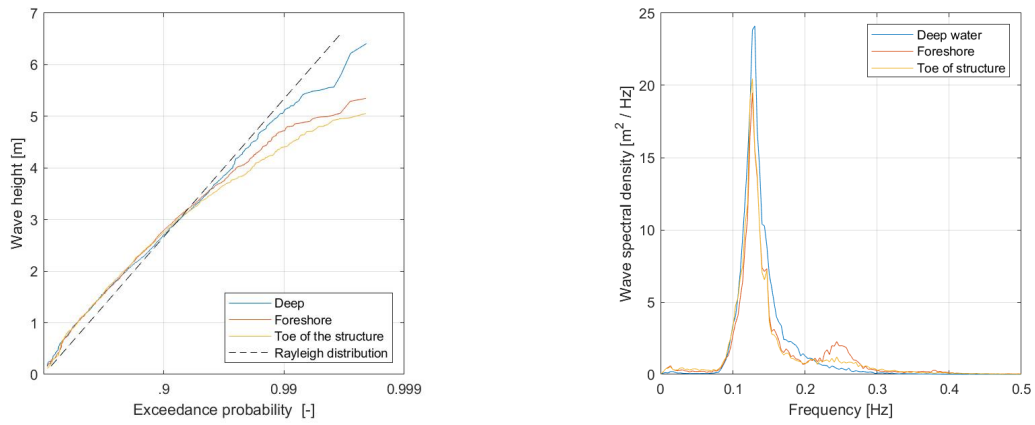
Figure B.2: Exceedance probability (left) and frequency energy density spectrum (right)

SWL [m + NAP]	H_{m0} [m]	T_p
5.13	3.68	7.75

Table B.1: Target wave conditions at deep water

B.1.2. Bottom profile 8a-179
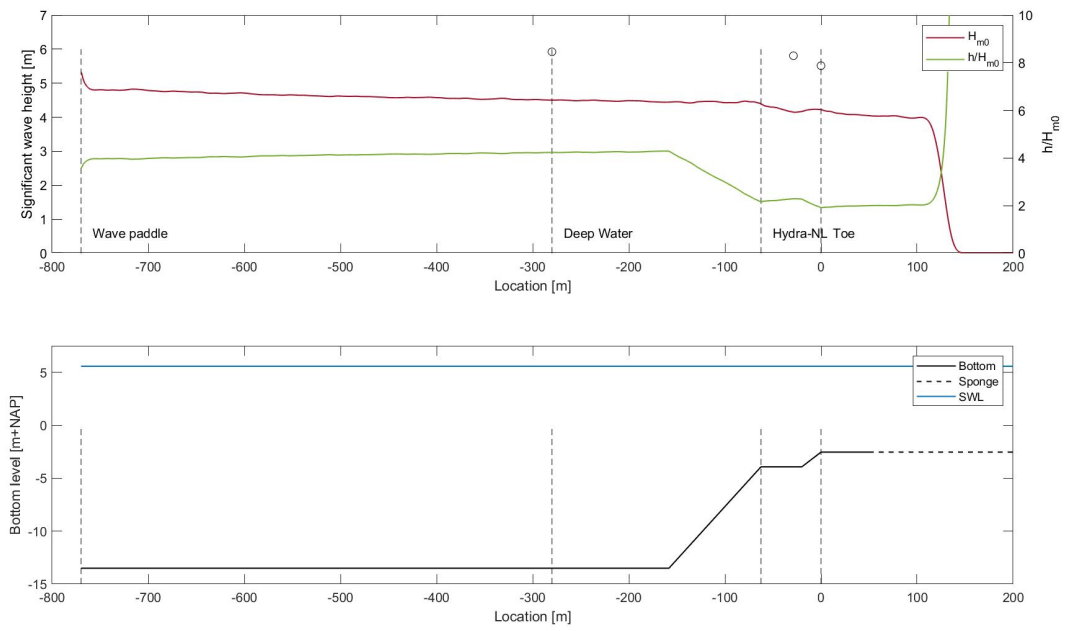
Figure B.3: Significant wave height over spatial domain
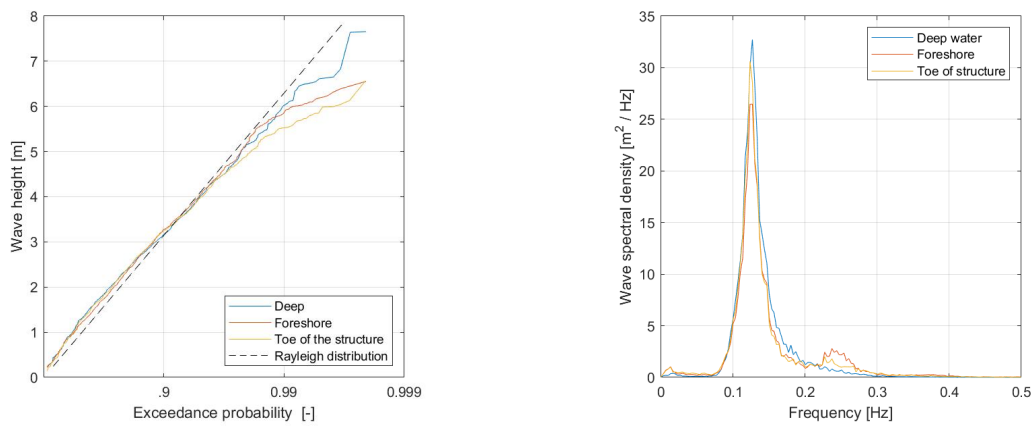
Figure B.4: Exceedance probability (left) and frequency energy density spectrum (right)

SWL [m + NAP]	H_{m0} [m]	T_p
5.57	4.36	7.9

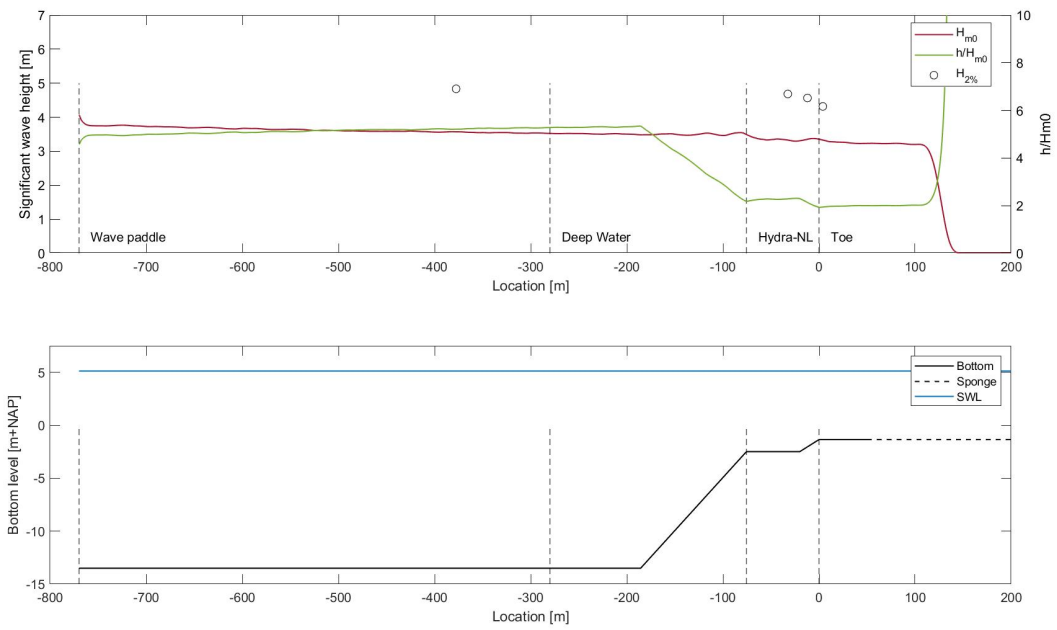Table B.2: Target wave conditions at deep water
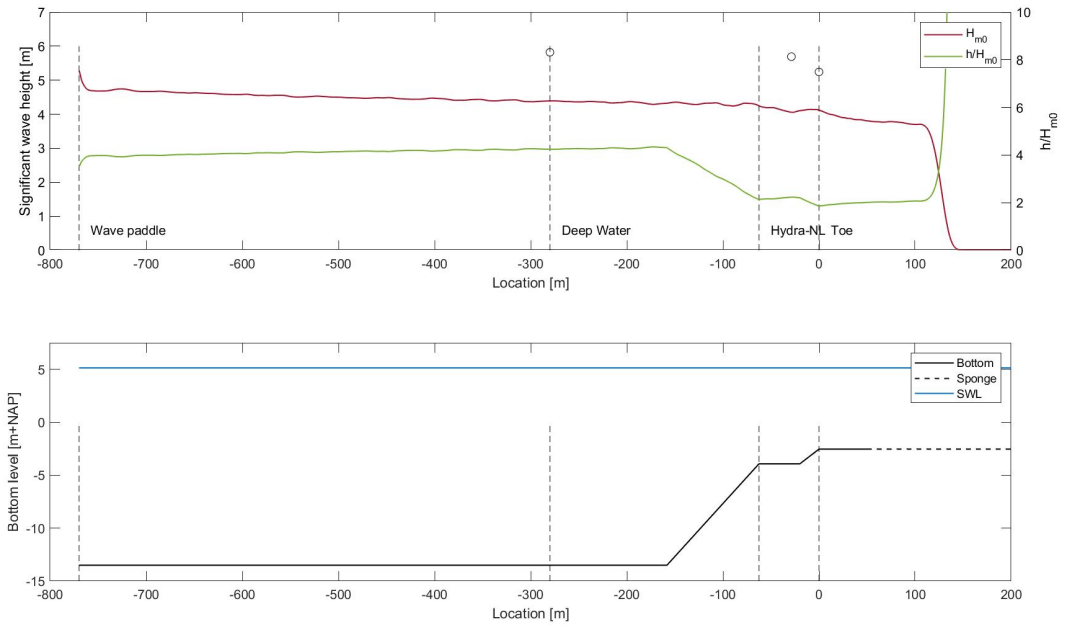
Figure B.5: Significant wave height over spatial domain
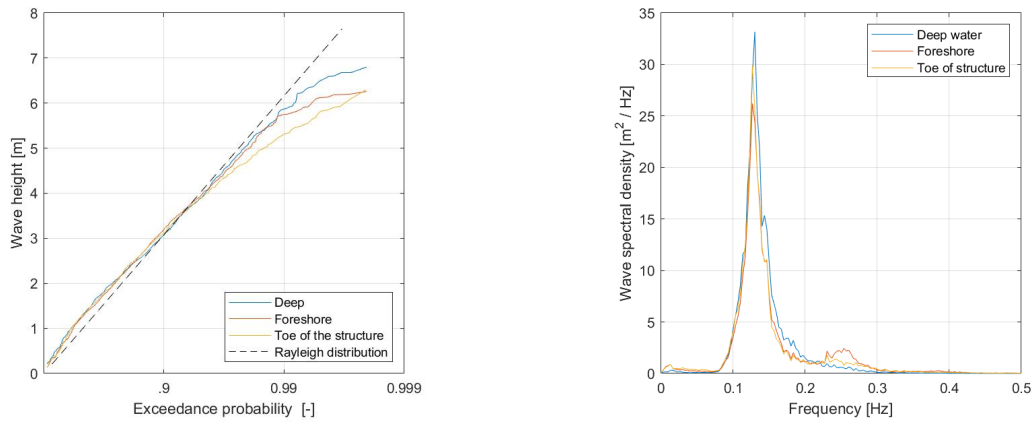
Figure B.6: Exceedance probability (left) and frequency energy density spectrum (right)

SWL [m + NAP]	H_{m0} [m]	T_p
5.13	4.21	7.56

Table B.3: Target wave conditions at deep water

B.1.3. Bottom profile 8b-208
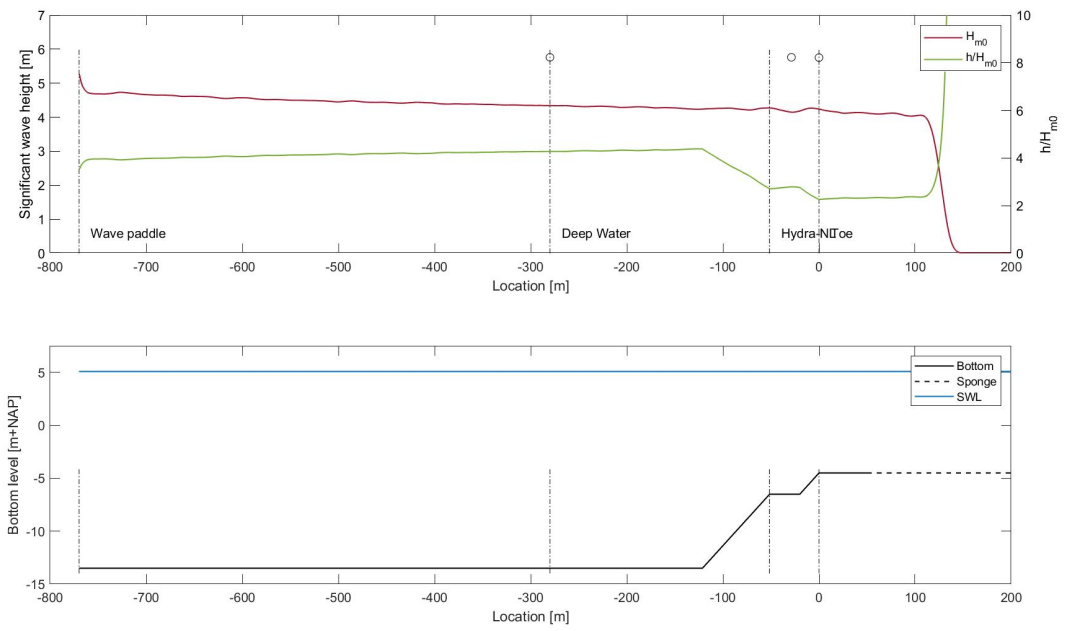
Figure B.7: Significant wave height over spatial domain
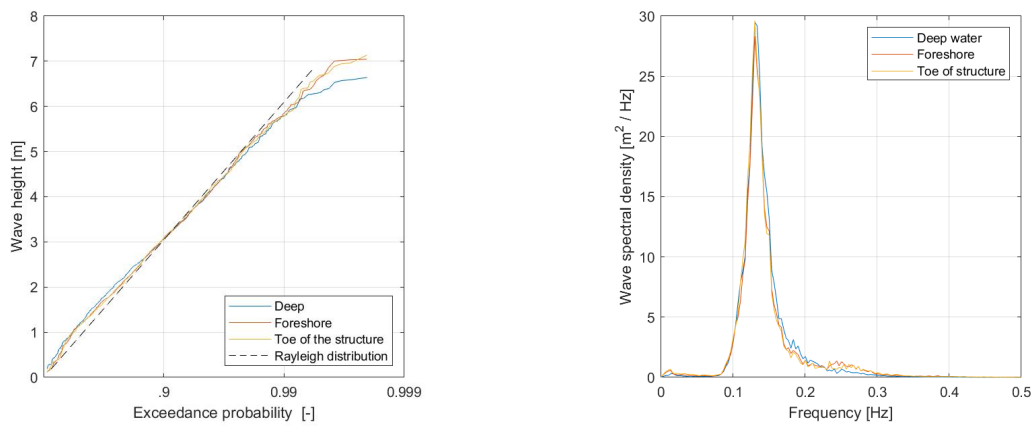
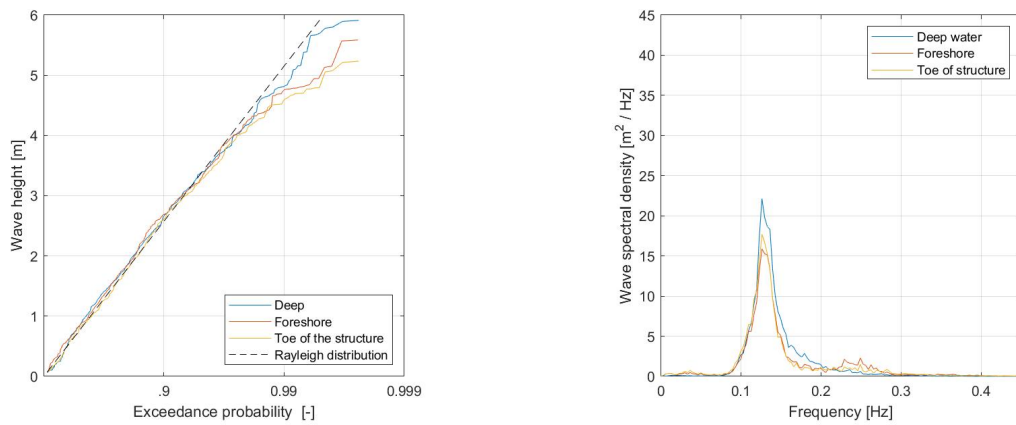Figure B.8: Exceedance probability (left) and frequency energy density spectrum (right)

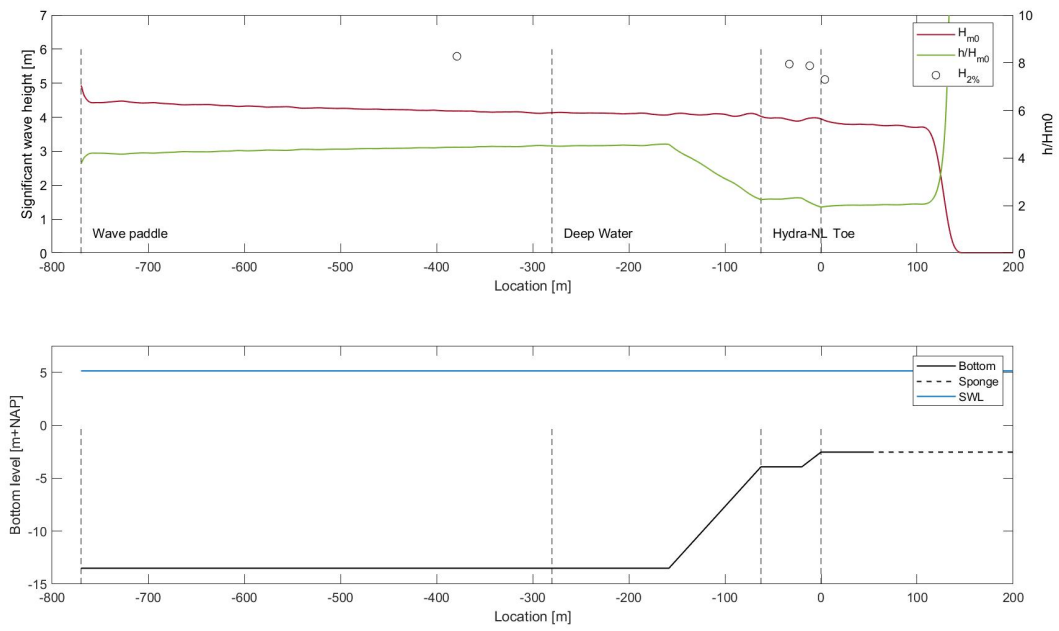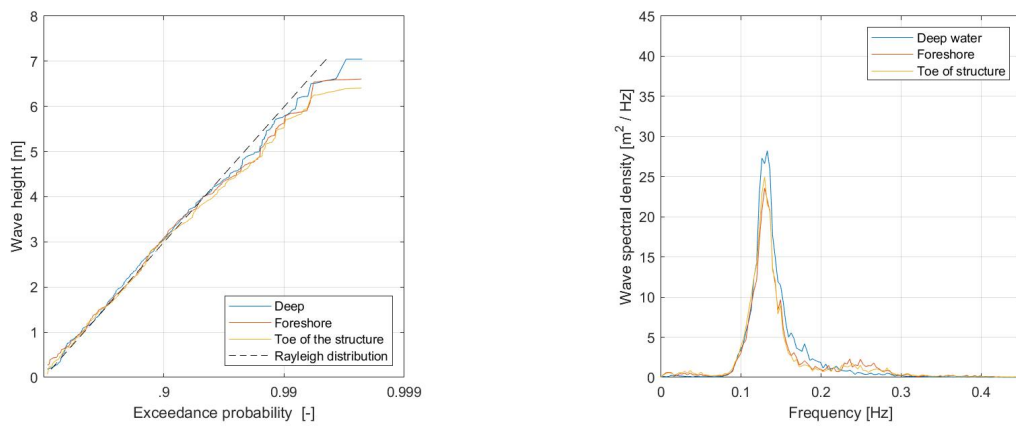| SWL [m + NAP]	H_{m0} [m]	T_p
5.07	4.21	7.56

Table B.4: Target wave conditions at deep water

Figure B.9: Significant wave height over spatial domain
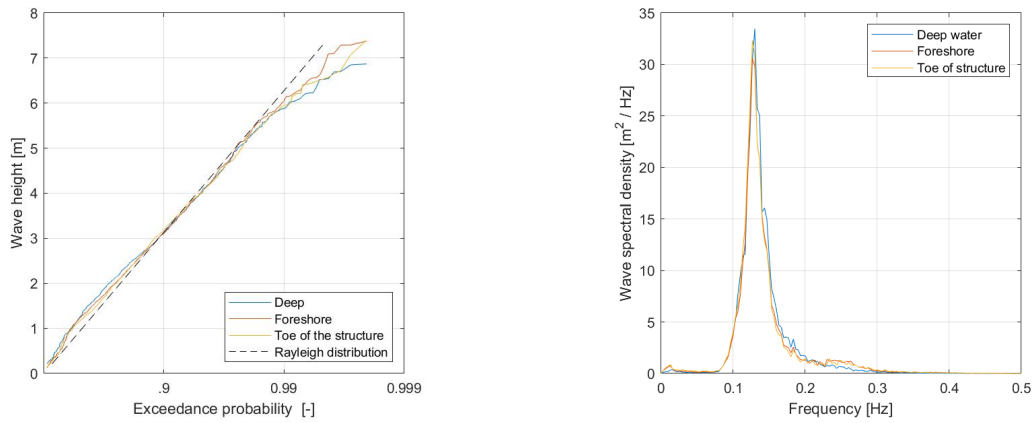
Figure B.10: Exceedance probability (left) and frequency energy density spectrum (right)

SWL [m + NAP]	H_{m0} [m]	T_p
5.21	4.33	7.63

Table B.5: Target wave conditions at deep water

Figure B.11: Significant wave height over spatial domain
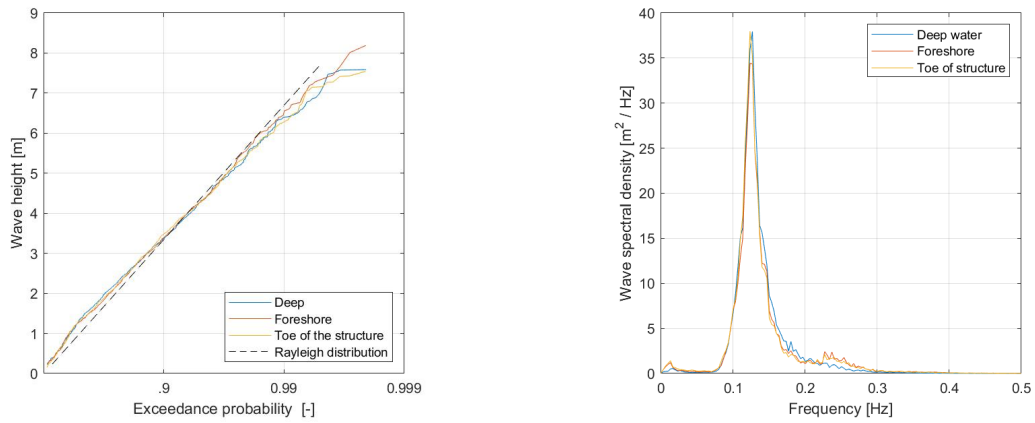
Figure B.12: Exceedance probability (left) and frequency energy density spectrum (right)

SWL [m + NAP]	H_{m0} [m]	T_p
5.07	4.63	7.93

Table B.6: Target wave conditions at deep water

B.2. Delta flume
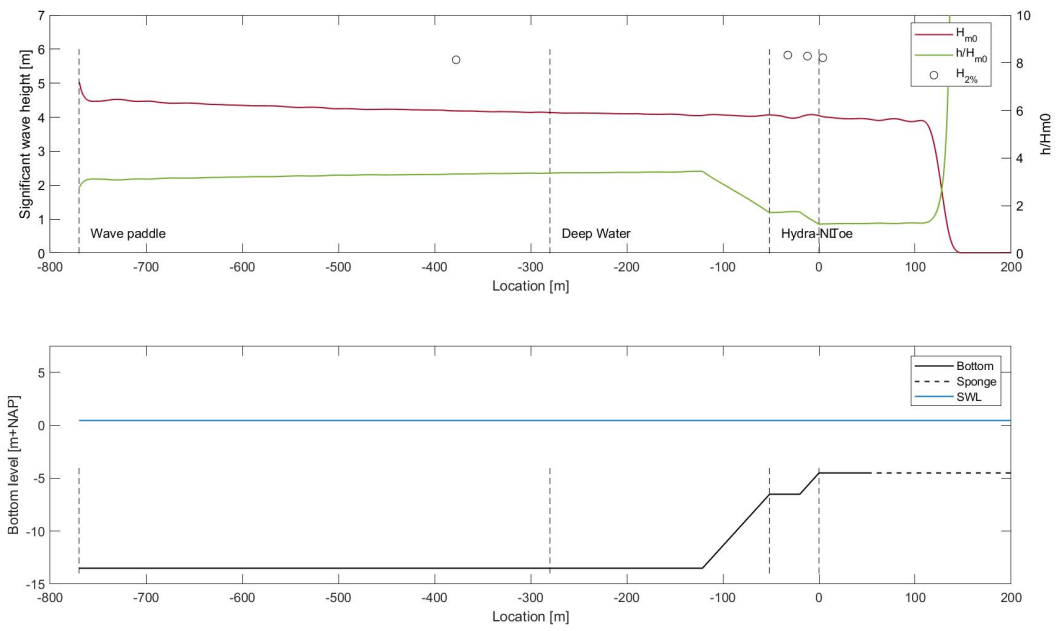### B.2.1. Bottom profile 6b-179

Figure B.13: Significant wave height over spatial domain

Figure B.14: Exceedance probability (left) and frequency energy density spectrum (right)

SWL [m + NAP]	H_{m0} [m]	T_p
5.12	3.60	7.75

Table B.7: Target wave conditions at deep water

B.2.2. Bottom profile 8a-179

Figure B.15: Significant wave height over spatial domain

Figure B.16: Exceedance probability (left) and frequency energy density spectrum (right)

SWL [m + NAP]	H_{m0} [m]	T_p
5.12	4.21	7.69

Table B.8: Target wave conditions at deep water

B.2.3. Bottom profile 8b-208

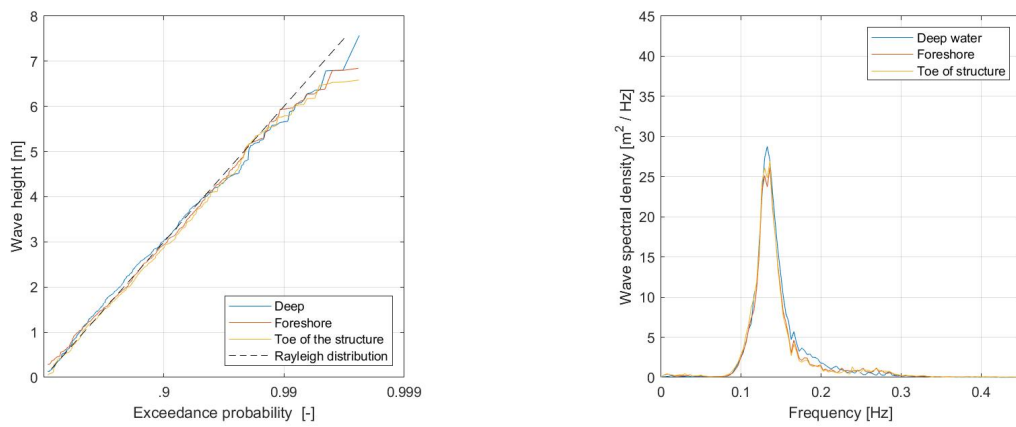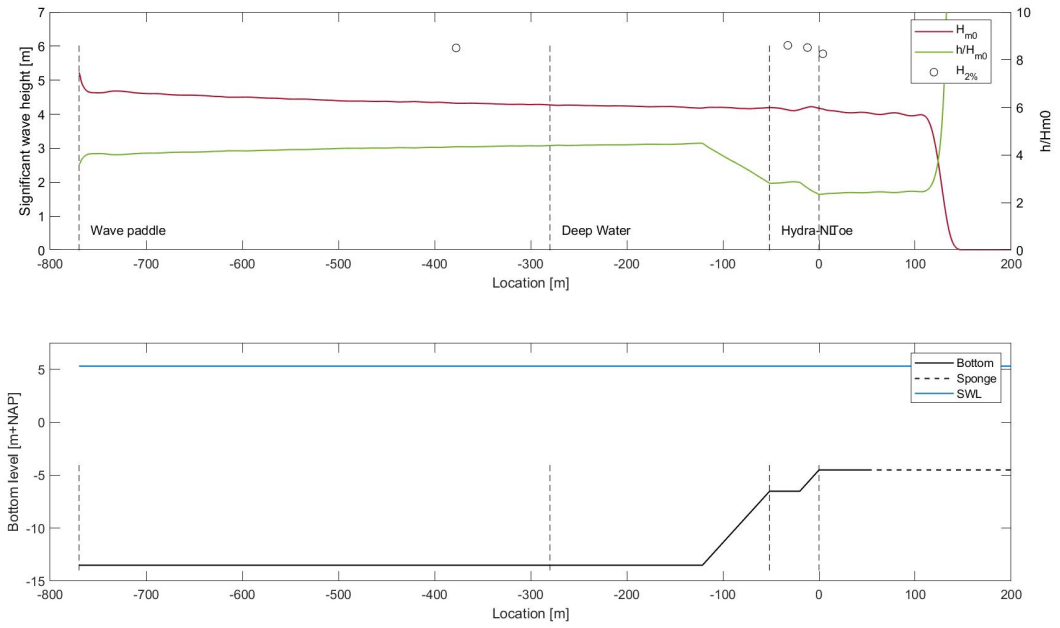

Figure B.17: Significant wave height over spatial domain

Figure B.18: Exceedance probability (left) and frequency energy density spectrum (right)

SWL [m + NAP]	H$_{m0}$ [m]	T$_p$
5.59	4.22	7.56

Table B.9: Target wave conditions at deep water
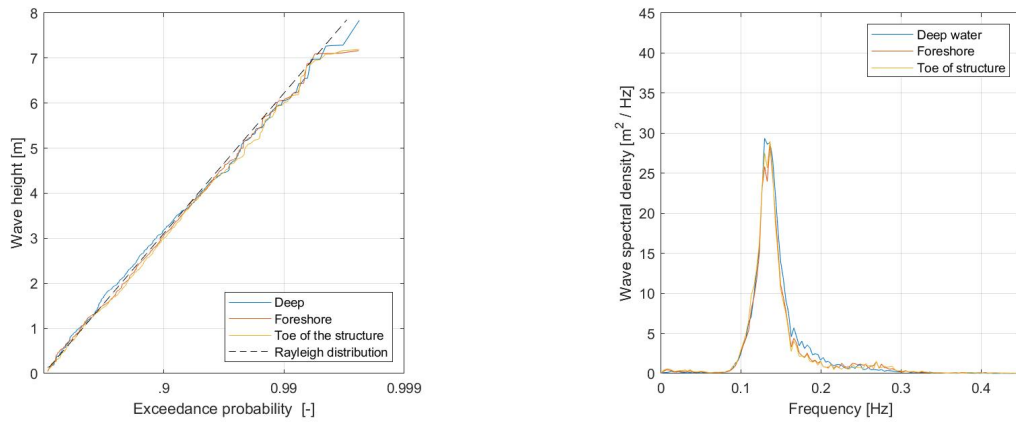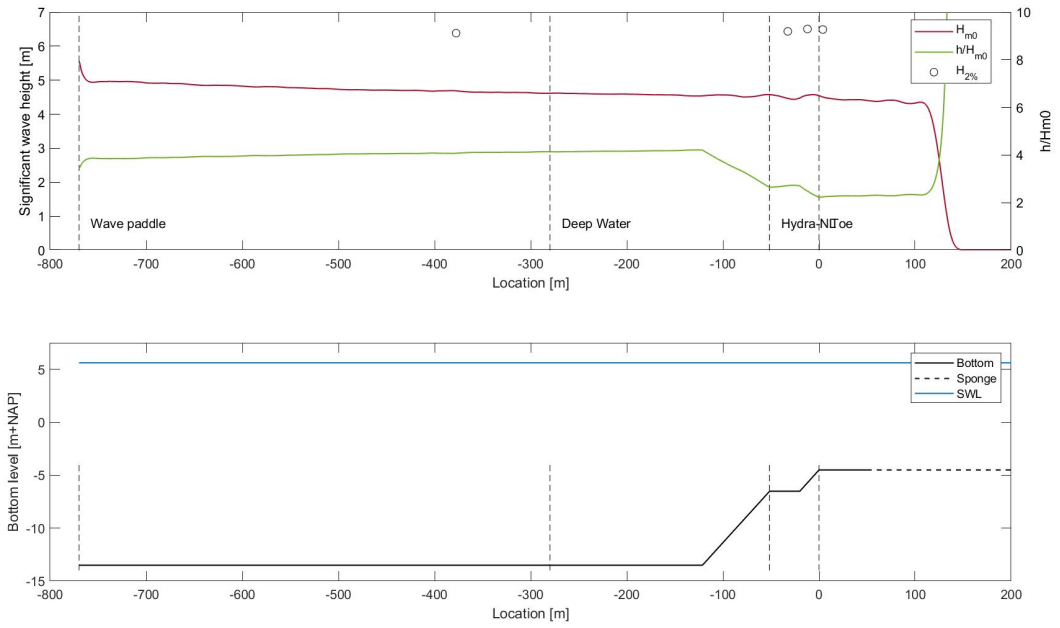
Figure B.19: Significant wave height over spatial domain

Figure B.20: Exceedance probability (left) and frequency energy density spectrum (right)

SWL [m + NAP]	H_{m0} [m]	T_p
5.30	4.33	7.63

Table B.10: Target wave conditions at deep water

Figure B.21: Significant wave height over spatial domain

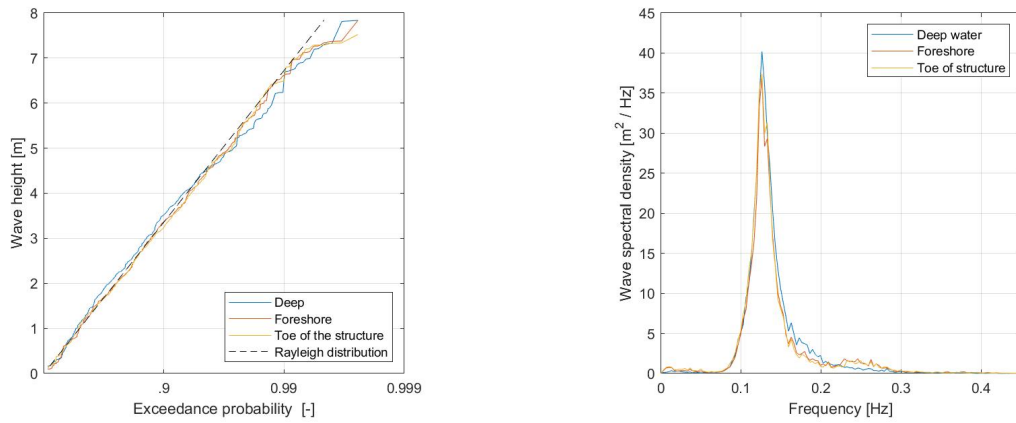Figure B.22: Exceedance probability (left) and frequency energy density spectrum (right)

SWL [m + NAP]	H_{m0} [m]	T_p
5.61	4.64	7.93

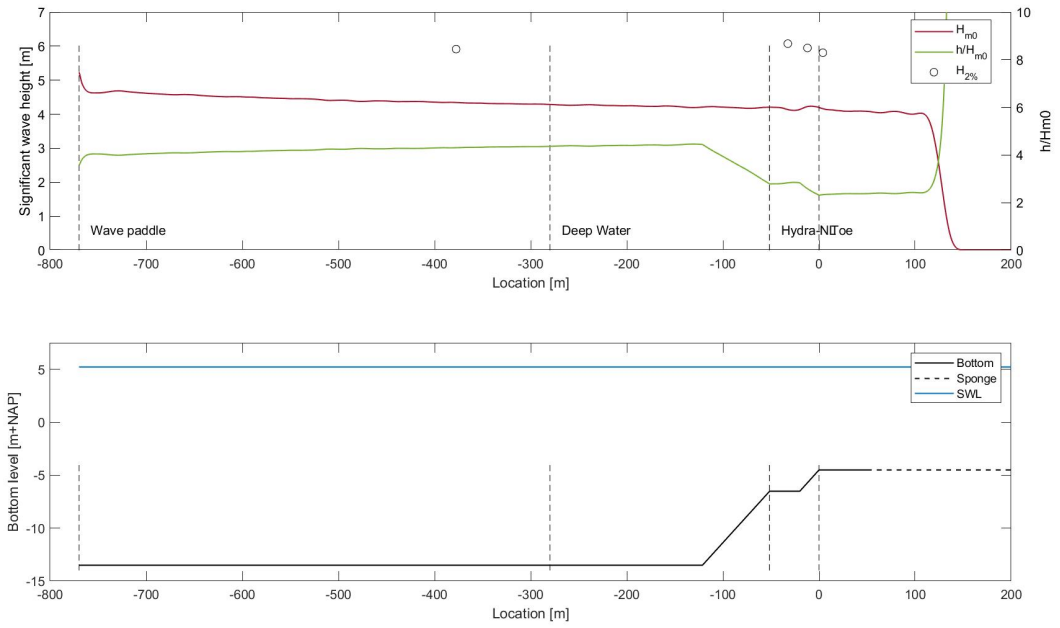Table B.11: Target wave conditions at deep water

Figure B.23: Significant wave height over spatial domain
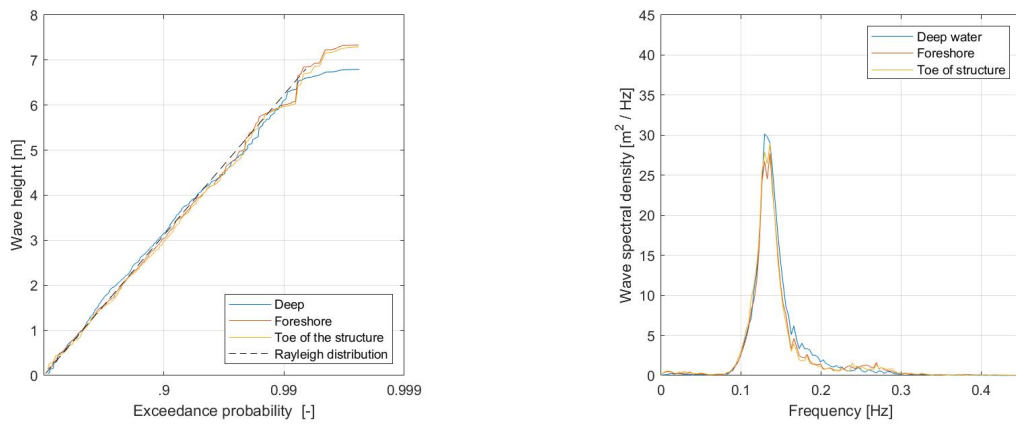
Figure B.24: Exceedance probability (left) and frequency energy density spectrum (right)

SWL [m + NAP]	H_{m0} [m]	T_p
5.22	4.33	7.63

Table B.12: Target wave conditions at deep water

B.2.4. Bottom profile 17-217

Figure B.25: Significant wave height over spatial domain

Figure B.26: Exceedance probability (left) and frequency energy density spectrum (right)

SWL [m + NAP]	H_{m0} [m]	T_p
5.47	3.4	7.21

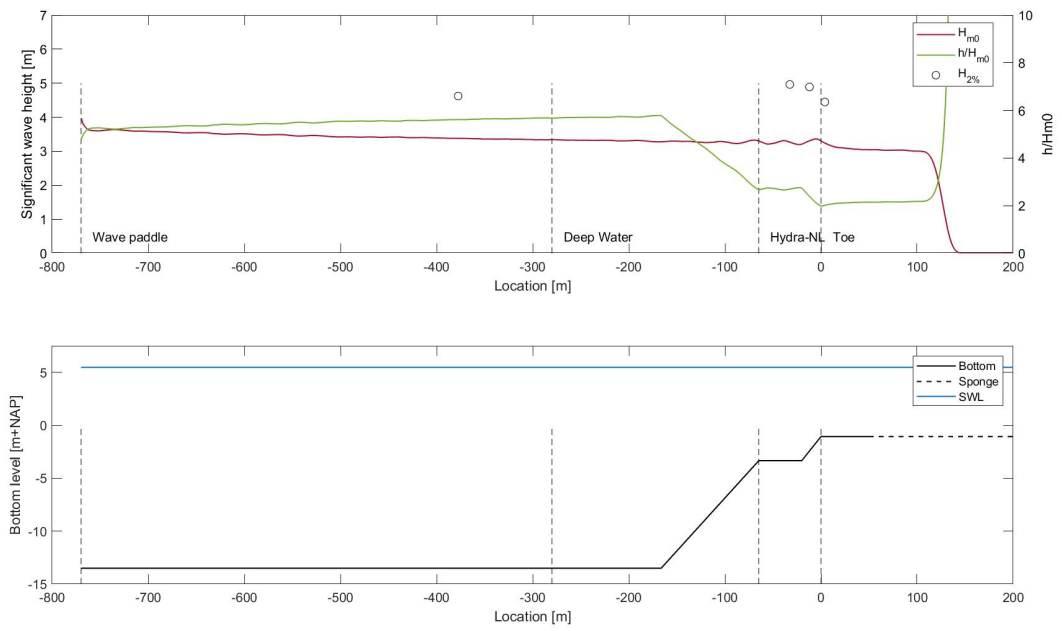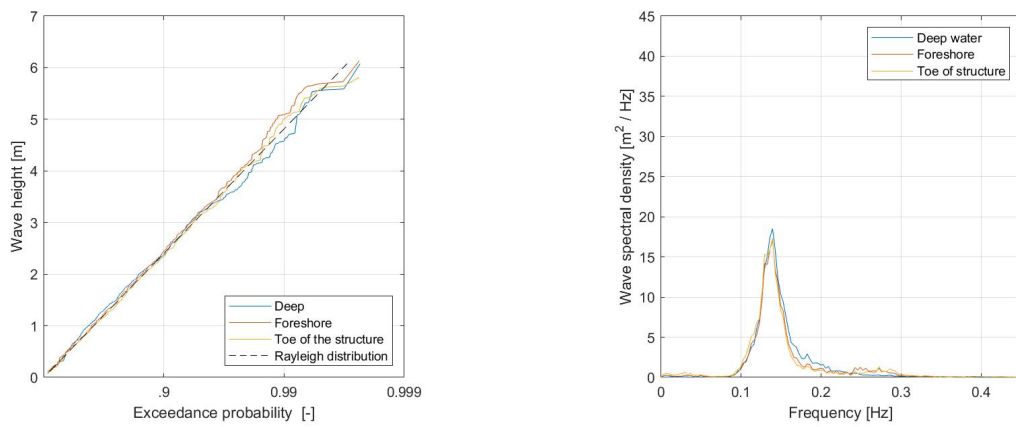Table B.13: Target wave conditions at deep water

Figure B.27: Significant wave height over spatial domain
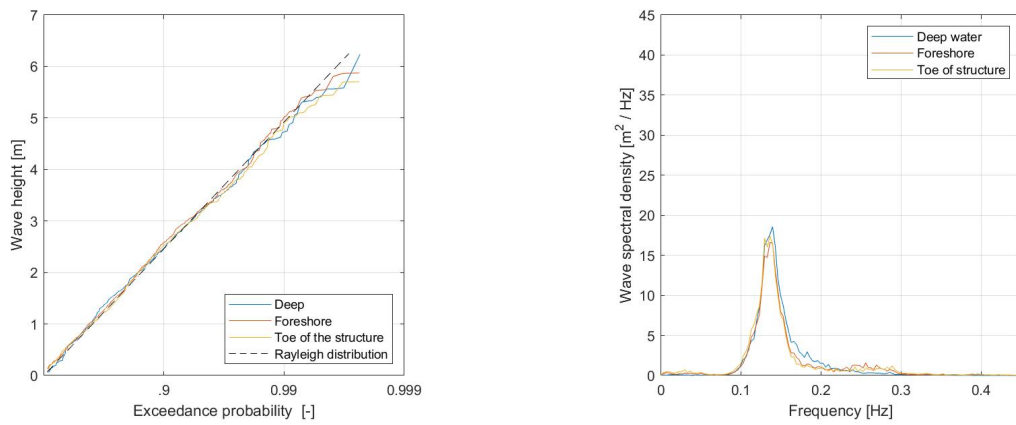
Figure B.28: Exceedance probability (left) and frequency energy density spectrum (right)

SWL [m + NAP]	H_{m0} [m]	T_p
5.20	3.4	7.21

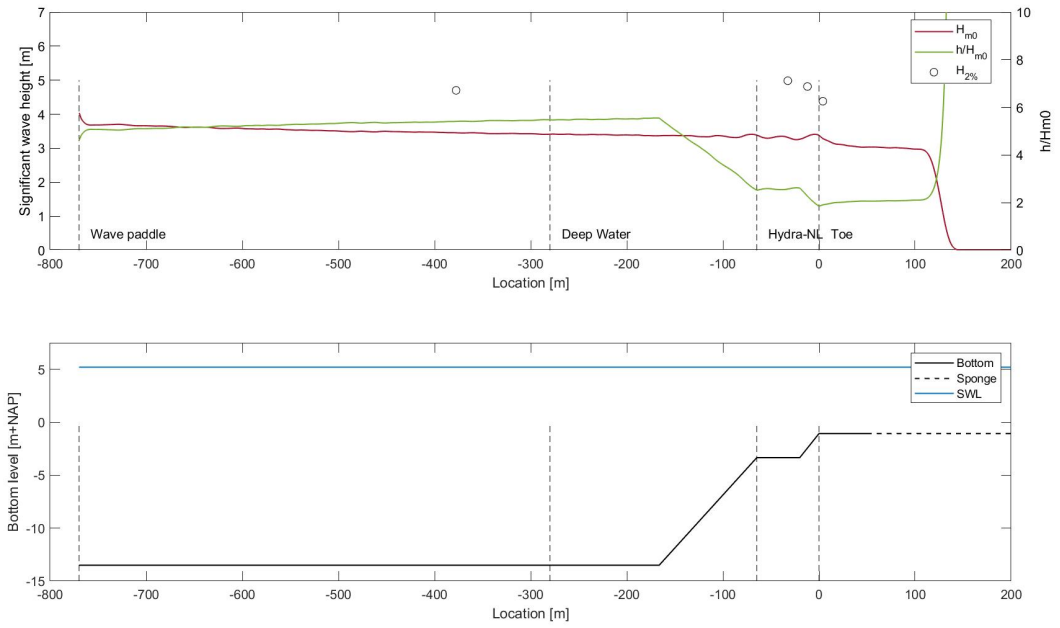Table B.14: Target wave conditions at deep water

Figure B.29: Significant wave height over spatial domain

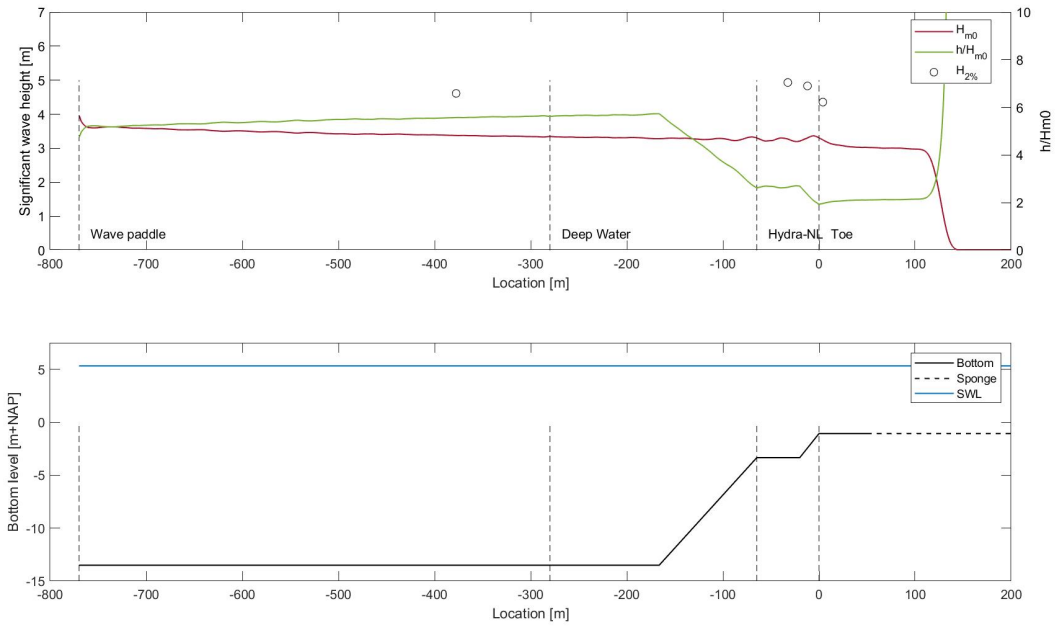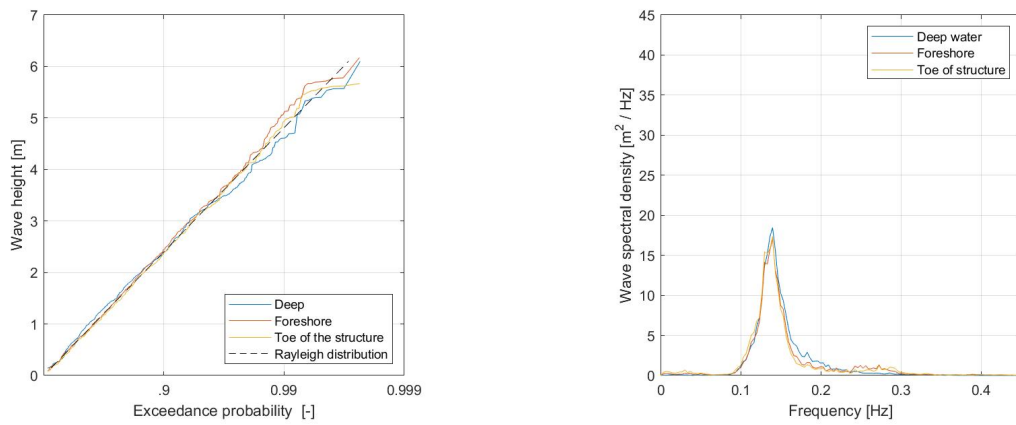Figure B.30: Exceedance probability (left) and frequency energy density spectrum (right)

SWL [m + NAP]	H_{m0} [m]	T_p
5.32	3.4	7.21

Table B.15: Target wave conditions at deep water

Here the equations to predict the average wave overtopping discharge are presented. In red the changes in the equations are visualized. The same structure as in chapter 6 is used. Every time the adjustment that is applied, the equations for the roughness influence factor, the wave overtopping discharge and the two percent run-up are shown.

C.1. Add location weighting factor in combined roughness influence factor

An extra location weighting factor, α is implemented in the combined roughness influence factor. This factor is added so the roughness elements on the upper slope have a larger weight than on the berm. The berm has a larger weight than the roughness elements on the lower slope.

$$\gamma_{f,weighted} = \frac{\sum_{i=1}^{n} \alpha_i \cdot \gamma_{f,i} \cdot L_i}{\sum_{i=1}^{n} L_i} \tag{C.1}$$

$$\frac{q}{\sqrt{g \cdot H_s^3}} = \frac{0.027}{\sqrt{\tan(\alpha)}} \cdot \xi_{m-1,0} \cdot \exp(-6.5 \cdot \frac{R_c}{3.45 \cdot \tanh(0.65 \cdot \xi_{m-1,0}) \gamma_b \cdot \gamma_{f,weighted} \cdot H_s}) \tag{C.2}$$

$$R_{u2\%} = 3.45 \cdot \tanh(0.65 \cdot \xi_{m-1.0}) \cdot \gamma_b \cdot \gamma_{f,weighted} \cdot H_s \tag{C.3}$$

C.2. Replacing combined roughness influence factor

The first adjustment, was replacing the combined roughness influence factor by the roughness influence factor of the upper slope.

$$\gamma_{f,weighted} \Rightarrow \gamma_f \tag{C.4}$$

$$\gamma_f = 1 - (0.585 \cdot \sqrt{0.075 - s'_{m-1,0}} \cdot \rho_{\gamma f}^{0.5} \cdot (6.9 \cdot \frac{Rc}{R_{u2\%}} - \ln(q_0)) \tag{C.5}$$

$$\frac{q}{\sqrt{g \cdot H_s^3}} = \frac{0.027}{\sqrt{\tan(\alpha)}} \cdot \xi_{m-1,0} \cdot \exp(-6.5 \cdot \frac{R_c}{3.45 \cdot \tanh(0.65 \cdot \xi_{m-1,0}) \gamma_b \cdot \gamma_f \cdot H_s}) \tag{C.6}$$

$$R_{u2\%} = 3.45 \cdot \tanh(0.65 \cdot \xi_{m-1.0}) \cdot \gamma_b \cdot \gamma_f \cdot H_s \tag{C.7}$$

C.3. Implement foreshore influence factor

To take into account the changing wave height distribution due to the limited water depth at the toe of the structure an extra influence factor is implemented.

$$\gamma_h = \frac{H_{2\%}}{1.4 \cdot H_s} \tag{C.8}$$

$$\gamma_f = 1 - (0.585 \cdot \sqrt{0.075 - s'_{m-1,0}} \cdot \rho_{\gamma f}^{0.5} \cdot (6.9 \cdot \frac{Rc}{R_{u2\%}} - \ln(q_0)) \tag{C.9}$$

$$\frac{q}{\sqrt{g \cdot H_s^3}} = \frac{0.027}{\sqrt{\tan(\alpha)}} \cdot \xi_{m-1,0} \cdot \exp(-6.5 \cdot \frac{R_c}{3.45 \cdot \tanh(0.65 \cdot \xi_{m-1,0}) \gamma_b \cdot \gamma_f \cdot \gamma_h \cdot H_s}) \tag{C.10}$$

$$R_{u2\%} = 3.45 \cdot \tanh(0.65 \cdot \xi_{m-1.0}) \cdot \gamma_b \cdot \gamma_f \cdot \gamma_h \cdot H_s \tag{C.11}$$

C.4. Replace local wave steepness by deep water wave steepness

Since it was expected that the wave could not adapt quickly to the foreshore. It was expected that the wave steepness at the toe of the structure corresponds better to the calculated deep water wave steepness than to the calculated local wave steepness.

$$s'_{m-1,0} \Rightarrow s_{m-1,0} \tag{C.12}$$

$$\gamma_f = 1 - (0.585 \cdot \sqrt{0.075 - s_{m-1,0}} \cdot \rho_{\gamma f}^{0.5} \cdot (6.9 \cdot \frac{Rc}{R_{u2\%}} - \ln(q_0)) \tag{C.13}$$

$$\frac{q}{\sqrt{g \cdot H_s^3}} = \frac{0.027}{\sqrt{\tan(\alpha)}} \cdot \xi_{m-1,0} \cdot \exp(-6.5 \cdot \frac{R_c}{3.45 \cdot \tanh(0.65 \cdot \xi_{m-1,0}) \gamma_b \cdot \gamma_f \cdot \gamma_h \cdot H_s}) \tag{C.14}$$

$$R_{u2\%} = 3.45 \cdot \tanh(0.65 \cdot \xi_{m-1.0}) \cdot \gamma_b \cdot \gamma_f \cdot \gamma_h \cdot H_s \tag{C.15}$$

C.5. Flow depth run-up and blocking factor

As described in section 6.3.4, the wave overtopping discharge might be related to the rib height and the flow depth of the run-up. This is expressed in a new parameter. This parameter will replace the roughness influence factor in the equation of the average wave overtopping discharge.

$$\gamma_{rib} = 1 - \frac{1}{\frac{\sum h(z)}{\sum \delta(z)}} \tag{C.16}$$

$$\gamma_f = 1 - (0.585 \cdot \sqrt{0.075 - s_{m-1,0}} \cdot \rho_{\gamma f}^{0.5} \cdot (6.9 \cdot \frac{Rc}{R_{u2\%}} - \ln(q_0)) \tag{C.17}$$

$$\frac{q}{\sqrt{g \cdot H_s^3}} = \frac{0.027}{\sqrt{\tan(\alpha)}} \cdot \xi_{m-1,0} \cdot \exp(-6.5 \cdot \frac{R_c}{3.45 \cdot \tanh(0.65 \cdot \xi_{m-1,0}) \gamma_b \cdot \gamma_{rib} \cdot \gamma_h \cdot H_s}) \tag{C.18}$$

$$R_{u2\%} = 3.45 \cdot \tanh(0.65 \cdot \xi_{m-1.0}) \cdot \gamma_b \cdot \gamma_f \cdot \gamma_h \cdot H_s \tag{C.19}$$

C.6. Flow depth run-up with local wave steepness

Now the deep water wave steepness is replaced by the local wave steepness.

$$s_{m-1,0} \Rightarrow s'_{m-1,0} \tag{C.20}$$

$$gamma_{rib} = 1 - \frac{1}{\frac{\sum h(z)}{\sum \delta(z)}} \tag{C.21}$$

$$\gamma_f = 1 - (0.585 \cdot \sqrt{0.075 - s_{m-1,0}} \cdot \rho_{\gamma f}^{0.5} \cdot (6.9 \cdot \frac{Rc}{R_{u2\%}} - \ln(q_0)) \tag{C.22}$$

$$\frac{q}{\sqrt{g \cdot H_s^3}} = \frac{0.027}{\sqrt{\tan(\alpha)}} \cdot \xi_{m-1,0} \cdot \exp(-6.5 \cdot \frac{R_c}{3.45 \cdot \tanh(0.65 \cdot \xi_{m-1,0}) \gamma_b \cdot \gamma_{rib} \cdot \gamma_h \cdot H_s}) \tag{C.23}$$

$$R_{u2\%} = 3.45 \cdot \tanh(0.65 \cdot \xi_{m-1.0}) \cdot \gamma_b \cdot \gamma_f \cdot \gamma_h \cdot H_s \tag{C.24}$$

D
Matlab Scripts

The table below presents the used Matlab scripts, the function of the script and the writer of the script. The scripts are adjusted for this study.

Name script	Function	Written by
calibrate_swash	Calibrates SWASH by changing the input conditions	Luuk Jordans
capel_roughness_calculate	Calculates influence factor of roughness for Capel	Luuk Jordans
capel_roughness_fit	Fits roughness influence factor for Capel	Luuk Jordans
comparison_swash	Post processes data and creates figures	Luuk Jordans
convert_swash_table	Convert SWASH output file to Matlab struct	Gerbrant van Vledder
create_bottom	Creates bottom profile	Gerbrant van Vledder
create_points	Creates measurement points	Gerbrant van Vledder
make_movie_gif	Makes a gif of the surface elevation	Gerbrant van Vledder
master_swash_runs	Generates input data for SWASH	Gerbrant van Vledder
mod_textfile	Modification of textfile	Gerbrant van Vledder
post_processing	Creates figures for report	Luuk Jordans
show_propagation	Shows the surface elevation	Gerbrant van Vledder
spec_tps	Smoothens peak period	Gerbrant van Vledder
reflexng	Decomposes surface elevation using Zelt and Skelbreia	Alessandro Antonini
spectral_analysis	Obtain spectral parameters	Gerbrant van Vledder
time_domain_analysis	Obtain time domain parameters	Gerbrant van Vledder
van_der_meer_roughness_calculate	Calculates roughness influence factor for Van der Meer	Luuk Jordans
van_der_meer_roughness_fit	Fits roughness influence factor for Van der Meer	Luuk Jordans

Table D.1: Overview of used Matlab scripts

E
CLASH database

The CLASH database is created to develop a prediction method on wave overtopping of coastal structures. A more extended description of this database is given by Steendam et al. (2004). In this database all type of coastal structures are included. This database includes data of 10.532 tests from 163 independent studies. Each test in the database is described by 31 parameters. These parameters can be separated in three groups. These groups are:

- General parameters
- Hydraulic parameters
- Structural parameters

In order to filter the tests with structures that look similar as the structure of the Afsluitdijk from this database, a few limits are used. First, dikes should be filtered from breakwaters. The representative slope should be gentler than 1:2 and the roughness should be between 0.6 and 1.0. Than all the tests without berm are excluded from the dataset. From the total database approximately 300 tests were left. Based on the source of approximately 120 tests was decided that these did not correspond to the structure of the Afsluitdijk. Less than 200 tests are left, of which the source can not be identified, in the CLASH database where equation 3.29 is based on. This is less than 2% of the total data base. So the equation is not validated for this type of structure.

F
Roughness influence factor Xbloc$^{\text{plus}}$

To determine the roughness influence factor of the armour unit Xbloc$^{\text{plus}}$ the cases without ribs on the upper slope are and the Xbloc$^{\text{plus}}$ on the upper slope are considered. From these test cases is know that the roughness influence factor of the berm and upper slope are 1. The berm influence factor is calculated with the equation 3.11. Based on the measured average wave overtopping discharge, the combined roughness influence factor is calculated with equation 3.16. Then the roughness influence factor of the lower slope is fitted, until it corresponds to this combined roughness influence factor. There are three tests without ribs on the upper slope. Based on these tests the roughness influence factors for the lower slope are 0.75 and 0.91 in the Scheldt flume and 1.33 in the Delta flume.